

## Departure of a bubble growing on a horizontal wall

**Citation for published version (APA):**

Zijl, W. (1978). *Departure of a bubble growing on a horizontal wall*. [Phd Thesis 1 (Research TU/e / Graduation TU/e), Applied Physics and Science Education]. Technische Hogeschool Eindhoven.  
<https://doi.org/10.6100/IR33762>

**DOI:**

[10.6100/IR33762](https://doi.org/10.6100/IR33762)

**Document status and date:**

Published: 01/01/1978

**Document Version:**

Publisher's PDF, also known as Version of Record (includes final page, issue and volume numbers)

**Please check the document version of this publication:**

- A submitted manuscript is the version of the article upon submission and before peer-review. There can be important differences between the submitted version and the official published version of record. People interested in the research are advised to contact the author for the final version of the publication, or visit the DOI to the publisher's website.
- The final author version and the galley proof are versions of the publication after peer review.
- The final published version features the final layout of the paper including the volume, issue and page numbers.

[Link to publication](#)

**General rights**

Copyright and moral rights for the publications made accessible in the public portal are retained by the authors and/or other copyright owners and it is a condition of accessing publications that users recognise and abide by the legal requirements associated with these rights.

- Users may download and print one copy of any publication from the public portal for the purpose of private study or research.
- You may not further distribute the material or use it for any profit-making activity or commercial gain
- You may freely distribute the URL identifying the publication in the public portal.

If the publication is distributed under the terms of Article 25fa of the Dutch Copyright Act, indicated by the "Taverne" license above, please follow below link for the End User Agreement:

[www.tue.nl/taverne](http://www.tue.nl/taverne)

**Take down policy**

If you believe that this document breaches copyright please contact us at:

[openaccess@tue.nl](mailto:openaccess@tue.nl)

providing details and we will investigate your claim.

DEPARTURE OF A BUBBLE GROWING  
ON A HORIZONTAL WALL

W.ZIJL

**DEPARTURE OF A BUBBLE GROWING ON A HORIZONTAL WALL**

# DEPARTURE OF A BUBBLE GROWING ON A HORIZONTAL WALL

PROEFSCHRIFT

ter verkrijging van de graad van doctor in de  
technische wetenschappen aan de Technische  
Hogeschool Eindhoven, op gezag van de rector  
magnificus, prof.dr. P.van der Leeden, voor  
een commissie aangewezen door het college  
van dekanen in het openbaar te verdedigen op  
dinsdag 19 september 1978 te 16.00 uur

door

WOUTER ZIJL

geboren te Amsterdam

Dit proefschrift is goedgekeurd door  
de promotoren:

Prof. dr. D. A. de Vries,

Prof. dr. ir. G. Vossers.

*Aan mijn Ouders,  
Aan Beatrijs,  
Aan Gomaar en Firmijn*

1. INTRODUCTION AND BRIEF SURVEY OF LITERATURE	
1.1. Subject matter and contents of the thesis	1
1.2. Early theories on bubble departure	4
1.3. Growth of a free bubble	6
1.4. Micro- and adsorption layers. Dry areas	8
1.5. Bubble departure	11
1.6. The equations describing the evolution of the coupled temperature and flow fields	
1.6.1. The basic equations of motion	12
1.6.2. The boundary conditions for solid walls and free interfaces	13
1.6.3. The initial conditions	14
1.6.4. Well-posedness of the partial differential system	15
1.6.5. Methods of solution	15
2. INTRODUCTION TO BUBBLE DYNAMICS: GROWTH AND DEPARTURE OF A SPHERICAL BUBBLE	
2.1. Introduction to the basic equations	18
2.2. Bubble growth	
2.2.1. The equations of radial motion	23
2.2.2. Diffusion-controlled bubble growth	28
2.2.3. Bubble growth affected by liquid inertia	33
2.3. Bubble departure	
2.3.1. Initial acceleration of a free bubble	39
2.3.2. Acceleration controlled bubble departure	40
2.3.3. The validity of acceleration controlled bubble departure and other modes of bubble departure	43
2.4. Vapour bubbles at a wall	
2.4.1. Enhancement of growth rate by microlayer evaporation	47
2.4.2. The influence of non-homogeneous initial temperature fields on growth and departure	51
2.5. Volume oscillations	57

3.	DEVIATIONS FROM THE SPHERICAL SHAPE	
3.1.	Introduction	62
3.2.	Initial acceleration of non-growing bubbles	
3.2.1.	The equations of motion	63
3.2.2.	The global collocation method	66
3.2.3.	Convergence of orthogonal collocation	71
3.3.	Departure of water vapour bubbles under low pressure	
3.3.1.	Introduction	73
3.3.2.	The thermal equations	74
3.3.3.	Example of growth and departure of a bubble in a non-homogeneous temperature field	81

4.	THIN LIQUID LAYERS IN RELATION TO BUBBLES GROWING AT A WALL	
4.1.	The thickness of formation of the liquid microlayer	
4.1.1.	Creeping flow in the meniscus region	88
4.1.2.	Inertia effects in the meniscus region	94
4.1.3.	Thickness of microlayer formation	97
4.2.	The growth rate of a dry area	
4.2.1.	Formation of an adsorption layer. Contact angle between the adsorption layer and the microlayer	103
4.2.2.	Dry area growth under the influence of surface tension	105
4.3.	Gas bubble departure as governed by the growth of the bubble contact perimeter	108
4.4.	Conclusions	112

APPENDICES

A	Equations of motion for potential flow around sperical bubbles	114
B	Product rules for the generalized Riemann-Liouville operator	118



C	The equations of motion of the gas-liquid interface of a thin liquid layer at a horizontal wall under the influence of forces normal to that interface	
C 1.	Division of the flow field in finite elements	121
C 2.	Normal stress and normal velocity conditions	126
C 3.	Tangential stress and volumetric flux conditions	128
C 4.	Conditions at the triple interfacial line and at the place of outflow	130
C 5.	Kinematic boundary condition and global continuity	131
C 6.	Discussion	135
	LIST OF SYMBOLS	138
	REFERENCES	145
	SUMMARY	153
	SAMENVATTING	155
	DANKWOORD	157
	CURRICULUM VITAE	157

## CHAPTER 1

### INTRODUCTION AND BRIEF SURVEY OF LITERATURE

#### *1.1. Subject matter and contents of the thesis*

Heat or mass transfer processes are important in many fields of engineering. Extensive research on these subjects is strongly demanded by the need to control large amounts of energy for industrial and domestic use. For example, understanding of heat transfer processes is of paramount importance in electricity-producing plants, where heat is produced either by combustion of conventional fuels like coal, oil or gas, or by nuclear processes. This heat is required to generate steam for a turbine and either water under high pressure or liquid metals are used as an intermediate heat transport medium.

A field of renewed interest, in which mass transfer plays an important part, is in apparatus for the production of hydrogen and oxygen from water by electrolysis. Alternative energy sources producing the electricity required for electrolysis may be the sun or the wind. However, it is also possible that nuclear energy will become a main source of energy. Hydrogen is attractive as a fuel of the future because it is ecologically clean, can be transported efficiently through underground pipelines, and eventually can be mixed with natural gas; cf. Mathis (1976).

In most practical cases, heat and mass transfer takes place at the interface between a solid wall and a fluid; the transport characteristics are strongly dependent on the geometry of the set-up. Another important parameter is the strength of the acceleration field in which the fluid is situated. In this thesis, restriction has been made to horizontal walls upon which a fluid is initially at rest in the earth's gravitational field. The more complex case, where a fluid is forced to flow parallel to the wall, will not be considered despite its great practical importance in engineering.

One of the most characteristic features in such a configuration is the occurrence of buoyancy effects in the fluid. Buoyancy forces arise as a result of density variations in a fluid subject to gravity. In heat transfer the so-called Bénard problem, where a horizontal layer of fluid is heated from below, is well-known ; cf. Bénard (1901). In that case, density differences are caused by variations in temperature. It has been shown by Rayleigh (1906) that the so-called Rayleigh number plays a dominant part in the Bénard problem. When the Rayleigh number exceeds a critical value, the flow pattern becomes unstable and heat transfer by natural convection occurs. Similar behaviour can be observed when, instead of differences in temperature, differences in concentration of a solute are present in a liquid (e.g. salt in water). Here the so-called salinity Rayleigh number has the same significance as the ordinary Rayleigh number in heat transfer. A comparatively recent development in the field of natural convection has been the study of fluids in which there are gradients of two or more properties with different diffusivities. This is the case in binary mixtures and the stability properties of such a system have been reviewed by Turner (1973).

Another well-known buoyancy problem, which has certain similarities to the systems previously discussed, occurs when differences in density are caused by liquid-gas or liquid-vapour transitions. This is the case during electrolysis and boiling respectively. It is this problem to which this thesis will be devoted.

At the wall, transitions from liquid to vapour can occur when the wall is superheated, i.e. when it has a temperature which is higher than the saturation temperature at ambient pressure. Vapour bubbles nucleate at the wall in tiny cavities which have dimensions of approximately  $10^{-6}$  m and smaller. A review of the mechanism of this so-called heterogeneous nucleation has been presented by Cole (1974). It is noted that the nucleation properties of these cavities are not readily reproducible ; also, the way in which the cavities and their different sizes are distributed over the wall can hardly be controlled in most engineering applications. These facts represent a major cause of the difficulty of predicting

adequately heat transfer rates in boiling.

In a similar way, gas bubbles are formed when there is supersaturation of gas dissolved in the liquid directly above the wall. In this thesis no further attention will be paid to the physico-chemical aspects of nucleation.

In practical engineering, heat and mass transfer processes with phase transitions are often more advantageous than transfer processes in which only natural convection plays a part ; in the former processes the periodic growth and departure of bubbles causes forced liquid convection on a small scale which contributes substantially more to the transport rate than natural convection does.

Unfortunately, there is an upper limit to the heat or mass flow obtained in this way. For a sufficiently high driving temperature difference, respectively concentration difference, the number of bubbles at the wall becomes so large that these bubbles coalesce to form a coherent vapour or gas film that separates the wall from the bulk liquid. It has been shown experimentally by Yu and Mesler (1977) that, in boiling near the peak heat flux (i.e. in transitional boiling), a thin liquid layer remains at the wall between vapour and wall. Yu and Mesler called this layer the *macro-layer* and the properties of this layer are very important for an understanding of the transition from nucleate boiling, or pool boiling, to film boiling. One of the characteristic properties of this macro-layer is the rate of growth of dry areas within it. When this dry-area growth rate is large, a rapid transition to film boiling occurs, often leading to damage of the wall. However, except for the aspect of dry area growth in a liquid film at a horizontal solid wall, the transition to film boiling or to film mass transfer will not be considered in the present work.

In this thesis, only situations with sufficiently low superheating or supersaturation will be considered, under conditions where the so-called single-bubble approach may be used. This means that the distance between the individual bubbles is so large that one bubble may be considered as infinitely far away from its neighbours.

To understand the physics of the transport process and consequently ultimately to be able to find means of increasing the peak flux and thus the efficiency of engineering set ups, knowledge of the time of adherence at the wall and of the departure diameter of the bubble is essential. This is also illustrated by the many (semi-empirical) correlations for heat and mass transfer rates that are available in literature. Almost all of these correlations require knowledge of the frequency of bubble departure and of the bubble size.

*The description of the mechanisms of bubble departure, for the completely different cases of both rapidly-growing vapour bubbles and slowly-growing gas bubbles, forms the subject of this thesis.*

*In Chapter 2 of this thesis both the departure phenomena and the underlying growth processes will be illustrated with the aid of relatively simple models in which the bubble is represented as a sphere or a spherical segment. On the basis of the insight in the bubble behaviour and its mathematical description, obtained in this way, an extension will be presented in Chapter 3 to cylindrically symmetric vapour bubbles in water under subatmospheric pressures. Numerical methods will be used to calculate the bubble shape, and the results are compared to experimental data obtained by high-speed cinematography. In Chapter 4 both the hydrodynamic mechanism of microlayer formation and the mechanism of dry area growth under the influence of capillary forces will be investigated. The importance of these processes for bubble departure has already been stressed in Chapter 2.*

### *1.2. Early theories on bubble departure*

The earliest and even now perhaps best known expression for the departure diameter was presented by Fritz (1935). Although Fritz suggests that his equation can be applied for growing vapour bubbles, his model is only derived for static bubbles where the hydrostatic force balances the normal component of the capillary force and where the upward buoyancy force balances the downward force of adhesion at the wall. Fritz himself already remarked that in case of rapid evaporation a situation of exact dynamic equilibrium will hardly be reached, but he adds that experiments show his equation to be

approximately valid. Indeed, it turns out that, for many liquids boiling in the region of atmospheric pressures, Fritz's equation holds when the contact angle, occurring in this equation, is considered as an empirical parameter which has to be fitted to the experimental data for departure radii. This has been shown experimentally by Han and Griffith (1965), and by Cole and Rohsenow (1969) among others. In Section 2.4.2, this fact, which accounts for the success of Fritz's equation, will be explained theoretically. It is, however, stressed there that the agreement with experiment is purely accidental since, in reality, for rapidly growing vapour bubbles, surface tension forces and the force of adhesion do not play an important part as compared with inertia forces.

When adhering, slowly-growing gas bubbles are considered, the surface tension and adhesion forces do play important parts, and Fritz's equation agrees fairly well with experimental data, provided that the apparent contact angle at the time of break-off is known.

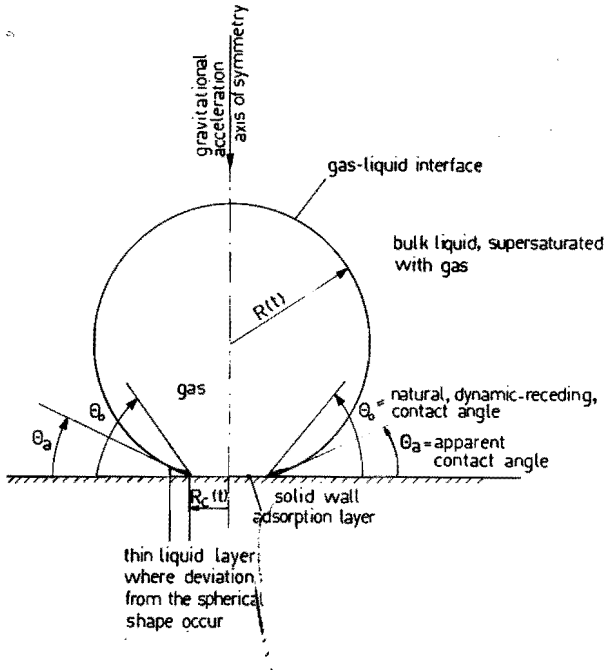


Fig. 1.1. Regions around a quasi-static gas bubble. Frictional forces cause the bubble to deviate from the static shape near the wall

However, even for slowly-growing gas bubbles, dynamic equilibrium does not hold everywhere. Apart from the fact that growth induces a pressure field which diminishes the total upward force, deformations from the static shape may be expected near the wall since the bubble contact perimeter is growing. Since this growth has the character of slip along the wall, with a growth rate often lagging behind the bubble growth rate, shear stresses will occur locally. As a consequence, an apparent contact angle, with a value varying in time, is observed. This apparent contact angle is a result of the hydrodynamics of the process. It must not be confused with the dynamic-receding contact angle, which is independent of the hydrodynamics of the process, and is purely determined by the local intermolecular interactions at the bubble contact perimeter ; cf. Section 4.2.2, and Fig. 1.1.

Consequently, in addition to Fritz's treatment, a description for the apparent contact angle has to be developed. In Section 4.3, the latter problem will be considered in more detail.

### *1.3. Growth of a free bubble*

It will be clear from the foregoing discussion that it is of paramount importance to have an accurate knowledge of the mechanism of bubble growth in order to be able to predict departure radii and times. In addition, for gas bubbles, which always grow relatively slowly, additional information is required for the growth rate of the bubble contact radius in order to be able to calculate the downward force of adhesion. For these reasons much attention will be paid to the subjects of both bubble growth and growth of a dry area caused by capillary effects.

The earliest expression for bubble growth follows from a treatment given by Rayleigh (1917), who considered the collapse of a spherical cavity in an infinitely extended, incompressible liquid. In the bubble, a constant pressure was assumed to be present. Since the expression for bubble growth based on Rayleigh's approach did, in general, not agree with experimental growth rates of gas and vapour bubbles, it was obvious that the problem had to be considered from

a different point of view. Bošnjacović (1930) neglected the hydrodynamics of the problem by assuming that the excess pressure in the bubble is negligible. In that case the bubble only grows by diffusion of gas into the bubble, or by diffusion of heat to the bubble, the sensible heat being converted into latent heat of vaporization at the vapour-liquid interface.

Experiments performed by Jakob (1958) showed that Bošnjacović's approach was very fruitful. However, strictly speaking, Bošnjacović's result is not completely correct. For rapidly-growing vapour bubbles, heat transport by radial convection must also be included ; for slowly-growing gas bubbles, a correction due to the curvature of the spherical bubble boundary has to be taken into account. Birkhof, Margulies and Horning (1958) and Scriven (1959) independently derived the correct expressions. In Section 2.2.3 the points-of-view of Rayleigh and Bošnjacović are brought together. It will be shown that initially, shortly after nucleation, a Rayleigh-type of growth exists, whereas later, after a transitional period, the Bošnjacović-mode of growth is reached asymptotically. This growth behaviour will be presented in one algebraic expression. Thus, a unified treatment of bubble growth is obtained. Comparison will be made to the unified treatment of Prosperetti and Plesset (1978), and it is shown that the agreement with the models reviewed by them is good.

Experimental investigations show that, under many conditions, the growth rate of a vapour bubble oscillates around an average value. Not only oscillations in the bubble shape, but also oscillations in the bubble volume have been observed ; cf. Van Stralen (1968), and Schmidt (1977), who pointed out that oscillations in the bubble shape may be caused by surface tension. However, volume oscillations cannot be explained in this way. One explanation may be that periodic evaporation and condensation occur around a mean rate of evaporation ; cf. Zijl, Moalem and Van Stralen (1977). Another explanation is that compressibility effects in the vapour become important, and that there is a periodic expansion and compression. In Section 2.5, these two possibilities will be considered theoretically ; it turns out that the first process, which shows a strong damping, will indeed occur for sufficiently small bubbles.



For relatively large bubbles the second mechanism, which has a much lower damping, is the governing process. For gas bubbles similar results can be obtained. However, in the latter case the oscillation frequency will be very high. Consequently, oscillations cannot be observed with equipment having a response time which is only a few orders of magnitude smaller than the bubble adherence time. In the following Chapters it will be assumed that the amplitude of the bubble oscillations is so small that they have negligible effect on bubble departure and may consequently be ignored for the present purpose.

#### 1.4. *Micro- and adsorption layers. Dry areas*

In principle, the theory for bubble growth mentioned above only applies to free bubbles in an infinitely-extended, initially uniformly superheated or supersaturated liquid under zero gravity conditions. Cooper and Lloyd (1969) and, independently, Van Ouwkerk (1970, 1971) extended the theory for heat transfer controlled vapour bubble growth at a horizontal wall, again under zero gravity conditions in a uniformly superheated liquid. Although, qualitatively speaking the results do not differ greatly from Bošnjacović's result for the growth rate of a free bubble, the hydrodynamic and heat transfer processes in this case are much more complex because of the existence of a thin liquid layer between the bubble and the wall ; cf. Fig. 1.2. The generally accepted name for this layer in literature is the (evaporating) *micro-layer*. This name has for the first time been proposed by Moore and Mesler (1961). Since the micro-layer evaporates during adherence, it contributes considerably to the bubble growth rate.

The determination of the thickness of formation of this liquid layer is presented in Section 4.1. Use will be made of Landau and Levich's (1942) solution for the free coating problem, rather than of the boundary layer approach suggested by the forementioned authors. Van Ouwkerk also considered the rate of growth of the dry area in the micro-layer. During nucleate boiling this growth rate is almost completely determined by evaporation from the micro-layer for common materials like water on steel. Important conclusions from Van Ouwker-

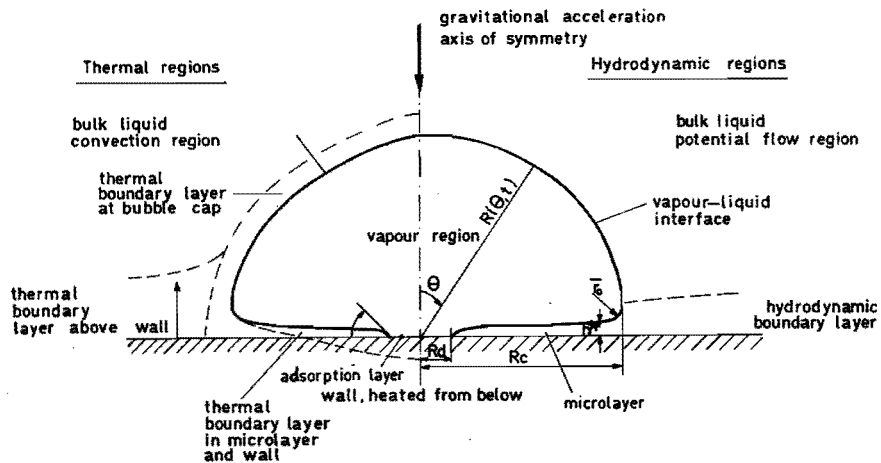


Fig. 1.2. Flow- and thermal regions around a rapidly-growing vapour bubble

kerk's analysis are that the bubble growth rate is hardly affected by the existence of a dry area and is almost independent of the thermal properties of the wall as well.

In contrast to vapour bubbles, the almost quasistatic gas bubbles do not have a similar liquid microlayer between bubble and wall. For these bubbles the thickness of formation, as calculated with Landau and Levich's expression, results in a value which is large with respect to the bubble dimensions ; i.e., the latter model does not hold for that case. Gas bubbles have almost the shape of spherical segments and the radius of the bubble base in contact with the wall (the so-called bubble contact radius) is equal to the dry area radius. Since vaporization does not play an important part for gas bubbles, the growth of this dry area is governed by capillary effects.

In reality, this so-called "dry" area is not completely dry, for complete drying would be a violation of the adherence or no-slip condition for the liquid at the wall. In fact, a microscopically thin liquid layer remains at the wall ; cf. Scheludko, Tschaljowska and Fabrikant (1970). In this non-Newtonian layer, with a thickness of  $10^{-7}$ m and smaller, the adsorption force field near boundaries plays an important part, resulting in the so-called disjoining pressure ; cf. e.g. De Feijter and Vrij (1972). The earlier mentioned microlayer, which has a thickness varying from approximately  $10^{-6}$ m to  $10^{-4}$ m, may, from this point of view, be considered as a bulk liquid, that can be described by the theory of Newtonian fluids. It is somewhat misleading that the name *micro-layer* is already in use for this macroscopic layer. In this thesis, the name *adsorption layer* will be used for the microscopic layer in which the disjoining pressure plays a dominant part. Since an adsorption layer at a wall does not evaporate completely ; cf. Wayner, Kao and Lacroix (1976), the wall surface covered by this layer forms a thermal insulation for the heat flux, in a similar way as a dry area does. For this reason, the name dry area for the wall surface covered by the adsorption layer is acceptable for the present purpose.

In literature hardly any attention has been paid to the process of dry area formation caused by capillary forces. Experiments on this subject have been reported by Scheludko, Tschaljowska and Fabrikant (1970), and by Cooper and Merry (1972) ; however, a theoretical treatment has not yet been given. For that reason a model has been proposed in Section 4.2 and in Appendix C. In contrast to this, the process of dry area formation by evaporation, i.e. the so-called dry-out, will not be considered in this thesis, since this subject has been treated extensively in the literature; cf. e.g. Cooper and Merry(1972, 1974), and Yu and Mesler (1977).

### 1.5. Bubble departure

Knowing the growth rate of the bubble, the acceleration of the centre of mass of a free bubble with the same growth rate can be determined by Green's momentum equation ; cf. Lamb (1974). When the latter equation may be considered as an approximation for bubbles at a wall, the following description holds : when the displacement of the bubble centre from the wall has become equal to the bubble radius, the bubble will depart, provided that the upward buoyancy force exceeds the downward force of adhesion at the wall. For vapour bubbles this is the case, and the departure radii obtained in this way agree quantitatively with experimental results obtained by Moalem, Zijl and Van Stralen (1977), and by Cooper, Judd and Pike (1978) ; cf. Section 2.3.2.

It is stressed here that in the fore-mentioned case, liquid acceleration is the governing mechanism for departure, and in general, during adherence there is no balance between upward buoyancy force and downward inertia and adhesion forces. Of course, the model of an accelerating growing sphere is a simplification, since in reality the growing bubble foot is decelerating ; cf. Chapter 3. However, in both cases, liquid accelerated by gravity determines the departure radius and adherence time. Models for prediction of the adherence time based on a balance of forces in fact only present a lower limit for the adherence time ; cf. e.g. Witze, Schrock and Chambré (1968), and Kiper (1971).

Since gas bubbles grow very slowly with respect to vapour bubbles, the above-mentioned explanation of departure does not apply, and a balance of the upward buoyancy force and the downward force of adhesion determines the adherence time and break-off radius. In Section 4.2 this equilibrium of forces has been treated in the way discussed by Kabanow and Frumkin (1933).

An expression for the bubble growth rate has to be substituted in the expressions for departure mentioned above. For vapour-bubbles, growing in a realistic non-uniformly-superheated liquid at a wall, it is relatively simple to express the parameter describing bubble growth in other physical parameters like ambient pressure and

surface tension in the following way. After bubble departure, cold bulk liquid, with a temperature approximately equal to the saturation temperature at ambient pressure, flows to the superheated wall. Initially, this liquid is heated only by conduction and, after some time, when the thermal penetration thickness has grown so large that the Rayleigh number exceeds its critical value, it is also heated by natural convection. Next, when the thermal boundary layer has become sufficiently thick, nucleation takes place at a certain cavity. Since the required superheating for nucleation at a cavity with prescribed dimensions depends among others on surface tension, the final thickness of the thermal boundary layer will also depend on the value of the surface tension.

This process has been described by Han and Griffith (1965). Combination of their model with the theories of vapour bubble growth and departure developed in this thesis, results in an expression for the bubble departure radius which is independent of both the superheating and the dimensions of the cavity where the bubble has been nucleated; cf. Section 2.4.2.

The derivation of a similar expression relating the departure radius to the ambient pressure has not been attempted for gas bubbles because such an expression would depend greatly on the way in which supersaturation is produced at the wall (e.g. by electrolysis, or by leading a gas through the liquid etc.).

## *1.6. The equations describing the evolution of the coupled temperature and flow fields*

### *1.6.1. The basic equations of motion*

Until now, relatively simple algebraic expressions have been discussed in order to understand, at least approximately, the main aspects of bubble departure and of the underlying growth processes. However, from a fundamental point of view, the picture obtained in this way is not fully satisfactory, since, in the models mentioned before, deviations from the spherical bubble shape have been neglected; i.e. the hydrodynamic theory holding for free spherical bubbles has

been used. Another unsatisfactory approximation was the determination of the contribution of the evaporating liquid microlayer to bubble growth. The presentation given in Section 2.4.1 only holds for the rather unrealistic case of bubble growth in an initially uniformly superheated liquid under zero gravity conditions.

For these reasons the growth and departure of cylindrically symmetric vapour bubbles in water boiling at subatmospheric pressures has been treated numerically and the results are compared to experimental data in Chapter 3.

Theoretically speaking, the flow and temperature fields of the gas and vapour in the bubble and of the liquid surrounding the bubble can adequately be described by the basic continuum formulation for Newtonian fluids, expressing conservation of mass, of momentum and of energy, complemented with a diffusion equation for the gas dissolved in the liquid and with expressions for the normal and tangential stresses ; cf. e.g. Bird, Stewart and Lightfoot (1960). In order to obtain a solution of these equations, appropriate boundary and initial conditions have to be prescribed.

#### *1.6.2. The boundary conditions for solid walls and free interfaces*

In general, boundary conditions at the solid wall are the condition of impermeability and of no-slip or adherence.

At the gas-liquid interface there is a discontinuity in normal stress caused by surface tension. This effect is described mathematically by the Laplace-Kelvin equation. There is also a discontinuity in the tangential stress over the gas-liquid interface. This effect is described by the Marangoni-Gibbs condition; cf. Traykov and Ivanov (1977). However, in the flow field around the bubble, potential flow may be assumed, cf. Section 3.1, and in that case, the Marangoni-Gibbs condition must be disregarded.

For the thermal or energy equation it is usually assumed that there is no jump in temperature across a vapour-liquid interface. This has been verified experimentally by Prüger (1944). Also for gas bubbles it may be assumed that there is no jump in concentration across the interface.

The pressure at the gas-liquid or vapour-liquid interface may be approximated by the thermodynamic equilibrium expressions of Henry and Clapeyron respectively.

At the bubble boundary the displacement of this interface can be related to the inflow of gas or vapour, thus resulting in a second boundary condition for respectively the mass or heat diffusion equation.

As a result of the solution for an initially prescribed gas-liquid interface, the normal component of the liquid velocity is also known at  $t = 0$ . Equating the rate of displacement of the gas-liquid interface to this normal velocity component results in a so-called kinematic boundary condition from which the evolution in time of the interfacial coordinates can be determined.

At the location of the dry area radius, where the adsorption layer and the microlayer meet, both the thickness of the layer and the so-called contact angle between the adsorption layer and the microlayer have to be prescribed. From these two conditions the a priori unknown position of the perimeter of the adsorption layer or dry area can be determined as a function of time from a partial differential equation of the parabolic type ; cf. Section 4.2.

### *1.6.3. The initial conditions*

Initial conditions must be prescribed for the position and the normal component of the velocity of the vapour-liquid, or gas-liquid, interface. For growing bubbles, the choice of these conditions is not of great consequence since their influence damps away rapidly. This is in contrast to imploding bubbles where small variations in the initial conditions are amplified; cf. Plesset (1954 a).

However, the choice of the initial temperature field in which the bubble grows is shown to be of great influence on the rate of growth and the adherence time. In Section 3.3.2, measurements of initial temperature fields will be reported. The latter fields have been used

as initial conditions for the temperature field and comparison of shape and size of computed bubbles with experimental bubbles, growing in similar temperature fields, will be reported.

#### *1.6.4. Well-posedness of the partial differential system*

After having derived the partial differential equations and the relevant boundary and initial conditions, the first question which must be answered is whether the resulting system represents a well-posed problem. This is a crucial question, especially for the application of the collocation method, which will be used in this thesis, since this method will also produce "solutions" of ill-posed problems. In this thesis, the well-posedness will not be proved mathematically, but comparison with situations where well-posedness is established in the literature has served as a guideline.

#### *1.6.5. Methods of solution*

The advent of fast digital computers with a large memory capacity has made it possible to find solutions for problems by application of numerical approximation methods where analytical methods are hard to apply. In this thesis numerical methods are considered as methods which map the space-time continuum in a finite number of discrete space-time points.

This definition of a numerical method does not touch upon the question whether it is convenient or not to use a digital computer to evaluate the values of the variables at the discrete points.

An example of an analytical solution, inspired by a numerical method, will be presented in Appendix C. There the equation of motion of the gas-liquid interface of a liquid layer under the action of forces normal to that interface has been derived from the equations of steady Stokes or creeping flow and their boundary conditions, by use of the local collocation approximation ; cf. Finlayson (1972).

Even when numerical approximation methods are adopted, finding the solution of the problem is far from trivial both for theoretical and



practical reasons. To know how good an approximation method is, error bounds must be determined. An engineering approach rather than a mathematical approach is adopted here; the error is considered to be sufficiently small when an approximation with smaller discretization interval did not result in an obvious change in the solution. Furthermore, the convergence of the method is proved in Section 3.2.3. The theoretical results will receive support from comparisons with experiments.

The treatment is complicated because many length- and time scales are involved. (e.g. low bubble departure frequency, high volume oscillation frequency ; large bulk region, thin boundary layers). Consequently, it is impossible to obtain one general numerical solution that covers the complete flow and temperature fields from bulk liquid to liquid microlayer.

Another difficulty in bubble dynamics stems from the fact that, at the gas-or vapour-liquid interface, the pressure is prescribed as a boundary condition. This is in contrast to the situation at a solid wall, where the velocity is prescribed instead. In order to solve for the flow field in the liquid, this pressure condition has to be transformed into a velocity condition by integration of the momentum equations. In general, such an integration is not possible beforehand.

There are, however, three important cases where this pressure problem does not arise, i.e. where the momentum equations can easily be integrated without knowing the solution of the velocity field beforehand. These cases are : (i) potential flow, (ii) boundary layer type flow, (iii) Stokes flow. Consequently, only these three kinds of flow have been considered in this thesis.

For reasons of computational efficiency the *global* orthogonal collocation method, cf. Finlayson (1973), has been chosen for the solution of the potential flow field in the bulk liquid. As has already been mentioned, the creeping flow field in the liquid microlayer has been treated by the *local* collocation method. Different methods have been used by Yeh (1967), Plesset and Chapman (1971), and Hermans (1973) for describing the behaviour of a bubble

in a potential flow field.

In the way described above, the hydrodynamical theory for finding the bubble shape results in a set of coupled, non-linear, ordinary differential equations which can easily be solved numerically with the aid of a computer.

Simultaneously with the hydrodynamic equations, the temperature or diffusion equation has to be solved. However, a full description of the temperature or concentration field is not required ; only knowledge of the temperature or concentration at the vapour-liquid interface is needed in order to determine the excess pressure in the bubble. For that reason, finding the temperature or concentration at the bubble boundary will supply the necessary condition for solving the hydrodynamic equations. From this point of view plausible simplifications will be introduced, resulting in one additional ordinary differential equation, coupled with the hydrodynamic equations mentioned before ; cf. Section 3.3. For the formulation of the diffusion problem use has been made of the formulation with fractional derivatives ; cf. Oldham and Spanier (1974).

CHAPTER 2

INTRODUCTION TO BUBBLE DYNAMICS :  
GROWTH AND DEPARTURE OF A SPHERICAL BUBBLE

2.1. Introduction to the basic equations

This Chapter provides an introduction to the physics of bubble growth and departure, and presents the main results based on the assumption that the bubble keeps its spherical shape.

The starting point of all calculations will be the equations of conservation of mass, momentum and energy, complemented by the diffusion equation and by expressions for the components of the stress tensor. Because of their frequent use in this thesis, the latter equations will be presented here in rotationally symmetric spherical coordinates for an incompressible liquid with constant viscosity  $\eta$ , constant thermal conductivity  $\lambda$ , constant specific heat  $c$ , and constant diffusion coefficient  $\kappa$  in case of diffusion of a dissolved gas. Furthermore, viscous dissipation will be neglected. Under these restrictions the equations are ; cf. e.g. Bird, Stewart and Lightfoot (1960), and cf. Fig. 2.1.

$$\nabla \cdot \underline{u} = \frac{1}{r^2} \frac{\partial}{\partial r} (r^2 u_r) + \frac{1}{r \sin \theta} \frac{\partial}{\partial \theta} (u_\theta \sin \theta) = 0, \text{ (continuity)} \quad (2.1.1)$$

$$\rho \left( \frac{\partial u_r}{\partial t} + u_r \frac{\partial u_r}{\partial r} + \frac{u_\theta}{r} \frac{\partial u_r}{\partial \theta} - \frac{u_\theta^2}{r} \right) = - \frac{\partial p}{\partial r} + \rho g_r + \eta \left( \nabla^2 u_r - \frac{2u_r}{r^2} - \frac{2}{r^2} \frac{\partial u_\theta}{\partial \theta} - \frac{2u_\theta \cot \theta}{r^2} \right), \text{ (r-momentum)} \quad (2.1.2)$$

$$\rho \left( \frac{\partial u_\theta}{\partial t} + u_r \frac{\partial u_\theta}{\partial r} + \frac{u_\theta}{r} \frac{\partial u_\theta}{\partial \theta} + \frac{u_r u_\theta}{r} \right) = - \frac{1}{r} \frac{\partial p}{\partial \theta} + \rho g_\theta + \eta \left( \nabla^2 u_\theta + \frac{2}{r^2} \frac{\partial u_r}{\partial \theta} - \frac{u_\theta}{r^2 \sin^2 \theta} \right), \text{ (\theta-momentum)} \quad (2.1.3)$$

$$\rho c \left( \frac{\partial T}{\partial t} + u_r \frac{\partial T}{\partial r} + \frac{u_\theta}{r} \frac{\partial T}{\partial \theta} \right) = \lambda \nabla^2 T, \text{ (energy)} \quad (2.1.4)$$

$$\frac{\partial C}{\partial t} + u_r \frac{\partial C}{\partial r} + \frac{u_\theta}{r} \frac{\partial C}{\partial \theta} = \kappa \nabla^2 C. \text{ (diffusion)} \quad (2.1.5)$$

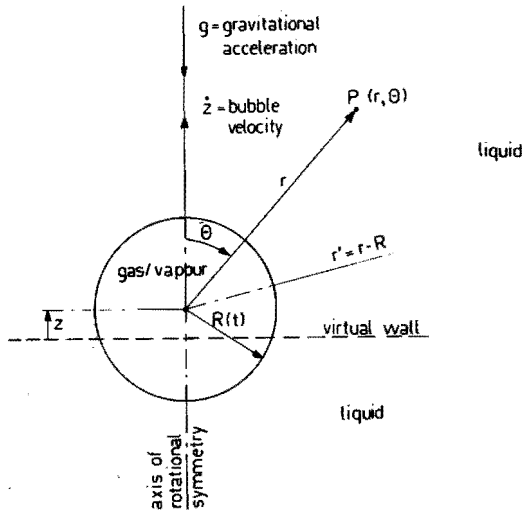


Fig. 2.1. Gas or vapour bubble in an infinitely extended liquid.  
 The plane  $z = 0$  represents a virtual wall which does not represent a boundary for the liquid; cf. also Section 2.3.2.

In equations (2.1.2, 3, 4, 5) the Laplace operator  $\nabla^2$  is given by :

$$\nabla^2 = \frac{1}{r^2} \frac{\partial}{\partial r} \left( r^2 \frac{\partial}{\partial r} \right) + \frac{1}{r^2 \sin \theta} \frac{\partial}{\partial \theta} \left( \sin \theta \frac{\partial}{\partial \theta} \right). \quad (2.1.6)$$

Since the gas or vapour phase is compressible, the basic conservation equations for that phase are more complex. However, the latter equations will hardly be used, and will only be mentioned at the appropriate places. For the same reasons, the components of the stress tensor will not be presented explicitly in this Section.

As will be clear from comparison of equation (2.1.4) with equation (2.1.5), heat transport and mass diffusion are described by similar equations.

This similarity has even been stressed by using  $\kappa$  for the mass diffusion coefficient in (2.1.5) instead of the usual symbol  $D$ . In the following, the thermal diffusivity will be defined in the usual way as  $\kappa = \lambda/\rho c$ . It will be clear from the context whether  $\kappa$  represents the heat or mass diffusion coefficient. In this way a unified treatment has been made possible.

As is well-known in the theory of fluid dynamics, it is often advantageous to introduce a stream function  $\psi$  in order to satisfy the continuity equation (2.1.1). This stream function is defined as follows :

$$u_r = - \frac{1}{r^2 \sin \theta} \frac{\partial \psi}{\partial \theta}, \quad (2.1.7)$$

$$u_\theta = \frac{1}{r \sin \theta} \frac{\partial \psi}{\partial r}. \quad (2.1.8)$$

In this way the continuity equation (2.1.1) has been replaced by equations (2.1.7, 8), and only the momentum equations (2.1.2, 3) remain.

By taking the  $\partial/\partial \theta$  of (2.1.2) and the  $\partial/\partial r$  of (2.1.3) the following equation, in which the pressure is eliminated, replaces the two equations (2.1.2, 3) :

$$\frac{\partial}{\partial t} (D^2 \psi) + \frac{\partial(\psi, \frac{D^2 \psi}{r^2 \sin^2 \theta})}{\partial(r, \theta)} \sin \theta = \nu D^4 \psi, \quad (2.1.9)$$

where

$$D^2 = \frac{\partial^2}{\partial r^2} + \frac{\sin \theta}{r^2} \frac{\partial}{\partial \theta} \left( \frac{1}{\sin \theta} \frac{\partial}{\partial \theta} \right), \quad (2.1.10)$$

and the Jacobian is defined by

$$\frac{\partial(\psi, \xi)}{\partial(r, \theta)} = \frac{\partial \psi}{\partial r} \frac{\partial \xi}{\partial \theta} - \frac{\partial \psi}{\partial \theta} \frac{\partial \xi}{\partial r}. \quad (2.1.11)$$

The vorticity  $\underline{\omega} = \text{rot } \underline{u}$  has only one component, normal to the cross-sectional plane under consideration :

$$\underline{\omega} = (0, 0, \omega) = \left( 0, 0, \frac{D^2 \psi}{r \sin \theta} \right). \quad (2.1.12)$$

Consequently, equation (2.1.9) describes the diffusion and convection of vorticity in the flow field.

Equation (2.1.9) shows that no vorticity is produced in the flow field, i.e.  $\omega = 0$  is a possible solution of (2.1.9). As can be inferred from the boundary conditions for (2.1.9), vorticity is produced at the boundaries of the flow field, and equation (2.1.9) describes the diffusion and convection of vorticity into the flow field. Sufficiently far away from the boundaries, or initially after start of motion, the flow field may be assumed to be vortex-free, hence  $D^2\psi = 0$ . The latter equation can be satisfied identically by the introduction of a velocity potential  $\phi$ . The velocity potential is defined in such a way that:

$$(u_r, u_\theta) = \nabla\phi \quad , \quad (2.1.13)$$

where

$$\nabla = \left( \frac{\partial}{\partial r} , \frac{1}{r} \frac{\partial}{\partial \theta} \right) \quad . \quad (2.1.14)$$

Substitution of (2.1.13) in the continuity equation (2.1.1) results in the Laplace or potential equation for the velocity potential :

$$\nabla^2\phi = 0 \quad . \quad (2.1.15)$$

In this case of so-called potential flow, the momentum equations can be integrated, resulting in an explicit expression for the pressure in the flow field. Substitution of (2.1.13) in (2.1.2, 3) results in the well-known Bernoulli equation :

$$p + \rho g r \cos\theta - p_\infty(t) = -\rho \left( \frac{\partial\phi}{\partial t} + \frac{1}{2} (\nabla\phi)^2 \right) + \eta \nabla^2\phi \quad . \quad (2.1.16)$$

In (2.1.16)  $p_\infty$  is a function of  $t$  only ; it represents the pressure far away from the bubbles under consideration. Substitution of (2.1.15) in (2.1.16) shows that viscous effects vanish in the formulation of incompressible potential flow. However, this does not mean that there are no viscous stresses present in the flow field.

In Chapters 2 and 3 of this thesis, the flow in the bulk liquid surrounding the bubbles has been described using potential flow

theory. The solution of the diffusion equations (2.1.4, 5) enters in the calculations since the boundary conditions for (2.1.15) depend on the concentration or temperature at the bubble boundary.

In Section 2.2 an introduction to the phenomenon of bubble growth will be presented, starting from the assumption of radially symmetric flow and temperature fields. The latter assumption is the starting point of many approaches presented in the literature. The case of radially symmetric flow and temperature fields has been considered because in this way the basic steps, also required in more complex calculations, can be shown in a relatively simple way. The treatment given in this Section also shows the assumptions on which various well-established theories are based. In this way, a unified treatment of these theories is presented.

In Section 2.3 and Appendix A, the assumption of a spherically symmetric flow field will be relaxed, and the combined process of growth and translation of spherical bubbles will be considered. In this way a preliminary discussion of various modes of bubble departure will be presented. The latter results will be applied in Section 2.4 for vapour bubbles in a non-homogeneous initial temperature field.

In Section 2.5 the assumption of spherical symmetry is used again when considering oscillations in the bubble volume, and the assumption of negligible vapour compressibility.

In Chapter 3 the assumption of a spherical bubble shape will be relaxed, and deviations from the spherical shape will be considered, assuming a rotationally symmetric potential flow field. It will be shown there, that an important mode of bubble departure is governed by concentration of the bubble foot, caused by gravitational acceleration.

Finally, it is noted that, in the thin liquid layer between bubble and wall, the potential flow approximation no longer holds. In that case, either boundary layer flow or Stokes flow will be assumed. The appropriate equations will be presented in Chapter 4 and Appendix C.

## 2.2. Bubble growth

### 2.2.1. The equations of radial motion

For a radially expanding bubble, growing in a superheated or supersaturated liquid, the behaviour of the gas or vapour phase will be considered first. In this thesis, only the case  $\rho_1 \ll \rho$ , i.e. the case where the gaseous phase has a density which is much smaller than the liquid density, will be considered. For gases surrounded by a liquid, e.g.  $H_2$ - or  $CO_2$ -bubbles in water, this condition is always satisfied. For boiling, it represents a restriction to situations sufficiently far away from the critical point.

Since  $\rho_1 \ll \rho$ , and since the gaseous phase is kept within a relatively small volume, disturbances in the pressure of the gaseous phase are damped away much more rapidly than in the liquid. Consequently, the pressure in the gaseous phase is assumed to be homogeneous, i.e.  $\partial p_1(r,t)/\partial r = 0$ .

Further, when the process of evaporation at the vapour-liquid interface is considered, it is assumed that the vapour is in thermodynamic equilibrium with the liquid. Consequently, when no other gases or vapours are present in the bubble, it follows from Clapeyron's law that the temperature is homogeneous along the bubble boundary.

For sufficiently small variations around the saturation temperature  $T_s(p_\infty)$ , belonging to the pressure  $p_\infty$ , the Clapeyron equation may be linearized, resulting in:

$$p_{1R}(t) = p_\infty + \frac{\rho_1 \ell}{T_s} \{T_{1R}(t) - T_s\}. \quad (2.2.1)$$

In (2.2.1)  $p_{1R}$  represents the vapour pressure at the bubble boundary  $r = R(t)$ ,  $p_\infty$  represents the pressure far away from the bubble where the saturation temperature is equal to  $T_s(p_\infty)$ , and  $T_{1R}$  represents the vapour temperature at the bubble wall. In (2.2.1) it is also assumed that the vapour density  $\rho_1$  and the latent heat of vaporization  $\ell$  vary so little that they may be considered as constant over the temperature and pressure ranges involved.



For a spherical vapour bubble, fed by evaporation at its boundary, Cho and Seban (1969) derived the following expression for the radial vapour velocity at the vapour-liquid interface  $r = R(t)$  :

$$u_{1r}(R(t), t) = \frac{1}{P_{\infty}} \left[ \frac{c_{1p} - c_{1v}}{c_{1p}} \lambda_1 \left( \frac{\partial T}{\partial r} \right)_{r=R(t)} - \frac{c_{1v} \rho_1 \ell R(t)}{3c_{1p} T_s} \dot{T}_{1R}(t) \right] \quad (2.2.2)$$

Here Cho and Seban's expression has been presented in a linearized form, combined with the linearized Clapeyron equation (2.2.1).

The first term between brackets in the right-hand side of (2.2.2) results from the influence of temperature on vapour density. The second term represents the effect of pressure on the compressible vapour.

Equation (2.2.2) must be coupled to the hydrodynamic and thermal equations of the liquid. In order to show the basic steps, a free bubble, far away from walls and under zero gravity conditions will be considered in this Section.

In that case, conservation of total (liquid and vapour) mass at the spherical interface  $r = R(t)$  results in ; cf. Hsieh (1965) :

$$\rho \left( \dot{R}(t) - u_{1r}(R(t), t) \right) = \rho_1 \left( \dot{R}(t) - u_{1r}(R(t), t) \right) \quad (2.2.3)$$

In the case under consideration, where compressibility effects in the vapour are negligible, the vapour velocity is so small that  $(\rho_1/\rho) u_{1r} \ll u_r$ . Since also  $\rho_1 \ll \rho$ , equation (2.2.3) becomes equivalent to the well-known *kinematic boundary condition* that holds at the interface of two immiscible fluids without phase transitions:

$$u_{1r}(R(t), t) = \dot{R}(t). \quad (2.2.4)$$

Equation (2.2.4) expresses that *in the hydrodynamics of the determination of  $R(t)$ , only the liquid motion needs to be considered.*

Combining (2.2.4) with the continuity equation for the liquid (2.1.1) results for spherical symmetry in :

$$u_r(r, t) = \left( \frac{R(t)}{r} \right)^2 \dot{R}(t). \quad (2.2.5)$$

In this case, the momentum equation for the liquid (2.1.2) in the  $r$ -direction can be integrated, resulting in an explicit expression for the pressure in the liquid:

$$p(r,t) = p_{\infty}(t) + \rho \left( \frac{R^2 \ddot{R} + 2R\dot{R}^2}{r} - \frac{R^4 \dot{R}^2}{2r^4} \right). \quad (2.2.6)$$

Application of equation (2.2.6) at  $r = R(t)$  results in the so-called Rayleigh equation:

$$R\ddot{R} + \frac{3}{2}\dot{R}^2 = \frac{p_R(t) - p_{\infty}}{\rho}. \quad (2.2.7)$$

For prescribed  $p_R(t)$ , equation (2.2.7), expressing the balance between inertia and pressure effects, constitutes the so-called *dynamic boundary condition*.

The normal stress at the vapour-liquid interface can be calculated using (2.2.5), resulting in:

$$\tau_{n_R}(t) = -p_R(t) + 2\eta \left( \frac{\partial u_r}{\partial r} \right)_{r=R} = -p_R(t) - 4\eta \frac{\dot{R}}{R}. \quad (2.2.8)$$

The Laplace-Kelvin equation for the discontinuity of normal stresses over the curved gas-liquid interface, substituted into a momentum balance at the gas-liquid interface, cf. Hsieh (1965), results in:

$$p_{l_R} = -\tau_{n_R} + \frac{2\sigma}{R}. \quad (2.2.9)$$

Combination of (2.2.7, 8, 9) results in the so-called extended Rayleigh equation, cf. Van Stralen (1968), or Rayleigh-Plesset equation, cf. Plesset and Prosperetti (1977):

$$R\ddot{R} + \frac{3}{2}\dot{R}^2 = \frac{p_{l_R}(t) - p_{\infty}}{\rho} - \frac{2\sigma}{R} - \frac{4\eta\dot{R}}{\rho R}. \quad (2.2.10)$$

When pure vapour bubbles are considered, the pressure term in (2.2.10) is given by the Clapeyron equation (2.2.1). It follows from (2.2.10) that, for a certain bubble radius  $R = R_e$ , a situation of (unstable) dynamic equilibrium exists. The superheating  $T_{R_e} - T_s$  of the vapour in this dynamic equilibrium situation is given by:

$$T_{R_e} - T_s(p_\infty) = \frac{2\sigma T_s(p_\infty)}{\rho_1 \ell R_e} . \quad (2.2.11)$$

A *thermal* boundary condition at the vapour-liquid interface  $r' = r - R(t) = 0$ , cf. Fig. 2.1, is given by the heat requirement for vaporization or condensation at the bubble boundary :

$$\lambda \left( \frac{\partial T}{\partial r'} \right)_{r'=0} - \lambda_1 \left( \frac{\partial T}{\partial r'} \right)_{r'=0} = \rho_1 \ell \left( \dot{R}(t) - u_{1r}(R(t), t) \right) . \quad (2.2.12)$$

In (2.2.12), terms accounting for compressibility of the vapour, mechanical work, and viscous dissipation have been neglected with respect to the term containing the enthalpy of vaporization  $\ell$ ; cf. Hsieh (1965).

Since  $\kappa_1 \gg \kappa$ , the temperature gradients in the vapour are smoothed out more rapidly than in the liquid. Since also  $\lambda_1 \ll \lambda$ , the term  $\lambda_1 (\partial T / \partial r')_{r'=0}$  may be neglected with respect to the term  $\lambda (\partial T / \partial r')_{r'=0}$  in the left-hand side of equation (2.2.12). Substitution of (2.2.2) in (2.2.12) then results in :

$$\lambda \left( \frac{\partial T}{\partial r'} \right)_{r'=0} = \rho_1 \ell \dot{R}(t) + \frac{c_{1v} \rho_1 \ell}{3c_{1p} T_s p_\infty} R(t) \dot{T}_{1R}(t) \quad (2.2.13)$$

A second thermal boundary condition is that the temperature of the liquid at the vapour-liquid interface  $T_R(t)$  equals the vapour temperature at the interface  $T_{1R}(t)$ , i.e.  $T_R(t) = T_{1R}(t)$ . From this latter condition, combined with equation (2.2.13), it is seen that, *for finding the temperature field in the liquid, the vapour phase needs no further consideration.*

When steady growth of vapour bubbles is considered with no implosions or oscillations, the temperature  $T_{1R} = T_R$  at the bubble boundary decreases so slowly that the second term in the right-hand side of (2.2.13) may be neglected, resulting in :

$$\lambda \left( \frac{\partial T}{\partial r'} \right)_{r'=0} = \rho_1 \ell \dot{R}(t) . \quad (2.2.14)$$

In Section 2.5, however, the full equation (2.2.13) will be considered in the context of bubble oscillations, where compressibility of the vapour may not be neglected.

The energy equation (2.1.4) for spherically symmetric flow and temperature fields in the liquid reads :

$$\frac{\partial T}{\partial t} + \left(\frac{R}{r}\right)^2 \dot{R} \frac{\partial T}{\partial r} = \kappa \left( \frac{\partial^2 T}{\partial r^2} + \frac{2}{r} \frac{\partial T}{\partial r} \right) . \quad (2.2.15)$$

The transformation  $r' = r - R$  results in :

$$\frac{\partial T}{\partial t} - \frac{r'(r' + 2R)}{(r' + R)^2} \dot{R} \frac{\partial T}{\partial r'} = \kappa \left[ \frac{\partial^2 T}{(\partial r')^2} + \frac{2}{r'+R} \frac{\partial T}{\partial r'} \right] \quad (2.2.16)$$

As a mathematical simplification, the non-linear term in the left-hand side of (2.2.16) will be neglected. This means that heat transport by radial convection is approximated by assuming that all liquid in the thermal boundary layer surrounding the bubble has radial velocity  $\dot{R}(t)$ , independent of  $r'$ . This can also be seen from equation (2.2.15). When taking  $r = R$  in the non-linear term, the remaining expression  $\partial T / \partial t + \dot{R}(\partial T / \partial r)$  equals the time derivative in a coordinate system moving with the velocity of the bubble boundary. Later on, in Section 2.2.2, this latter assumption will be relaxed.

If initially, at  $t = 0$ , the temperature in the liquid is homogeneous, i.e.  $T(r, 0) = T_\infty$ , the solution of the simplified equation (2.2.16) also satisfies the following equation; cf. Oldham (1973):

$$-\kappa^{\frac{1}{2}} {}_0 D_t^{-\frac{1}{2}} \frac{\partial T(r', t)}{\partial r'} = T(r', t) - T_\infty + \kappa^{\frac{1}{2}} {}_0 D_t^{-\frac{1}{2}} \frac{T(r', t) - T_\infty}{R(t) + r'} . \quad (2.2.17)$$

In (2.2.17),  ${}_0 D_t^{-\frac{1}{2}}$  represents the so-called Riemann-Liouville integral operator of order  $1/2$ . In general, the Riemann-Liouville integral of order  $-v > 0$  is defined by; cf. Ross (1975), and Appendix B:

$${}_c D_t^v f(t) = \frac{1}{\Gamma(-v)} \int_{t'=c}^t \frac{f(t')}{(t-t')^{1+v}} dt' , \quad v < 0 . \quad (2.2.18)$$

Substitution of (2.2.14) into (2.2.17) results in:

$$D_o^{-\frac{1}{2}} \dot{R}(t) = \kappa^{\frac{1}{2}} Ja \frac{T_\infty - T_R(t)}{T_\infty - T_s} + \kappa Ja D_o^{-\frac{1}{2}} \left[ \frac{T_\infty - T_R(t)}{T_\infty - T_s} \frac{1}{R(t)} \right], \quad (2.2.19)$$

where the dimensionless Jakob number is defined as:

$$Ja = \frac{\rho c (T_\infty - T_s)}{\rho_1 \ell}. \quad (2.2.20)$$

When pure gas bubbles are considered, equation (2.1.5) for the concentration field  $C(r,t)$  in a spherically symmetric situation has to be solved. In an analogous way, the equations equivalent to the set (2.2.19,20) can be derived; cf. also Epstein and Plesset (1950):

$$D_o^{-\frac{1}{2}} \dot{R}(t) = \kappa^{\frac{1}{2}} Ja \frac{C_\infty - C_R(t)}{C_\infty - C_s} + \kappa Ja D_o^{-\frac{1}{2}} \left[ \frac{C_\infty - C_R(t)}{C_\infty - C_s} \frac{1}{R(t)} \right]. \quad (2.2.21)$$

Here  $\kappa$  represents the diffusivity of the gas in the liquid, and the dimensionless Jakob number becomes:

$$Ja = \frac{C_\infty - C_s}{\rho_1}. \quad (2.2.22)$$

In this case, the equation equivalent to Clapeyron's law (2.2.1) is given by Henri's law:

$$P_{1R} = p_\infty + k(C_R - C_s). \quad (2.2.23)$$

### 2.2.2. Diffusion-controlled bubble growth

The diffusion equations (2.2.19) or (2.2.21) have to be solved simultaneously with the extended Rayleigh equation (2.2.10). However, as will be proved in Subsection a, in many practical situations inertia, viscous and surface tension effects are negligible and equations (2.2.1) and (2.2.23), combined with equation (2.2.10), simplify to  $T_R = T_s$  and  $C_R = C_s$  respectively. In that case, equations (2.2.19,20) simplify to:

$$D_o^{-\frac{1}{2}} \dot{R}(t) = \kappa^{\frac{1}{2}} Ja + \kappa Ja D_o^{-\frac{1}{2}} \frac{1}{R(t)}. \quad (2.2.24)$$

The solution of (2.2.24) can be determined with Euler's equation; cf. Oldham and Spanier (1974):

$${}_0 D_t^v t^q = \frac{\Gamma(q+1)}{\Gamma(q-v+1)} t^{q-v}, \quad q > -1. \quad (2.2.25)$$

From (2.2.25), it follows that the solution of (2.2.24), when  $R(0) = 0$  is prescribed as the initial condition, becomes:

$$R(t) = \frac{Ja}{\pi^{\frac{1}{2}}} \left( 1 + \left( 1 + \frac{2\pi}{Ja} \right)^{\frac{1}{2}} \right) (\kappa t)^{\frac{1}{2}}. \quad (2.2.26)$$

In the following two Subsections, the two limiting approximations  $Ja \ll 2\pi$  and  $Ja \gg 2\pi$  will first be discussed in connection with their most obvious physical interpretation.

*a).  $Ja \ll 2\pi$ . Gas bubbles*

When gas bubbles are considered, the approximation  $Ja \ll 2\pi$  usually applies. In that case, equation (2.2.26) simplifies to:

$$R(t) = (2Ja\kappa t)^{\frac{1}{2}}. \quad (2.2.27)$$

The thickness  $\delta$  of the diffusion boundary layer around the gas-liquid interface is of the order of  $(\kappa t)^{\frac{1}{2}}$ ; consequently, in this case  $\delta \gg R$ . Substitution of  $r' = \delta$  into the radial convection term of (2.2.16) shows that this term is negligible with respect to the last term between brackets in the right-hand side (the curvature term).

If  $R(0) \neq 0$ , then deviations from equation (2.2.27) may initially be expected; cf. Manley (1960). Equation (2.2.27) has also been verified experimentally by the latter author for air bubbles in water.

Substitution of (2.2.27) into (2.2.7,23) shows that, if the time of growth is sufficiently long, the assumption  $C_R = C_S$  holds indeed, as will be shown in the following example:

*Numerical example: hydrogen bubbles in water*

Substitution of expression (2.2.27) into the inertia, surface tension and viscous terms of the Rayleigh equation (2.2.10) results in:

$R\ddot{R} + \frac{3}{2} \dot{R}^2 + 2\sigma/\rho R + 4\eta\dot{R}/\rho R = \text{Jak}/4t + (\sigma/\rho)(2/\text{Jakt})^{\frac{1}{2}} + 2\eta/\rho t$ . At atmospheric pressure (100 kPa) and room temperature (293 K),  $\kappa = 3 \times 10^{-9} \text{ m}^2/\text{s}$ ,  $\nu = \eta/\rho = 1 \times 10^{-6} \text{ m}^2/\text{s}$  and  $C_s/\rho_1 = 1.5 \times 10^{-6}$ .

As an example, the case  $C_\infty = 11C_s$  will be considered, i.e.

$\text{Ja} = 1.5 \times 10^{-5}$ ; cf. equation (2.2.22). From the numerical values it follows that inertia effects are negligible with respect to viscous effects. Under the assumption that surface tension effects are negligible, it follows from Henri's equation (2.2.23) that the viscous term in the Rayleigh equation (2.2.10) may be neglected when  $2\nu/t \ll \kappa C_\infty/\rho$ . Since, at atmospheric pressure and room temperature,  $\kappa\rho_1/\rho = 6.7 \times 10^7 \text{ m}^2/\text{s}^2$ , the latter condition becomes:  $t \gg 2 \times 10^{-9} \text{ s}$ .

When surface tension is dominating over viscous effects, the following condition must hold for the validity of (2.2.27):  $\sigma(2/\text{Jakt})^{\frac{1}{2}} \ll \kappa C_\infty$ .

Since  $\sigma = 0.07 \text{ N/m}$  and  $\rho = 10^3 \text{ kg/m}^3$ , the latter condition becomes:  $t \gg 0.2 \text{ s}$ .

When the hydrogen bubble does not immediately depart from the wall after formation, cf. Section 2.3, the latter time is short with respect to the adherence time; cf. Section 4.3. Consequently, for gas bubbles adhering at a wall, only the diffusion controlled mode of growth has a practical meaning.

*b).  $\text{Ja} \gg 2\pi$ . Vapour bubbles*

When  $\text{Ja} \gg 2\pi$ , expression (2.2.26) results in an equation, also obtained by Bošnjacovič (1930):

$$R(t) = \frac{2}{\pi^{\frac{1}{2}}} \text{Ja}(\kappa t)^{\frac{1}{2}}. \quad (2.2.28)$$

The assumption  $\text{Ja} \gg 2\pi$  is a common one when vapour bubbles are considered.

In the latter case, it follows that the thermal boundary layer has a thickness  $\delta$  which is small compared to  $R$ . Substitution of  $r' = \delta$

into the radial convection term of equation (2.2.16) shows that the latter term has the same order of magnitude as the second order term  $\kappa \partial^2 T / (\partial r')^2$ . That is, the radial convection term must be taken into account.

Equation (2.2.28) has in fact been derived by assuming that the radial velocity of the liquid is equal to  $\dot{R}$  for every  $r$  in the flow field. The latter approach has been relaxed by Plesset and Zwick (1952), who derived a more accurate equation than (2.2.19), taking into account radial convection. However, their result is restricted to bubble growth with  $Ja \gg 1$  only; cf. also Prosperetti and Plesset (1978).

Plesset and Zwick's approximation has the following form:

$$\int_0^{\infty} D_{t^*}^{-\frac{1}{2}} (R^2 \frac{dR}{dt^*}) = \kappa^{\frac{1}{2}} Ja \frac{T_{\infty} - T_R(t^*)}{T_{\infty} - T_s} . \quad (2.2.29)$$

In (2.2.29) the variable  $t^*$  is related to  $t$  by:

$$t^*(t) = \int_0^t R^4(t') dt' . \quad (2.2.30)$$

Comparison of equations (2.2.29,30) with equation (2.2.19) shows that, in Plesset and Zwick's result, the curvature term is missing. Due to their improved description of radial convection, the left-hand side of (2.2.19) has been changed in the left-hand side of (2.2.29) where the 'time' variable  $t^*$  has been introduced.

Substitution of the trial solution  $R = \gamma' t^s$  into the left-hand side of (2.2.29) and use of (2.2.30) results in:

$$\int_0^{\infty} D_{t^*}^{-\frac{1}{2}} (R^2 \frac{dR}{dt^*}) = \frac{\Gamma(\frac{3s}{4s+1})}{\Gamma(\frac{3s}{4s+1} + \frac{1}{2})} \frac{s}{(4s+1) \frac{2s+1}{4s+1}} \gamma' t^{s-\frac{1}{2}} . \quad (2.2.31)$$

In (2.2.31) use has also been made of Euler's equation (2.2.25).

In the special case where  $s = \frac{1}{2}$ , equation (2.2.31) results in:



$$\int_0^D \frac{dR}{t^{3/2}} (R^2 \frac{dR}{dt^2}) = \frac{1}{2} \left(\frac{\pi}{3}\right)^{1/2} \gamma' \quad (2.2.32)$$

From (2.2.32) combined with (2.2.29) it follows that, when the vapour temperature  $T_{iR} = T_R$  is independent of  $t$ , and equal to the saturation temperature  $T_s$ , the growth constant  $\gamma'$  equals  $2(3/\pi)^{1/2} Ja \kappa^{1/2}$ , or equivalently; cf. also Plesset and Zwick (1954 b, 1955):

$$R(t) = 2 \left(\frac{3}{\pi}\right)^{1/2} Ja (\kappa t)^{1/2} \quad (2.2.33)$$

In the limit  $Ja \rightarrow \infty$ , both Birkhof, Margulies and Horning (1958) and, independently, Scriven (1959) presented an exact proof of (2.2.33) based on a similarity transform. However, their starting point was the assumption  $T_R(t) = T_s$  and, therefore, their method cannot be extended to situations where  $T_R(t)$  depends on time, as will be the case in the following Sections.

In view of the important contribution of radial convection, the frequently used expression 'diffusion-controlled mode of growth' is somewhat misleading in the case  $Ja \gg 2\pi$ .

Substitution of (2.2.33) into (2.2.1,10) shows that, for a sufficiently long time of growth, the condition  $T_R = T_s$  indeed applies. However, especially in water boiling at subatmospheric pressures and in boiling liquid metals, this condition is usually not reached during adherence at the wall. For these cases, surface tension and viscous effects may be neglected. However, inertia effects must be included; cf. Section 2.2.3.

*c). Intermediate values of Ja*

In view of solution (2.2.33), expression (2.2.26) can be modified to the following expression for intermediate values of the Jakob number:

$$R(t) = \gamma(\kappa t)^{1/2} = \left(\frac{3}{\pi}\right)^{1/2} Ja \left\{ 1 + \left(1 + \frac{2\pi}{3Ja}\right)^{1/2} \right\} (\kappa t)^{1/2} \quad (2.2.34)$$

Although this relation has no exact basis, it represents the correct values reasonably well, as has been shown in Table 2.1, where

Table 2.1. Comparison of equation (2.2.34) with Scriven's numerical result for the bubble growth constant  $\gamma$  when  $Ja \neq \infty$

Ja	$\gamma$	$\gamma_{\text{Scriven}}$	$\frac{\gamma - \gamma_{\text{Scriven}}}{\gamma_{\text{Scriven}}} \times 100$
$1.965 \times 10^{-4}$	$2.002 \times 10^{-2}$	$2.000 \times 10^{-2}$	0.1
$1.697 \times 10^{-2}$	$2.016 \times 10^{-1}$	$2.000 \times 10^{-1}$	0.8
$3.546 \times 10^{-2}$	$3.032 \times 10^{-1}$	$3.000 \times 10^{-1}$	1.1
$5.881 \times 10^{-2}$	$4.052 \times 10^{-1}$	$4.000 \times 10^{-1}$	1.3
$1.166 \times 10^{-1}$	$6.102 \times 10^{-1}$	$6.000 \times 10^{-1}$	1.7
$1.850 \times 10^{-1}$	$8.154 \times 10^{-1}$	$8.000 \times 10^{-1}$	1.9
$3.420 \times 10^{-1}$	1.226	1.200	2.2
$5.152 \times 10^{-1}$	1.637	1.600	2.3
$6.977 \times 10^{-1}$	2.046	2.000	2.3
1.175	3.064	3.000	2.1
1.668	4.078	4.000	2.0
2.671	6.096	6.000	1.6
3.683	8.106	8.000	1.3
5.719	1.212	1.200	1.0
7.760	1.613	1.600	0.8
9.803	$2.014 \times 10$	$2.000 \times 10$	0.7
$1.019 \times 10^2$	$2.002 \times 10^2$	$2.000 \times 10^2$	0.1
$8.182 \times 10^2$	$1.601 \times 10^3$	$1.600 \times 10^3$	0.04

comparison has been made to Scriven's (1959) numerical values of the bubble growth constant  $\gamma$  in the intermediate region as a function of the Jakob number  $Ja$ .

### 2.2.3. Bubble growth affected by liquid inertia

When inertia may not be neglected, the Plesset and Zwick equations (2.2.29,30) for  $T_{1R} = T_R$ , substituted into Clapeyron's equation (2.2.1), have to be solved simultaneously with the Rayleigh equation (2.2.10).

For the present purpose, Plesset and Zwick's formulation (2.2.29,30) of the heat transport process will be replaced by the following simpler equation:

$$\frac{1}{3^{\frac{1}{2}}} \circ D_t^{-\frac{1}{2}} \dot{R} = \kappa^{\frac{1}{2}} Ja \frac{T_{\infty} - T_R(t)}{T_{\infty} - T_s} . \quad (2.2.35)$$

Equation (2.2.35) is similar to expression (2.2.19) where the curvature term has been neglected. However, a correction term  $1/3^{\frac{1}{2}}$  has been introduced in the left-hand side of (2.2.19) to account for radial convection.

First, it will be shown that this correction represents a good approximation. Substitution of the trial solution  $R = \gamma' t^s$  into (2.2.35) results in:

$$\frac{1}{3^{\frac{1}{2}}} \circ D_t^{-\frac{1}{2}} \dot{R} = \frac{s}{3^{\frac{1}{2}}} \frac{\Gamma(s)}{\Gamma(s+\frac{1}{2})} \gamma' t^{s-\frac{1}{2}} . \quad (2.2.36)$$

When  $s = \frac{1}{2}$  is substituted into (2.2.36), the right-hand side of this equation becomes identical with the right-hand side of (2.2.32); i.e. in that case, (2.2.35) gives the same result as the more correct equations (2.2.29,30).

When  $s = 1$ , Plesset and Zwick's equations (2.2.29,30) result in:

$$\circ D_{t^*}^{-\frac{1}{2}} (R^2 \frac{dR}{dt^*}) = \frac{1}{5^{\frac{1}{2}}} \frac{\Gamma(\frac{3}{2})}{\Gamma(\frac{11}{10})} \gamma' t^{\frac{1}{2}} , \quad (2.2.37)$$

as can be deduced from (2.2.31).

In the latter case,  $s = 1$ , it follows from (2.2.36) that the left-hand side of approximation (2.2.35) equals:

$$\frac{1}{3^{\frac{1}{2}}} \circ D_t^{-\frac{1}{2}} \dot{R} = \frac{2}{(3\pi)^{\frac{1}{2}}} \gamma' t^{\frac{1}{2}} \quad (2.2.38)$$

From (2.2.37,38) it follows that for  $s = 1$ :

$$\frac{\frac{1}{3^{\frac{1}{2}}} {}_0D_t^{-\frac{1}{2}} \dot{R}}{{}_0D_{t^*}^{-\frac{1}{2}} (R^2 \frac{dR}{dt^*})} = 0.931 \quad (2.2.39)$$

Consequently, also for  $s = 1$ , (2.2.35) represents an acceptable approximation of the more correct equations (2.2.29,30).

As will be shown in the following part of this Section, inclusion of inertia effects will result in a gradual transition from growth with  $s = 1$  for small  $t$ , to growth with  $s = \frac{1}{2}$  for large times. In that case, equation (2.2.35) may be used during this transition as a reasonable approximation upon which the subsequent calculation can conveniently be based.

Since the surface tension and viscous stress terms in (2.2.10) are negligible with respect to inertia terms, substitution of (2.2.35) in (2.2.10) results in:

$$R\ddot{R} + \frac{3}{2}\dot{R}^2 + \frac{3}{2}\gamma_0^2 \left( \frac{{}_0D_t^{-\frac{1}{2}} \dot{R}}{(3\kappa)^{\frac{1}{2}} Ja} - 1 \right) = 0, \quad (2.2.40)$$

where

$$\gamma_0 = \left\{ \frac{2\rho_1 l (T_\infty - T_s)}{3\rho T_s} \right\}^{\frac{1}{2}}. \quad (2.2.41)$$

Initially, shortly after start of bubble growth,  $|{}_0D_t^{-\frac{1}{2}} \dot{R}| \ll \kappa^{\frac{1}{2}} Ja$  and, in that case, integration of (2.2.40) results in:

$$\dot{R}(t) = \left[ \left\{ \frac{R_0}{R(t)} \right\}^3 \dot{R}_0^2 + \gamma_0^2 \frac{R^3(t) - R_0^3}{R^3(t)} \right]^{\frac{1}{2}}. \quad (2.2.42)$$

After an initial stage of growth where, during a relatively short time,  $\dot{R} > 0$ ,  $R$  has grown to a value much larger than  $R_0$  and the solution of (2.2.42) is given by:

$$R(t) = \gamma_0 t. \quad (2.2.43)$$

Initially,  $R$  is so small that  $|RR'| \ll \dot{R}^2$ . In the limit for large time the term  $RR'$  is also unimportant, as has been shown in Section 2.2.2. As an approximation, this term will be neglected for all  $t$ . Furthermore, it is assumed that  $\dot{R}^2$  can be linearized to  $\gamma_0 \dot{R}$ . This approximation is motivated by the fact that initially  $\dot{R} = \gamma_0$  and, for advanced growth, the term  $\dot{R}^2$  does not play a part. Under these approximations, equation (2.2.40) simplifies to:

$$\dot{R}\left(\frac{t}{\tau}\right) + D_0^{-\frac{1}{2}} \frac{d}{d(t/\tau)} \dot{R}\left(\frac{t}{\tau}\right) - \gamma_0 = 0. \quad (2.2.44)$$

In (2.2.44) the characteristic time  $\tau$  is defined by:

$$\tau = 3 \left(\frac{Ja}{\gamma_0}\right)^2 \kappa. \quad (2.2.45)$$

The solution of (2.2.44) equals; cf. Oldham and Spanier (1974), and Appendix B:

$$\dot{R}(t) = \gamma_0 \exp\left(\frac{t}{\tau}\right) \operatorname{erfc}\left\{\left(\frac{t}{\tau}\right)^{\frac{1}{2}}\right\}. \quad (2.2.46)$$

Differentiation of (2.2.46) gives:

$$\ddot{R}(t) = \frac{\gamma_0}{\tau} \exp\left(\frac{t}{\tau}\right) \operatorname{erfc}\left\{\left(\frac{t}{\tau}\right)^{\frac{1}{2}}\right\} - \frac{\gamma_0}{(\pi\tau t)^{\frac{1}{2}}}. \quad (2.2.47)$$

Integration of (2.2.46) results in:

$$\frac{R(t)}{3^{\frac{1}{2}} Ja(\kappa\tau)^{\frac{1}{2}}} = \exp\left(\frac{t}{\tau}\right) \operatorname{erfc}\left\{\left(\frac{t}{\tau}\right)^{\frac{1}{2}}\right\} - 1 + \frac{2}{\pi^{\frac{1}{2}}} \left(\frac{t}{\tau}\right)^{\frac{1}{2}}. \quad (2.2.48)$$

From (2.2.46,47,48), it follows that, for  $t \rightarrow 0$ ,  $R \rightarrow 0$ ,  $\dot{R} \rightarrow \gamma_0$ ,  $\ddot{R} \rightarrow -\infty$  and  $RR' \rightarrow 0$ , which is in agreement with the previous assumptions. For  $t \gg \tau$  the diffusion controlled mode (2.2.33) is reached asymptotically.

In the previous discussion, a unified treatment of the coupled hydrodynamic and thermal processes occurring during bubble growth has been presented, resulting in equation (2.2.48) for the bubble radius as a function of time. However, in the literature both the expressions of Cooper and Vijuk (1970) and of Mikic, Rohsenow and Griffith (1970) are in frequent use.

The equation of Cooper and Vijuk is an ad hoc interpolation between equations (2.2.43) and (2.2.33) which hold for  $t/\tau \ll 1$  and  $t/\tau \gg 1$  respectively. Their expression reads:

$$\frac{R(t)}{3^{\frac{1}{2}} Ja(\kappa\tau)^{\frac{1}{2}}} = \frac{1}{\frac{1}{\frac{2}{\pi^{\frac{1}{2}}}\left(\frac{t}{\tau}\right)^{\frac{1}{2}}} + \frac{1}{\frac{t}{\tau}}} . \quad (2.2.49)$$

Also on the basis of an interpolation, Mikic, Rohsenow and Griffith solve the following equation instead of equation (2.2.44):

$$\frac{\dot{R}^2}{\gamma_0} + \left(\frac{\pi t}{\tau}\right)^{\frac{1}{2}} \dot{R} - \gamma_0 = 0. \quad (2.2.50)$$

In (2.2.50), the linearization of (2.2.40) with  $\dot{R}^2 = \gamma_0 \dot{R}$  has not been introduced. Instead, the semi-integral operator  ${}_0 D_t^{-\frac{1}{2}}$  has been replaced by  $(\pi t/\tau)^{\frac{1}{2}}$ . The latter approximation is only valid for asymptotic growth, i.e. for  $t/\tau \gg 1$ ; initially, when  $\dot{R} = \gamma_0$ , this approximation results in a value for the heat flux to the bubble which is  $\pi/2$  times larger. The expression for transitional growth, following from (2.2.50) is:

$$\frac{R(t)}{3^{\frac{1}{2}} Ja(\kappa\tau)^{\frac{1}{2}}} = \frac{\pi^{\frac{1}{2}}}{3} \left[ \left(\frac{t}{\tau} + \frac{4}{\pi}\right)^{\frac{3}{2}} - \left(\frac{t}{\tau}\right)^{\frac{3}{2}} - \left(\frac{4}{\pi}\right)^{\frac{3}{2}} \right]. \quad (2.2.51)$$

Fig. 2.2. compares the results of (2.2.48,49,51). It is observed that the differences are marginal.

For growing sodium vapour bubbles, Dalle Donne and Ferranti (1975) numerically solved the Rayleigh equation (2.2.10), coupled with the

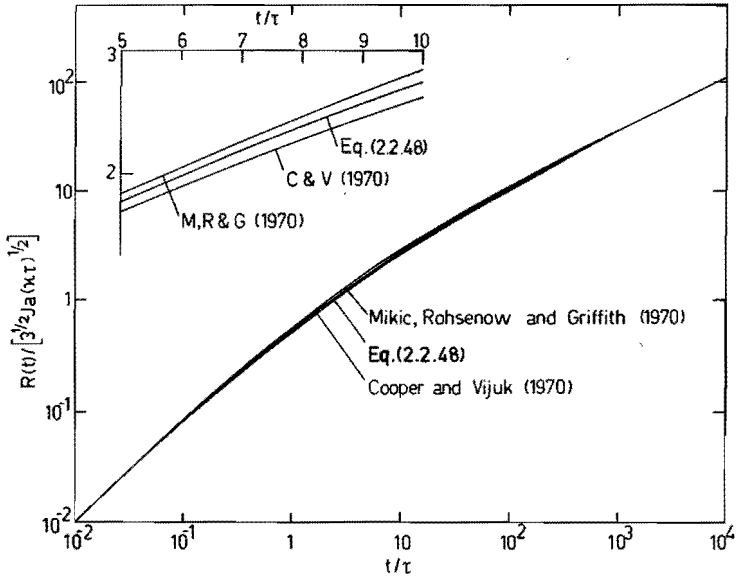


Fig.2.2. Comparison of the radius vs. time relationships represented by equations (2.2.48,49,51)

heat diffusion equation (2.2.15) and boundary condition (2.2.14). In this way, these authors did not make use of the thin boundary layer assumption upon which the Plesset and Zwick equation (2.2.29) is based.

Similarly, Prosperetti and Plesset (1978) solved the Rayleigh equation (2.2.10), coupled with the Plesset and Zwick equation (2.2.29) for the same sodium bubbles as considered by Dalle Donne and Ferranti. It is noted that both authors accounted for variations in  $\rho_1$  as a function of  $T_R$ , and they used the equilibrium pressure-temperature relationship instead of the linearized Clapeyron equation (2.2.1). For  $Ja \geq 10$  the agreement between the two approaches was good and, consequently, it was proved in this way that the Plesset and Zwick approximation (2.2.29) may be used when vapour bubble growth is considered.

Theofanous and Patel (1976) replaced the linearized Clapeyron equation (2.2.1) by  $p_1(T_R) = p_\infty + \{[p_1(T_\infty) - p_\infty]/(T_\infty - T_s)\}(T_R - T_s)$ . This turns out to be an improvement, especially when relatively high superheats are considered, as is often the case for boiling liquid metals.

Prosperetti and Plesset also compared Mikic, Rohsenow and Griffith's expression (2.2.51) (where Theofanus and Platel's suggestion was included) to their own results. The agreement was good; in the transitional stage, Mikic, Rohsenow and Griffith's equation results in a value which is only a few percents too low. As a matter of course, equations (2.2.48, 49, 51) do not represent the, usually unimportant, short time of growth after nucleation, where bubble growth is dominated by surface tension.

### 2.3. Bubble departure

#### 2.3.1. Initial acceleration of a free bubble

First, a free bubble, i.e. a bubble far away from walls, will be considered. However, in contrast to the situation described in Section 2.2, the bubble is growing in a gravitational field with a force per unit mass  $g$ .

Initially, after start of acceleration caused by the buoyancy force, the hydrodynamic boundary layer around the bubble and the thin viscous wake behind the bubble do not yet affect the rise velocity and, consequently, potential flow theory may be applied.

In Appendix A, the following coupled equations are derived on the basis of a cylindrically symmetric potential flow field around a growing, and translating, spherical bubble:

$$R\ddot{R} + \frac{3}{2} \dot{R}^2 = \frac{P_{1R} - P_{\infty}}{\rho} - \frac{2\sigma_0}{\rho R} + \left(\frac{\dot{z}}{4}\right)^2, \quad (2.3.1)$$

$$\frac{d}{dt} \left( \frac{2}{3} \pi \rho R^3 \dot{z} \right) = \frac{4}{3} \pi \rho R^3 g - \frac{8}{3} \pi \sigma' R. \quad (2.3.2)$$

In (2.3.1,2),  $z$  is the coordinate parallel to the axis of rotational symmetry, and  $\dot{z}$  is the upward translation velocity of the bubble centre; cf. Fig. 2.1. In (2.3.1,2), viscous effects have been neglected.



Equation (2.3.1) is the extended Rayleigh equation (2.2.10), modified by the addition of a term  $(\dot{z}/4)^2$ . However, in the following discussion, this term may be neglected with respect to other terms.

When a bubble translates, heat or mass transfer to the bubble wall by convection will become important with respect to diffusion, cf. e.g. Yao and Schrock (1976); however, also this effect is assumed to be so small that it may be neglected. Consequently, the solutions for bubble growth presented in Section 2.2, also apply during the initial stage of bubble acceleration.

Equation (2.3.2) expresses that the so-called impulse of the bubble is equal to the relative velocity between bubble and liquid multiplied by the so-called virtual mass of the bubble. The virtual mass is given by half the mass of the displaced liquid. Equation (2.3.2) will be referred to as the Green equation; cf. Lamb (1974).

In (2.3.1,2), the surface tension  $\sigma$  is written as  $\sigma = \sigma_0 + \sigma' \cos \theta$ , which expresses a possible change of surface tension along the bubble wall. The effect of this gradient is discussed in Section 2.3.3.

When surface tension gradients may be neglected, and when  $R(t) \propto t^{\frac{1}{2}}$ , cf. equation (2.2.34), the initial acceleration  $\ddot{z}$  follows from (2.3.2), and is given by:

$$\ddot{z} = \frac{4}{5} g. \quad (2.3.3)$$

Similarly, when  $R(t) \propto t$ , cf. equation (2.2.43), the initial acceleration of the bubble centre is given by:

$$\ddot{z} = \frac{1}{2} g. \quad (2.3.4)$$

### *2.3.2. Acceleration controlled bubble departure*

Up till now, only free bubbles, far away from walls, have been considered. However, in reality, the bubble originates, via a nucleation process, in a tiny cavity at the wall. This bubble starts growing, and between the solid wall and the bubble, a liquid layer remains, which is very thin when bubble growth is sufficiently rapid;

cf. Fig. 1.2. In Section 4.1, the formation of this so-called liquid microlayer will be considered in detail.

Due to the presence of this layer, it is as if the bubble starts growing as a hemisphere with its base moving smoothly over the solid wall, and because the microlayer evaporates, the growth rate, given by expression (2.2.34), predicts too low a value; a correction for this effect will be accounted for in Section 2.4.1.

In the following discussion, a model for bubble departure will be given, based on a more detailed description that is presented in Chapter 3.

The gravitational acceleration causes the bubble to depart from the wall. When it is assumed that expression (2.3.2) for a free bubble also holds approximately at a solid wall, it is found for the displacement of the centre of the bubble that, in the diffusion-controlled mode of growth; cf. also Fig. 2.1:

$$z = \frac{2}{5} g t^2. \quad (2.3.5)$$

After a certain time, the bubble has only one point of contact with the wall, i.e.  $z = R$ . When it is assumed that, at that instance, the bubble breaks away from the wall, then the following expressions are found for the adherence time and departure radius:

$$t_{\text{dep}} = \left(\frac{5\gamma}{2g}\right)^{\frac{2}{3}} \kappa^{\frac{1}{3}}, \quad (2.3.6)$$

and

$$R_{\text{dep}} = \left(\frac{5\gamma^4 \kappa^2}{2g}\right)^{\frac{1}{3}}, \quad (2.3.7)$$

where  $\gamma$  is the bubble growth constant, defined by  $R(t) = \gamma(\kappa t)^{\frac{1}{2}}$ .

During the process of acceleration, the bubble contact radius

$R_c = (R^2 - z^2)^{\frac{1}{2}}$  is given by:

$$R_c(t) = \left(\gamma^2 \kappa t - \frac{4g^2}{25} t^4\right)^{\frac{1}{2}}, \quad t < t_{\text{dep}}. \quad (2.3.8)$$

The growth rate of the bubble base,  $\dot{R}_c$ , is positive for  $t < t_{\text{dep}}/2^{2/3}$ , and contraction of the bubble base takes place for  $t > t_{\text{dep}}/2^{2/3}$ , as can be observed from the following expression:

$$\dot{R}_c(t) = \frac{\frac{1}{2}\gamma^2\kappa - \frac{8}{25}g^2t^3}{R_c(t)}. \quad (2.3.9)$$

Finally it is noted that  $\dot{R}_c$  is always negative. This turns out to be of great importance for the determination of the thickness of formation of the liquid microlayer; cf. Section 4.1. The expression for  $\dot{R}_c$  is given by:

$$\dot{R}_c(t) = \frac{-\frac{1}{4}\gamma^4\kappa^2 - \frac{16}{25}g^2\gamma^2\kappa t^3 + \frac{32}{625}g^4t^6}{R_c^3(t)}. \quad (2.3.10)$$

Experimentally, Cooper, Judd and Pike (1978) found expressions similar to (2.3.6,7), however, with the factor 5/2 replaced by 4 in (2.3.6), and with the factor 5/2 replaced by 13.5 in (2.3.7). Since these two factors have not the same value, it is concluded that deviations from the growth law  $R \propto t^{1/2}$  occurred in their experiment. This may be due to the fact that, in reality, the bubble does not grow in a uniformly superheated liquid; cf. also Section 2.4.2.

When the bubble growth rate is given by  $R(t) = \gamma_0 t$ , cf. equation (2.2.43), the following expressions are obtained in a similar way as discussed before:

$$z = \frac{1}{4}gt^2, \quad (2.3.11)$$

$$t_{\text{dep}} = \frac{4\gamma_0}{g}, \quad (2.3.12)$$

$$R_{\text{dep}} = \frac{4\gamma_0^2}{g}, \quad (2.3.13)$$

$$R_c(t) = \left(\gamma_0^2 t^2 - \frac{g^2 t^4}{16}\right)^{1/2}, \quad t < t_{\text{dep}}, \quad (2.3.14)$$

$$\dot{R}_c(t) = \frac{\gamma_0^2 t - g^2 t^3/8}{R_c(t)}, \quad (2.3.15)$$

$$\dot{R}_c(t) = \frac{-5\gamma_0^2 g^2 t^4 / 16 + g^4 t^6 / 128}{R_c^3(t)}. \quad (2.3.16)$$

From equation (2.3.15), it is observed that the bubble contact radius grows when  $t < t_{\text{dep}}/2^{1/2}$ , and contraction of the bubble foot takes place when  $t > t_{\text{dep}}/2^{1/2}$ . From equation (2.3.16) it is observed that also in the inertia-controlled mode of growth,  $\dot{R}_c < 0$ .

Finally, it is noted that equations (2.3.12,13) have been verified experimentally by Sabbotin, Sorokin, Orechkin and Rudryavtsev (1972) for boiling liquid potassium. In this case, the relationship  $R \propto t$  was verified as well.

### 2.3.3. *The validity of acceleration controlled departure and other modes of bubble departure*

In the previous Section, a model of departure caused by bubble acceleration was proposed. This model is based on a more detailed study, presented in Chapter 3, where it is shown that gravitational acceleration causes a deceleration of the growth rate of the bubble contact radius  $R_c$ . Both in Section 2.3.2 and in Chapter 3, it is assumed that departure takes place when  $R_c$  has become zero.

However, in reality, a small contact area with radius  $R_d$  can remain, where  $R_d$  is the so-called dry area radius; cf. Fig. 1.2. At this contact perimeter, a downward-directed force, with a maximum value equal to the surface tension force of adhesion is present. This surface tension force equals  $F_\sigma = 2\pi\sigma R_d \sin\theta_0$ ; cf. e.g. Kabanov and Frumkin (1933). Consequently, the upward buoyancy force,  $F_g = (4/3)\pi\rho g R^3$ , must be larger than the maximum downward force  $F_\sigma$  to cause bubble departure.

When the bubble is growing at a sufficiently high rate, an inertia force, resisting departure, must also be included in the force balance, as will be shown in the following discussion.

In Appendix A, expressions are presented for the equations of motion of a spherical bubble, a distance  $z$  away from a solid wall. The derivation of these equations is only valid when  $z \gg R$ ; however, in this Section, these expressions will be used as an approximation to show the behaviour of a spherical bubble attached to the wall at a relatively small contact area. In that case,  $z = R$ , and, with neglect of viscous effects and of surface tension gradients, the following expression is obtained from (A 19):

$$\frac{d}{dt} \left( \frac{1}{6} \pi \rho R^3 \dot{R} \right) = \frac{4}{3} \pi \rho R^3 g - F_d. \quad (2.3.17)$$

In (2.3.17), the downward force,  $F_d$ , exerted by the wall on the bubble, has been subtracted from the upward buoyancy force. When the left-hand side of (2.3.17) is positive, as is usually the case during adherence, the latter term represents a downward force of inertia  $F_i$ ; cf. Fig. 2.3.

When diffusion-controlled growth is considered, where  $R(t) = \gamma(\kappa t)^{\frac{1}{2}}$ , the inertia force becomes  $F_i = \pi \rho \gamma^4 \kappa^2 / 12$ . For this latter case, the downward inertia force has been calculated exactly by Witze, Schrock and Chambré (1968). The latter authors found a three times larger force than is obtained from approximation (2.3.17).

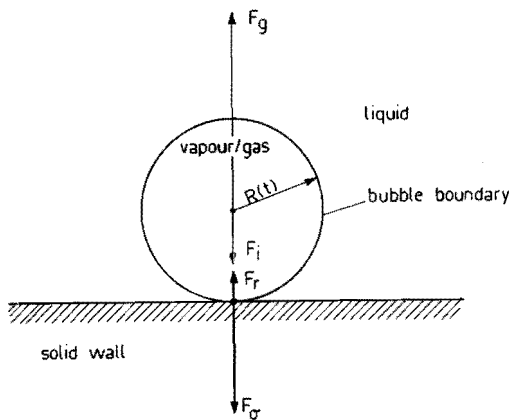


Fig.2.3. Force balance of a spherical bubble with one point of contact at a horizontal wall

Consequently, the bubble adheres at the wall as long as the following inequality is satisfied:

$$F_g = F_i + F_d < F_i + F_\sigma, \quad (2.3.18)$$

and in the mode of diffusion-controlled growth, the latter condition results in:

$$\rho \gamma^4 \kappa^2 < \frac{24}{37} \sigma R_d \sin \theta_o, \quad (2.3.19)$$

where use has been made of expression (2.3.7) to calculate  $F_g$ .

For rapidly-growing steam bubbles, at atmospheric and subatmospheric pressures, condition (2.3.19) is usually satisfied, and consequently, the adherence time and departure radius may be described by equations (2.3.4,5); cf. also Section 2.4.2.

On the other hand, for slowly-growing gas bubbles, the inequality (2.3.19) is usually not satisfied, and the bubble adheres until the following condition holds:

$$F_g = F_i + F_\sigma. \quad (2.3.20)$$

Since  $F_\sigma$  depends on the growing dry area radius, the departure of gas bubbles is governed by the growth of the dry area radius which, in this case, equals the bubble contact radius; cf. Fig. 1.1. The growth of the bubble contact area has been considered in Section 4.3, where equations for the prediction of the break-off radius are also discussed.

A third possible mode of departure exists, due to the occurrence of surface tension gradients along the bubble boundary.

From equation (2.3.2) it is observed that a surface tension gradient along the bubble boundary causes bubble acceleration in a direction

opposite to the direction of that gradient. Consequently, for departure assisted by a gradient in surface tension, the surface tension gradient must be negative in the z-direction and, since surface tension increases with decreasing temperature, there must be a positive temperature gradient in the z-direction along the bubble wall.

Such a gradient does not exist in usual boiling situations, where the temperature gradient outside the thermal boundary layer around the bubble is usually negative, and where hardly any temperature gradient exists along the bubble boundary; cf. Kenning and Toral (1977). Consequently, departure is not assisted by that force.

However, in boiling of binary mixtures, a positive gradient in concentration of the solute can exist, and since surface tension depends considerably on concentration, surface tension gradients possibly play a part in these systems. However, in this thesis, only one-component systems will be considered.

When hydrogen is formed electrolytically, a continuous jet of tiny  $H_2$ -bubbles is usually observed; cf. e.g. Trividi and Funk (1970). Also, during nucleate boiling at relatively high heat fluxes, the latter phenomenon can be observed. The buoyancy force at this stage is still quite small, and it does not significantly affect bubble dynamics. The mechanism by which this mode of departure is caused has not yet been clarified exactly. Han and Griffith (1965) suggest that the inertia force tends to lift the bubble off the surface if growth of the bubble decelerates rapidly enough. From equation (2.3.17), it is observed that, when  $R(t) \propto t^s$ , where  $s < 1/4$ , the inertia force is negative indeed, and  $F_i \rightarrow -\infty$  when  $t \rightarrow 0$ .

Finally, it is remarked that in the literature, the departure of rapidly-growing vapour bubbles is treated as a balance of forces, rather than by an acceleration process, as is proposed here; cf. e.g. Witze, Schrock and Chambré (1968), and Kiper (1971).

When the force balance (2.3.20) is applied, the surface tension force of adhesion may be neglected when sufficiently high bubble growth rates are considered. For diffusion-controlled growth, this force balance then results in:

$$R_{\text{dep}} = \left( \frac{3\gamma^4 \kappa^2}{16g} \right)^{\frac{1}{3}}. \quad (2.3.21)$$

Comparison of (2.3.21) with (2.3.7), shows that both the acceleration model and the force balance model yield a similar result, except for a difference in the numerical factors. However, as is clear from equations (2.3.8,9,10), the acceleration model also describes the contraction of the bubble foot during adherence.

## 2.4. Vapour bubbles at a wall

### 2.4.1. Enhancement of growth rate by microlayer evaporation

A detailed description of the hydrodynamic processes that occur in the liquid microlayer will be found in Chapter 4. However, as a preliminary to these more-detailed discussions, this Section provides a semi-quantitative treatment of the heat transfer process in the microlayer, and the treatment is extended for more realistic situations in Chapter 3.

For ease-of-presentation, consideration of bubble growth in this Section is restricted to diffusion-controlled growth only, and is further restricted to situations where the time of growth is short compared with departure time. Under these conditions, the bubble is hemispherical, and  $R(t) = R_c(t) = \gamma(\kappa t)^{\frac{1}{2}}$ ; cf. equation (2.3.8).

According to equation (2.2.34), the volume of vapour that has entered into the bubble because of evaporation of liquid at the vapour-liquid interface of the bubble cap is given by:

$$V_R = \frac{2}{3} \pi \left[ \left( \frac{3}{\pi} \right)^{\frac{1}{2}} \text{Ja} \left\{ 1 + \left( 1 + \frac{2\pi}{3\text{Ja}} \right)^{\frac{1}{2}} \right\} \right]^3 (\kappa t)^{\frac{1}{2}}. \quad (2.4.1)$$

The total volume of vapour that has entered into the bubble by evaporation of liquid, both at the bubble cap and at the vapour-liquid interface in the microlayer, is given by:



$$V = \frac{2}{3} \pi \gamma^3 (\kappa t)^{\frac{3}{2}}. \quad (2.4.2)$$

In the following treatment, the volume of vapour that has entered into the bubble by evaporation of liquid at the vapour-liquid interface in the microlayer, will be considered first.

At the location  $r = R_c$ , where the leading edge of the colder vapour moves over the hotter liquid at the wall, cf. Fig. 1.2, the heat flux is very high. This flux decreases with decreasing  $r$ . Moreover, the surface of the liquid microlayer in the region  $R_c - \Delta r \leq r \leq R_c$  is larger than a surface in a region  $R' - \Delta r \leq r \leq R'$  with  $R' < R_c$ . Consequently, most of the vapour that enters the bubble by evaporation of the liquid microlayer comes from the outer part of this layer. Since the thermal penetration thickness at that location is smaller than the microlayer thickness, the microlayer may be assumed as half infinite; cf. also Van Ouwkerk (1970, 1971).

Since there is negligible convection in the microlayer and heat fluxes in the radial direction are negligible with respect to the flux to the wall, the one-dimensional heat diffusion equation may be used. In a similar way as for equation (2.2.17), this equation can be written as:

$$\kappa^{\frac{1}{2}} \frac{1}{t_r} D^{-\frac{1}{2}} \frac{\partial T}{\partial z} = T(r, z, t) - T_{\infty}, \quad (2.4.3)$$

where  $t_r$  is determined by the implicit relationship

$$R_c(t_r) = r. \quad (2.4.4)$$

In the same way as in expression (2.2.12), the heat requirement for vaporization at the vapour-liquid interface in the microlayer is given by:

$$q_M(r, t) = -\lambda \left( \frac{\partial T}{\partial z} \right)_{z=h} = -\rho_1 \ell \left\{ \frac{\partial h(r, t)}{\partial t} - u_1(r, h, t) \right\}, \quad (2.4.5)$$

where  $h$  is the thickness of the microlayer and  $u_1(r, h, t)$  is the velocity of the vapour entering the bubble at  $z = h$ .

Since the thin liquid microlayer rests on the impermeable solid wall, the vapour-liquid interface of the microlayer cannot be 'blown away' as the bubble cap. Consequently,  $|\partial h/\partial t| \ll |u_1(r, h, t)|$ . Under this approximation, substitution of (2.4.5) in (2.4.3) results in:

$$-t_r D_r^{-\frac{1}{2}} u_1(r, h, t) = \kappa^{\frac{1}{2}} Ja \frac{T_M(t) - T_\infty}{T_\infty - T_s} \quad (2.4.6)$$

But  $T_M = T_s$  in the asymptotic diffusion-controlled mode of growth, and (2.4.6) results in:

$$\frac{q_M}{\rho_1 \ell} = u_1(r, h, t) = \frac{\kappa^{\frac{1}{2}} Ja}{\{\pi(t-t_r)\}^{\frac{1}{2}}}, \text{ for } t > t_r. \quad (2.4.7)$$

The total volumetric flow of vapour from the evaporating microlayer into the bubble can be found by integration of  $u_1(r, h, t)$  over the total wetted surface under the bubble. When the effect of a possible dry area is neglected this results in:

$$\dot{V}_M = 2\pi \int_{r'=0}^{R_c(t)} u_1(r', h, t) r' dr' = 2\pi \int_{t_r=0}^t u_1(t_r, h, t) R_c(t_r) \dot{R}_c(t_r) dt_r. \quad (2.4.8)$$

For small adherence times, where  $R_c(t) = \gamma(\kappa t)^{\frac{1}{2}}$ , equation (2.4.8) can easily be integrated, resulting in:

$$\dot{V}_M = 2\pi^{\frac{1}{2}} \gamma^2 Ja \kappa^{\frac{3}{2}} t^{\frac{1}{2}}, \quad (2.4.9)$$

or, after integration with respect to time:

$$V_M = \frac{4}{3} \pi^{\frac{1}{2}} \gamma^2 Ja (\kappa t)^{\frac{3}{2}}. \quad (2.4.10)$$

Since the saturated vapour may be considered as incompressible for the relatively slow process of bubble growth, the requirement of conservation of vapour mass results in:

$$V = V_R + V_M. \quad (2.4.11)$$

Substitution of expressions (2.4.1,2,10) in (2.4.11) results in a simple expression for  $\gamma$  in the limiting case of  $Ja \gg 1$  only. When  $x$  is defined so that  $\gamma = 2x(3/\pi)^{1/2}Ja$ , then (2.4.11) gives the following equation for  $x$ :

$$x^3 - \frac{1}{3^{1/2}} x^2 - 1 = 0. \quad (2.4.12)$$

The real solution of (2.4.12) gives  $x = 1.234$ .

When there is no contribution to growth due to microlayer evaporation,  $x = 1$ . When there is only growth caused by microlayer evaporation,  $x = 1/3^{1/2} = 0.5773$ . It follows therefore that the combined effect of both modes of growth is smaller than the sum of the separate effects.

*A dry area with radius  $R_d$  will be formed both by capillary effects and by evaporation of the microlayer. Dry area formation caused by capillary effects will be treated in detail in Section 4.2. Dry area formation by evaporation, or 'dry-out' as it is called, has been treated numerically by many authors; cf. e.g. Yu and Mesler (1977), and Cooper and Merry (1972, 1973).*

In the analysis of dry-out, thermal properties of both the wall and the liquid play an important part, and an analytical solution for  $R_d(t)$  cannot be found.

Van Ouwkerk (1970, 1971) presented an analytical solution for equal thermal properties of liquid and wall under the assumption that the thickness of formation of the microlayer  $\delta^*$  is proportional to  $t^{1/2}$ . However, as will be shown in Section 4.1, a more complex analysis results in  $\delta^* \propto t^{1/3}$ , which makes an analytical solution for  $R_d(t)$  even more difficult. Consequently, dry-out will not be considered further in this thesis.

2.4.2. *The influence of non-homogeneous initial temperature fields on growth and departure*

In practical situations, the liquid above the superheated wall with temperature  $T_w$  is not superheated uniformly, but its temperature decreases with increasing distance from the wall until the homogeneous temperature of the bulk liquid  $T_B < T_w$  is reached.  $T_B$  may even be lower than the saturation temperature  $T_s$ .

During bubble growth, the bubble pushes the hot liquid upwards, resulting in a convection process that will be described numerically in Section 3.3.2. Consequently, the temperature  $T_\infty$  at the edge of the thermal boundary layer around the bubble cap is a function of the azimuthal angle  $\theta$  and of time  $t$ .

In principle, expression (2.2.17) is only valid for time independent  $T_\infty(\theta)$  at all values of  $\theta$ . However, in the following treatment, it is assumed that  $T_\infty(\theta, t)$  changes sufficiently slowly, so that equation (2.2.17) may be used as an approximation when  $T_\infty(\theta, t)$  varies.

The total heat flow to the vapour-liquid interface at the bubble cap can be found by integrating  $q_R(\theta, t)$  over the surface of the bubble cap, resulting in:

$$\Phi_R(t) = 2\pi R^2(t) \int_{\theta=0}^{\pi-\theta_a(t)} q_R(\theta, t) \sin \theta \, d\theta, \quad (2.4.13)$$

where  $\theta_a(t)$  is the apparent contact angle, which is entirely determined by the bubble dynamics; cf. also Fig. 2.1.

The surface area of the bubble cap  $A(t)$  equals:

$$A(t) = 2\pi R^2(t) \int_{\theta=0}^{\pi-\theta_a(t)} \sin \theta \, d\theta = 2\pi R^2(t) \{1 + \cos \theta_a(t)\}. \quad (2.4.14)$$

The mean temperature  $\bar{T}_\infty$  at the edge of the thermal boundary layer is defined as:

$$\bar{T}_\infty(t) = \frac{2\pi R^2(t)}{A(t)} \int_{\theta=0}^{\pi-\theta_a(t)} T_\infty(\theta, t) \sin \theta \, d\theta. \quad (2.4.15)$$

The factor  $1 + \cos \theta_a(t)$  in (2.4.14) is a slowly varying function of  $t$  compared to  $R(t)$  and  $\dot{R}(t)$ . For that reason, this factor can be brought under the Riemann-Liouville integral operator  ${}_0 D_t^{-\frac{1}{2}}$  in (2.2.19), resulting in an equation similar to (2.2.19):

$${}_0 D_t^{-\frac{1}{2}} \frac{\dot{V}_R(t)}{A(t)} = (3\kappa)^{\frac{1}{2}} Ja \frac{\bar{T}_\infty(t) - T_R(t)}{T_w - T_s} + \kappa Ja {}_0 D_t^{-\frac{1}{2}} \left[ \frac{\bar{T}_\infty(t) - \bar{T}_R(t)}{T_w - T_s} \frac{1}{R} \right], \quad (2.4.16)$$

where the dimensionless Jakob number is defined as

$$Ja = \rho c (T_w - T_s) / \rho_1 \ell.$$

In (2.4.16), the correction factor  $3^{\frac{1}{2}}$ , accounting for radial convection has been introduced, as well as the global heat requirement  $\dot{\Phi}_R = \rho_1 \ell \dot{V}_R$ .

If vaporization at the vapour-liquid interface in the liquid micro-layer is negligible, then  $V_R(t) = V(t)$ . When it is further assumed that the dependence on  $t$  of  $T_R - \bar{T}_\infty = T_s - \bar{T}_\infty$ , as is the case in the diffusion controlled mode of growth, is negligible, the solution of (2.4.16) results in expression (2.2.34) where  $Ja$  has been replaced by  $Ja(\bar{T}_\infty - T_s) / (T_w - T_s)$ .

In the following discussion, this result will be used to calculate the bubble departure radius as a function of ambient pressure.

After a bubble has departed from the wall, cold liquid with bulk temperature  $T_B$  flows to the wall. This liquid is heated through contact with the wall which has a temperature  $T_w$  and, when a sufficient part of the liquid above the heated wall becomes superheated, nucleation will start again. This process repeats itself continuously, and for that reason, the thermal boundary layer in contact with the wall is sometimes called the relaxation layer; cf.

Van Stralen, Cole, Sluijter and Sohal (1975).

According to a theory for a perfectly conducting wall, described by Han and Griffith (1965), the time between bubble departure and nucleation, the so-called waiting time, is given by:

$$t_w = \frac{144(T_w - T_B)^2 T_s^2 \sigma^2}{\pi \kappa \rho_l^2 \ell^2 (T_w - T_s)^4} \quad (2.4.17)$$

Further, according to Han and Griffith's theory, the required wall superheating to nucleate a cavity with radius  $R_0$  is given by:

$$T_w - T_s = \frac{4\sigma T_s}{\rho_l \ell R_0} \quad (2.4.18)$$

From expressions (2.4.17,18), the initial thickness  $H$ , defined as  $H = (\pi \kappa t_w)^{\frac{1}{2}}$ , of the thermal boundary layer in which the bubble starts growing equals:

$$H = 3 \frac{T_w - T_B}{T_w - T_s} R_0 \quad (2.4.19)$$

As an approximation, it is assumed that the initial temperature profile in the relaxation layer is linear; cf. Section 3.3.2 for experimental evidence of this assumption. Consequently:

$$T_\infty(z) = \begin{cases} T_w + \frac{z}{H}(T_B - T_w) & \text{for } z \leq H \\ T_B & \text{for } z \geq H \end{cases} \quad (2.4.20)$$

During growth, the bubble pushes part of the hot liquid upward. However, after a sufficient growing time, the upper edge of the boundary layer surrounding the upper part of the bubble has a temperature  $T_B$ . Consequently, the temperature profile in the relaxation boundary layer may again be approximated by expression (2.4.20), corrected by replacing  $H$  by  $\zeta H$ , where  $\zeta$  represents the ratio in which the initial temperature profile has been stretched.

At the time of departure, where  $R = R_{dep}$ , the surface of the bubble

in contact with the thermal relaxation boundary layer equals  $2\pi\zeta HR_{\text{dep}}$ . In that case, the mean temperature defined by equation (2.4.15) follows from (2.4.20), resulting in:

$$\bar{T}_{\infty} = T_B + \frac{\zeta H}{4R_{\text{dep}}} (T_w - T_B) = T_B + \frac{3\zeta R_o}{4R_{\text{dep}}} \frac{(T_w - T_B)^2}{(T_w - T_s)}. \quad (2.4.21)$$

In the following discussion, restriction will be made to the case  $T_B = T_s$  and  $Ja \gg 1$ . Under these conditions, the bubble radius vs. time, near the time of departure, following from equations (2.4.16,21) is given by; cf. also equation (2.2.33):

$$R(t) = 2 \left(\frac{3}{\pi}\right)^{\frac{1}{2}} \frac{3\zeta R_o}{4R_{\text{dep}}} Ja(\kappa t)^{\frac{1}{2}}. \quad (2.4.22)$$

From (2.4.22), an expression for the bubble growth constant  $\gamma = R(\kappa t)^{\frac{1}{2}}$  near the departure time can easily be derived.

Substitution of the latter expression in equation (2.3.7) for the departure radius results in:

$$R_{\text{dep}} = \left(\frac{3^6 5}{2^5 \pi^2}\right)^{\frac{1}{7}} \frac{(R_o Ja \zeta)^{\frac{4}{7}} \kappa^{\frac{2}{7}}}{g^{\frac{1}{7}}}. \quad (2.4.23)$$

From (2.4.23), it follows that the radius of departure depends only slightly on the value of  $g$ . This effect has been found experimentally by Siegel and Keshock (1964).

Introduction of expression (2.2.20) for the Jakob number (where  $T_{\infty}$  is replaced by  $T_w$ ) and equation (2.4.18) for  $R_o$ , results in the following equation for  $R_{\text{dep}}$ :

$$R_{\text{dep}} = \left(\frac{2^3 3^6 5}{\pi^2}\right)^{\frac{1}{7}} \frac{(\rho_c T_s \sigma)^{\frac{4}{7}} \kappa^{\frac{2}{7}}}{(\rho_l \ell)^{\frac{4}{7}} g^{\frac{1}{7}}}. \quad (2.4.24)$$

The result (2.4.24) is independent of the initial superheating  $T_w - T_s$  and of the cavity radius  $R_o$ .

Equation (2.4.24) forms a theoretical proof of an empirical expression obtained by Cole and Rohsenow (1969), as will be shown in the following discussion.

Following the latter authors, equation (2.4.24) is non-dimensionalized by writing:

$$\frac{2R_{\text{dep}} \left(\frac{\rho g}{\sigma}\right)^{\frac{1}{2}}}{\left(\frac{\rho c T_s}{\rho_1 \ell}\right)^{\frac{5}{4}}} = 3.34 \left(\frac{\sigma^2 \kappa^8 g^{10} \zeta^{16} \ell^3 \rho_1^3}{\rho^5 c^{19} T_s^{19}}\right)^{\frac{1}{28}} = \alpha. \quad (2.4.25)$$

The dimensionless number  $\rho c T_s / \rho_1 \ell$  is approximately inversely proportional to pressure, and the right-hand side of (2.4.25) hardly depends on pressure.

Using experimental values of several authors for the departure diameter  $2R_{\text{dep}}$  of steam bubbles, Cole and Rohsenow found:

$$\alpha = 1.5 \times 10^{-4}. \quad (2.4.26)$$

For organic liquids like acetone, carbon tetrachloride and methanol they found:

$$\alpha = 4.65 \times 10^{-4}. \quad (2.4.27)$$

In the following discussion, Cole and Rohsenow's equation (2.4.25) will be compared with Fritz's (1935) equation for the maximum radius of static adhering bubbles. Fritz's equation reads:

$$R_{\text{dep}} = 0.0107 \theta_o \left(\frac{\sigma}{\rho g}\right)^{\frac{1}{2}}, \quad (2.4.28)$$

where  $\theta_o$  is the natural contact angle in degrees. For water boiling at atmospheric pressure,  $(\rho c T_s / \rho_1 \ell)^{\frac{5}{4}} \approx 10^4$ , and comparison of equations (2.4.25,27) with equation (2.4.28) shows that the latter equation gives the same result as Cole and Rohsenow's equation for  $\theta_o = 75^\circ$ . Probably this agreement, and the interpretation of  $\theta_o$  as a 'mean' contact angle, is the explanation of the frequent use of



Fritz's equation in the literature for cases far beyond its range of validity, which is restricted to static bubbles.

It is remarked that there must be a maximum pressure  $p_{tr}$  for which Cole and Rohsenow's expression holds. For higher pressures, the bubble growth rate given by equation (2.4.22) becomes so low that departure is no longer governed by acceleration; cf. Section 2.3.2, but by the rate of growth of the bubble contact radius; cf. Sections 2.3.3 and 4.3. In the latter case, the departure diameter is virtually independent of pressure, cf. e.g. equation (2.4.28), and consequently the adherence time will *increase* with increasing pressure, instead of the decrease predicted by equation (2.4.25).

The transitional pressure  $p_{tr}$ , where the surface tension force of adhesion at the bubble foot begins to play a part, can easily be estimated when it is assumed that the maximum bubble radius of this 'sticking' mode of adherence is described by Fritz's equation (2.4.28). This type of adherence will become important when  $R_{dep}$  calculated with Fritz's equation equals  $R_{dep}$  calculated with Cole and Rohsenow's equation.

Since Cole and Rohsenow's expression predicts that  $R_{dep} \propto 1/p_{\infty}$ , and in Fritz's expression  $R_{dep} \propto \theta_0$ , it follows, as a rough estimation, that  $p_{tr} = (75^\circ/\theta_0) \times 100$  kPa.

From (2.4.28) it is observed that the pressure  $p_{tr}$ , where transition from the accelerating to the sticking mode of departure takes place, strongly depends on the wetting properties of the system. When the heating wall is fatty, or when the wall is coated with a non-wetting agent (e.g. teflon),  $\theta_0$  may be in the range of  $90^\circ$  to  $110^\circ$  and the sticking mode will already be observed at atmospheric pressures.

On the other hand, the heat transfer process will be optimized when the walls are well-wetted. For example, with clean steel or copper walls  $\theta_0 \leq 5^\circ$ , and  $p_{tr} \geq 1500$  kPa. In this way, small bubbles with high departure frequency can be obtained at high pressures, resulting in a high peak heat flux.

A reduction of the peak heat flux has been observed experimentally by Diesselhorst, Grigull and Hahne (1977), where the wall is coated with the non-wetting material PTFE.

It is noted that there is also a lower limit for the pressures where (2.4.25) holds. For low pressures, bubble growth becomes inertia-controlled, and equations (2.2.33) and (2.3.7), upon which the previous treatment is based, lose their validity.

### *2.5. Volume oscillations*

In reality, an exact asymptotic, diffusion-controlled mode of growth is unlikely to occur. Deviations in ambient pressure, e.g. caused by the sudden start of growth of neighbouring bubbles, may cause fluctuations in the bubble growth rate. In the following discussion, deviations from the asymptotic diffusion-controlled mode of growth will be considered as an example.

When, during bubble growth, the temperature at the vapour-liquid interface is constant and equal to the saturation temperature, the flow of heat to the bubble is just sufficient to supply the required heat for vaporization to maintain this mode of bubble growth. If the growth rate decreases for some reason, less heat of vaporization is required, and the temperature of the liquid at the bubble boundary will increase. Consequently, the vapour temperature will rise, and an increase of vapour pressure will result. This pressure increase will cause an acceleration of the bubble growth process which, after some time, results in a higher bubble growth rate than the original one, and requires more heat of vaporization. This heat requirement causes the temperature of the liquid at the bubble boundary to decrease, resulting in a lowering of the pressure, etc..

From this qualitative description, it is learned that the interaction between inertia and thermal effects determines the character of the bubble response. To describe this process quantitatively for the case  $Ja \gg 1$ , it will be shown in the following discussion that radial convection does not play a part.

As becomes clear from the discussion of Section 2.2.2, heat transport takes place both by diffusion and by radial convection. Since the thermal boundary layer around the vapour-liquid interface at the bubble cap has a certain thickness, the radial velocity of the liquid at the edge of this boundary layer is lower than the velocity of the bubble boundary. Consequently, an additional convective contribution of  $3^{\frac{1}{2}} - 1 = 0.72$  times the heat flux without this effect is added to the heat transport rate and to the bubble growth rate; cf. Section 2.2.2.

When, due to inertia effects, the bubble growth rate is smaller than that given by the heat transfer controlled rate, the correction for radial convection will be smaller. It becomes zero for a non-growing, non-imploding bubble, and for an imploding bubble the radial convection phenomenon has to be accounted for by a negative correction.

Consequently, for a bubble growth rate oscillating around a mean value, the contribution of the oscillations to radial convection may be assumed to vanish in linear theory. This also follows from equations (2.2.29,30), as has been discussed by Plesset and Zwick (1952).

Under these conditions, the temperature oscillations of the vapour may be described by equation (2.2.19) with neglect of the second term in the right-hand side (the curvature term) since  $Ja \gg 1$ .

Substitution of (2.2.19) in the Rayleigh equation (2.2.10), with neglect of viscosity and surface tension, and combined with Clapeyron's equation (2.2.1), then results in equation (2.2.40) with a factor  $\kappa^{\frac{1}{2}}$  instead of the corrected factor  $(3\kappa)^{\frac{1}{2}}$ .

Let the perturbation in the bubble radius be represented by:

$$\varepsilon(t) = R(t) - R_{\infty}(t). \quad (2.5.1)$$

In (2.5.1),  $R_{\infty}(t)$  represents the diffusion-controlled mode of growth given by equation (2.2.33). In the following discussion, it will be assumed that  $|\varepsilon(t)| \ll R_{\infty}(t)$ , in such a way that terms in powers of  $\varepsilon$ ,  $\dot{\varepsilon}$ , and higher derivatives, greater than one, can be neglected.

In this way, substitution of (2.5.1) in (2.2.40), without the correction factor  $3^{\frac{1}{2}}$  for the disturbance  $\varepsilon$ , results in; cf. Appendix B:

$$R_{\infty} D_t^2 \varepsilon + 3\dot{R}_{\infty} D_t^1 \varepsilon + \frac{3^{\frac{3}{2}} \gamma_0}{2\tau^{\frac{1}{2}}} t_0 D_t^{-\frac{1}{2}} \varepsilon + \ddot{R}_{\infty} \varepsilon = 0. \quad (2.5.2)$$

In (2.5.2), it has been assumed that the perturbation is initiated at time  $t = t_0$  after onset of bubble growth at  $t = 0$  and, in the derivation of (2.5.2), use has been made of the following rule for piecewise defined functions; cf. Oldham and Spanier (1970):

$${}_0 D_t^{\nu} \varepsilon^*(t) = \begin{cases} 0 & 0 < t < t_0 \\ t_0 D_t^{\nu} \varepsilon(t) & t > t_0 \end{cases}, \quad (2.5.3)$$

where  $\varepsilon^*(t)$  is defined by:

$$\varepsilon^*(t) = \begin{cases} 0 & 0 < t < t_0 \\ \varepsilon(t) & t > t_0 \end{cases}. \quad (2.5.4)$$

For sufficiently large times  $t_0$ , the second term in (2.5.2) may be neglected since  $\dot{R}_{\infty} \propto 1/t^{\frac{1}{2}}$  and, similarly, the last term of (2.5.2) is negligible.

Further, equation (2.5.2) will be simplified by assuming that  $R_{\infty}(t)$  in the first term of (2.5.2) is only slowly depending on  $t$  with respect to the fast response of  $\varepsilon(t)$  to a sudden perturbation. In that case,  $R_{\infty}(t)$  may be replaced by  $R_{\infty}(t_0)$ , and (2.5.2) simplifies to:

$$D_t^2 \varepsilon + \left\{ \frac{3^{\frac{3}{2}} \gamma_0}{2\tau^{\frac{1}{2}} R_{\infty}(t_0)} \right\} t_0 D_t^{\frac{1}{2}} \varepsilon = 0, \quad (2.5.5)$$

where  $\tau$  is given by equation (2.2.45). In the derivation of (2.5.5), composition rule (B5) for  $\varepsilon(t_0) = 0$  has been used.

Taking the  $D_t^1 = \frac{d}{dt}$  of (2.5.5), and making use of the law of exponentials (B2), results in:

$$D_t^3 \epsilon + \left\{ \frac{3^{\frac{3}{2}} \gamma_0}{2\tau^{\frac{1}{2}} R_\infty(t_0)} \right\} t_0 D_t^2 \epsilon = 0. \quad (2.5.6)$$

Taking the  $t_0 D_t^{-\frac{1}{2}}$  of (2.5.5) and using composition rules (B5) and (B6) for  $\epsilon(t_0) = 0$ ,  $\dot{\epsilon}(t_0) = 0$  results in:

$$t_0 D_t^{\frac{3}{2}} \epsilon + \left\{ \frac{3^{\frac{3}{2}} \gamma_0}{2\tau^{\frac{1}{2}} R_\infty(t_0)} \right\} \epsilon = 0. \quad (2.5.7)$$

Substitution of (2.5.6) in (2.5.7), while eliminating the term  $t_0 D_t^{\frac{3}{2}} \epsilon$ , results in a third order ordinary differential equation:

$$\ddot{\epsilon} - \left\{ \frac{3^{\frac{3}{2}} \gamma_0}{2\tau^{\frac{1}{2}} R_\infty(t_0)} \right\}^2 \epsilon = 0. \quad (2.5.8)$$

The general solution of (2.5.8) is:

$$\begin{aligned} \epsilon = & A_0 \sin(\omega t) + B_0 \cos(\omega t) \exp\left(-\frac{\omega(t-t_0)}{3^{\frac{1}{2}}}\right) + \\ & + D_0 \exp\left(\frac{3^{\frac{3}{2}} \omega(t-t_0)}{2}\right), \end{aligned} \quad (2.5.9)$$

where

$$\omega = \frac{3^{\frac{13}{6}}}{2^{\frac{5}{3}}} \left[ \frac{\gamma_0 \tau}{R_\infty(t_0)} \right]^{\frac{2}{3}} \frac{1}{\tau} = \frac{3^{\frac{7}{6}}}{2} \left( \frac{\rho_1}{\rho} \right)^{\frac{4}{3}} \left( \frac{\ell}{cT_s} \right)^{\frac{2}{3}} \frac{\ell^{\frac{2}{3}}}{\kappa^{\frac{1}{3}} R_\infty(t_0)^{\frac{2}{3}}}. \quad (2.5.10)$$

Since  $D_t^2 \exp(t) = \exp(t)$  and, for sufficiently large  $t$ ,  $t_0 D_t^{\frac{1}{2}} \exp(t) \rightarrow \exp(t)$ , cf. Oldham and Spanier (1974), the last term in (2.5.9) cannot be a solution of the original equation (2.5.5). Consequently, the response in bubble growth rate to a perturbation in acceleration  $\ddot{\epsilon}(t_0)$ , introduced at time  $t = t_0$ , is given by:

$$\dot{\epsilon}(t) = \frac{\ddot{\epsilon}(t_0)}{\omega} \sin\{\omega(t-t_0)\} \exp\left\{-\frac{\omega(t-t_0)}{3^{\frac{1}{2}}}\right\}. \quad (2.5.11)$$

From (2.5.11), it follows that the asymptotic, diffusion-controlled mode of growth is stable with respect to small perturbations in growth rate. These perturbations and the corresponding inertia effects are cancelled almost immediately in the manner of a rapidly-damped oscillation.

In a similar way, it can be shown that the initial, inertia-controlled mode of growth is stable as well. In the latter mode of growth, the perturbations are damped out without oscillations.

From the extended Rayleigh-equation (2.2.10), combined with the Clapeyron equation (2.2.1), it follows that the temperature oscillates as  $T_R(t) - T_s = \rho T_s R_\infty(t_0) \ddot{\epsilon}(t) / \rho_1 l$ . Consequently, the first and second terms in the right-hand side of (2.2.13) have amplitudes of  $\ddot{\epsilon}(t_0) / \omega$  and  $\rho R_\infty^2(t_0) \omega \ddot{\epsilon}(t_0) p_\infty$  respectively. From this, it follows that compressibility effects in the vapour may only be neglected when the following condition is satisfied:

$$\omega^2 \ll \omega_M^2, \quad (2.5.12)$$

where  $\omega_M$  is the so-called Minnaert frequency, cf. Minnaert (1933), defined by:

$$\omega_M = \left( \frac{3c_1 p_\infty}{c_1 v \rho} \right)^{\frac{1}{2}} \frac{1}{R_\infty}. \quad (2.5.13)$$

If condition (2.5.12) is not satisfied, the vapour behaves as a compressible gas, as has also been shown numerically for imploding vapour bubbles by Cho and Seban (1969). In the latter case, the bubble has radial pulsations with frequency  $\omega_M$ , and the damping is low.

## CHAPTER 3

### DEVIATIONS FROM THE SPHERICAL SHAPE

#### *3.1. Introduction*

In Section 2.3.2, a model has been proposed to describe the departure of sufficiently large spherical vapour bubbles. The basis of this model has been Green's momentum equation for the initial acceleration of free spherical bubbles. The departure times and radii, determined in this way, were shown to be in good agreement with experimental data. However, in view of the oversimplifying assumption of a free, spherical bubble one must expect that equations (2.3.8, 9, 10) and (2.3.14, 15, 16) for the bubble contact radius  $R_c(t)$  only represent a semi-quantitative description of the evolution in time of  $R_c(t)$ .

In this Chapter, the assumption of a spherical bubble will be relaxed and the case where the flow field is bounded by a horizontal wall will be considered. Initially, at  $t = 0$ , it is assumed that a growing hemispherical bubble is formed. It will be further assumed that there is cylindrical symmetry, but that the bubble will deviate from the spherical shape due to gravity. As will be shown in this Chapter, the main distortion will be a decrease in growth rate of the bubble foot, leading to contraction and ultimately to departure. An effect of less importance will be a flattening of the bubble dome.

When the bubble growth rate is sufficiently high, the viscous boundary layers around the bubble cap and the solid wall will remain sufficiently thin during adherence; consequently, the assumption of potential flow is acceptable. The only region of importance for the bubble shape, namely the meniscus region near  $r = R_c$ , where viscous effects may play an important part, will be treated separately in Section 4.1.2.

Bubbles satisfying the above-mentioned conditions occur in water boiling at pressures lower than, say, 50 kPa. Comparison of theoretical results with experiments on such bubbles will be reported.

A situation which has many similarities with the above-discussed case has been considered by Walters and Davidson (1962, 1963). These authors considered the initial motion of a gas bubble in an infinitely-extended, inviscid liquid. Both for two-dimensional bubbles (Walters and Davidson (1962)) and for three-dimensional bubbles (Walters and Davidson (1963)) it was found that, at a certain time after bubble formation, a liquid tongue is formed at the rear of the ascending bubble. Comparison between non-growing and growing bubbles showed that for expanding bubbles the changes in shape occur more slowly; cf. Walters and Davidson (1963).

As a matter of course, tongue formation at the rear of the bubble cannot take place when the bubble is located at a solid wall, as is the case under consideration in this Chapter. However, since the bubble foot can move over the wall, cf. Section 2.3.2, it may be expected that contraction of the bubble foot will occur instead of tongue formation.

The departure of a non-growing bubble, initially formed as a hemisphere at a wall, will be discussed in Section 3.2. This enables us to describe the numerical method, the so-called global collocation method, which will be used to solve this non-linear problem. On the basis of the results obtained in Section 3.2, the departure of water vapour bubbles under low pressure will be considered in Section 3.3.

### 3.2. *Initial acceleration of non-growing bubbles*

#### 3.2.1. *The equations of motion*

The rotationally symmetric solution of potential equation (2.1.15), without singularities in  $\theta = 0$  and  $r \rightarrow \infty$ , has the following form when only one bubble is considered; cf. also appendix A:

$$\phi(r, \theta, t) = \sum_{j=0}^{\infty} \beta_j(t) \frac{P_j(\cos \theta)}{r^{j+1}}. \quad (3.2.1)$$

In (3.2.1), the expansion coefficient  $\beta_j$  is a function of time, but not of the spatial coordinates  $r, \theta$ .  $P_j(\cos \theta)$  represents the



Legendre polynomial of degree  $j$  with argument  $\cos \theta$ .

When the normal component of the velocity at the solid wall is zero, i.e. when  $(\partial\phi/\partial\theta)_{\theta=\pi/2} = 0$ , the coefficients for odd Legendre polynomials are zero, i.e.  $\beta_{2j+1} = 0$ ,  $j = 0, 1, \dots, \infty$ .

In the latter case, a series expansion similar to (3.2.1.) may be written as:

$$\phi(r, \theta, t) = \sum_{j=0}^{\infty} b_j(t) \frac{2_j(\cos \theta)}{r^{2j+1}}. \quad (3.2.2)$$

Following Yeh (1967) and Hermans (1973), the bubble radius is also expanded in Legendre polynomials:

$$R(\theta, t) = \sum_{j=0}^{\infty} \alpha_j(t) P_j(\cos \theta), \quad (3.2.3)$$

or, when a solid wall is present at  $\theta = \pi/2$ :

$$R(\theta, t) = \sum_{j=0}^{\infty} a_j(t) P_{2j}(\cos \theta). \quad (3.2.4)$$

The series expansions (3.2.2, 4) may be applied only when the bubble radius is single-valued, i.e. when for every angle  $\theta$  there is only one value for  $R(\theta)$ . The latter restriction is quite severe and is, for instance, not satisfied when bubble implosion and fragmentation are considered. However, when only bubble growth is treated, this difficulty does not arise.

Instead of the Rayleigh-Plesset equation (2.2.10), the Bernoulli equation (2.1.16), applied at the bubble boundary  $r = R(\theta, t)$ , will be used as the dynamic boundary condition. By neglecting the normal viscous stresses, the latter condition yields:

$$\begin{aligned} \frac{\partial\phi}{\partial t} = & -\frac{1}{2} \left[ \left( \frac{\partial\phi}{\partial r} \right)^2 + \left( \frac{1}{R} \frac{\partial\phi}{\partial\theta} \right)^2 \right] - \frac{P_1 R - P_\infty}{\rho} - gR \cos \theta + \\ & + \frac{\sigma}{\rho R} \left[ \frac{1 + 2 \left( \frac{1}{R} \frac{\partial R}{\partial\theta} \right)^2 - \frac{1}{R} \frac{\partial^2 R}{\partial\theta^2}}{\left[ 1 + \left( \frac{1}{R} \frac{\partial R}{\partial\theta} \right)^2 \right]^{3/2}} + \frac{1 - \frac{1}{R} \frac{\partial R}{\partial\theta} \cot \theta}{\left[ 1 + \left( \frac{1}{R} \frac{\partial R}{\partial\theta} \right)^2 \right]^{1/2}} \right], \quad (3.2.5) \end{aligned}$$

at  $r = R(\theta, t)$ .

The vapour pressure at the vapour-liquid interface,  $p_{1R}$ , follows from Clapeyron's equation (2.2.1). For the time being, it is assumed that  $p_{1R}$  is known. The term  $\rho g R \cos \theta$  represents the hydrostatic pressure. Equation (3.2.5) is the only equation where gravity occurs and, provided that the initial conditions represent spherical symmetry, deviations from the spherical bubble shape are due to this term only. Equation (3.2.5) may be considered as an equation of motion describing the evolution in time of the velocity potential at the bubble boundary. To find the evolution in time of the bubble boundary  $r = R(\theta, t)$ , a kinematic boundary condition must be prescribed as well. Similar to equation (2.2.4), this will be the condition that the normal component of the rate of displacement of the bubble boundary equals the normal component of the liquid velocity at the bubble wall.

In general, the coordinates of the moving interface are given by the following implicit relationship:

$$F(r, \theta, t) = 0 . \quad (3.2.6)$$

The unit vector normal to the interface is given by:

$$\underline{n} = (n_r, n_\theta) = \frac{\nabla F}{|\nabla F|} = \frac{\left( \frac{\partial F}{\partial r}, \frac{1}{r} \frac{\partial F}{\partial \theta} \right)}{\left\{ \left( \frac{\partial F}{\partial r} \right)^2 + \left( \frac{1}{r} \frac{\partial F}{\partial \theta} \right)^2 \right\}^{1/2}} . \quad (3.2.7)$$

Equation (3.2.6) generally has the form of a multivalued relation between  $r$  and  $\theta$ , but from physical considerations it is known that at least one solution exists which is written as:

$$r = R_\lambda(\theta, t) . \quad (3.2.8)$$

In (3.2.8), the index  $\lambda$  denotes the choice of the solution if equation (3.2.6) is multivalued for  $r$  with respect to  $\theta$ . Equation (3.2.8) can be written as  $r - R_\lambda(\theta, t) = 0$  and leads to the following expression for  $\underline{n}$ :

$$\underline{n}_\lambda = (n_{r\lambda}, n_{\theta\lambda}) = \frac{\left( 1, -\frac{1}{R_\lambda} \frac{\partial R_\lambda}{\partial \theta} \right)}{\left\{ 1 + \left( \frac{1}{R_\lambda} \frac{\partial R_\lambda}{\partial \theta} \right)^2 \right\}^{1/2}} . \quad (3.2.9)$$

At a fixed angle  $\theta$ , the time derivative of the coordinates of the bubble boundary is given by:

$$\frac{\partial}{\partial t}(r, \theta)_{\text{interface}} = \left( \frac{\partial R_\lambda}{\partial t}, 0 \right). \quad (3.2.10)$$

From (3.2.9,10), it follows that, for a fixed angle  $\theta$ , the normal component of the rate of displacement of the bubble boundary is given by:

$$\underline{n}_\lambda \cdot \frac{\partial}{\partial t}(r, \theta)_{\text{interface}} = \frac{\frac{\partial R_\lambda}{\partial t}}{\left\{ 1 + \left( \frac{1}{R_\lambda} \frac{\partial R_\lambda}{\partial \theta} \right)^2 \right\}^{1/2}}. \quad (3.2.11)$$

Equating the normal component  $(\underline{u} \cdot \underline{n}_\lambda)_{r=R_\lambda}$  of the liquid velocity at the vapour-liquid interface to the normal component of the rate of displacement of the vapour-liquid interface, results in:

$$\frac{\partial R_\lambda}{\partial t} + \left( \frac{1}{2} \frac{\partial \phi}{\partial \theta} \right)_{r=R_\lambda} \frac{\partial R_\lambda}{\partial \theta} = \left( \frac{\partial \phi}{\partial r} \right)_{r=R_\lambda}. \quad (3.2.12)$$

Equation (3.2.12) is a partial differential equation of the hyperbolic type for  $R_\lambda(\theta, t)$ . By making use of the method of characteristics, cf. e.g. Whitham (1974), a multivalued solution can be found. Sluyter (1978) performed such calculations for imploding gas bubbles. However, in the following Sections, multivaluedness will not be considered. Consequently, the index  $\lambda$  of  $R_\lambda$  will be omitted, and  $R(\theta, t)$  may be expanded in the series (3.2.3) or (3.2.4).

### 3.2.2. The global collocation method.

In this Section, a method will be presented for the determination of the expansion coefficients  $\alpha_i(t)$  and  $\beta_i(t)$  or  $a_i(t)$  and  $b_i(t)$ . Analytical methods will not be attempted, but a numerical solution method will be applied instead.

A finite number of  $N$  angles  $\theta_k$ ,  $k = 0, 1, \dots, N-1$ , is selected to discretize the continuous flow field. The way in which these angles are distributed over the interval of  $\theta$ -values will be discussed in Section 3.2.3.

When the values of the N bubble radii  $R_k(t) = R(\theta_k, t)$  have been calculated, the values of  $R(\theta, t)$  between the angles  $\theta_k$  can be found by interpolation. For that purpose, the series (3.2.4) will be cut after N terms, resulting in the following linear system for the expansion coefficients  $a_j(t)$ :

$$R_k(t) = \sum_{j=0}^{N-1} [P]_{kj} a_j(t), \quad (3.2.15)$$

where the matrix  $\underline{P}$  has elements  $[P]_{kj}$  which are:

$$[P]_{kj} = P_{2j}(\cos \theta_k). \quad (3.2.16)$$

Generally, the matrix denoted by (3.2.16) has a low condition number, and is therefore well-suited for machine computations; cf. e.g. Hayes (1970).

When the values of  $a_j(t)$ ,  $j = 0, 1, \dots, N-1$ , are obtained from the known values of  $R_k(t)$ ,  $k = 0, 1, \dots, N-1$ , at a certain time  $t$ , by solving numerically the linear set (3.2.15), the value of  $\partial R / \partial \theta$  can be determined by differentiation of series (3.2.4) which is cut after N terms.

Provided that  $(\partial \phi / \partial \theta)_{R_k}$  and  $(\partial \phi / \partial r)_{R_k}$  are known, the value of  $dR_k(t)/dt$  follows from the kinematic boundary condition (3.2.12). In this way, the kinematic boundary condition has only been satisfied at the N discrete angles  $\theta_k$ . A method where an equation is satisfied only at discrete points rather than over a complete continuous range of values is called a collocation method; cf. Finlayson (1972). The method applied here is the global collocation method, since only one interpolation function or so-called trial function has been used for the complete interval of  $\theta$ -values.

In the same way as with the series (3.2.4), the series (3.2.2) for  $\phi$  will also be cut after N terms, where each term is a solution of the potential equation (2.1.15). Defining  $\phi[R_k(t), \theta_k, t] = \phi_k(t)$ , the following set of linear equations for  $b_j(t)$  is derived from (3.2.2.):

$$\phi_k(t) = \sum_{j=0}^{n-1} [\underline{Q}(t)]_{kj} b_j(t), \quad (3.2.17)$$

where the matrix  $\underline{Q}(t)$  has elements  $[\underline{Q}(t)]_{kj}$  defined by:

$$[\underline{Q}(t)]_{kj} = \frac{P_{2j}(\cos \theta_k)}{R_k(t)^{2j+1}}. \quad (3.2.18)$$

Since  $R$ ,  $\partial R/\partial \theta$  and  $\partial^2 R/\partial \theta^2$  are known, the value of  $(\partial \phi/\partial t)_{r=R_k}$  can now be determined from (3.2.5), for prescribed values of  $\phi_k(t)$ , by solving the linear set (3.2.17) to find  $b_j(t)$  and, consequently,  $\partial \phi/\partial r$  and  $\partial \phi/\partial \theta$ . In order to find  $d\phi_k/dt$ , the following expression must be used:

$$\begin{aligned} \frac{d}{dt} \phi_k(t) &= \frac{d}{dt} \phi \{R_k(t), \theta_k, t\} = \left\{ \frac{\partial}{\partial t} \phi(r, \theta_k, t) \right\}_{r=R_k(t)} + \\ &+ \left\{ \frac{\partial \phi(r, \theta_k, t)}{\partial r} \right\}_{r=R_k(t)} \frac{dR_k(t)}{dt}. \end{aligned} \quad (3.2.19)$$

Since the matrix (3.2.18) is mostly ill-conditioned, the calculation of  $b_j(t)$  will be performed with the aid of a scaled matrix  $\underline{Q}^*(t)$ , with elements defined by:

$$[\underline{Q}^*(t)]_{kj} = \left\{ \frac{R^*(t)}{R_k(t)} \right\}^{2j+1} P_{2j}(\cos \theta_k). \quad (3.2.20)$$

In (3.2.20)  $R^*(t)$  is the mean radius defined by:

$$R^*(t) = \frac{1}{N} \sum_{k=0}^{N-1} R_k(t). \quad (3.2.21)$$

When the bubble has a hemispherical shape, then  $R_k(t) = R^*(t)$ , and the matrix  $\underline{Q}^*(t)$  becomes independent of  $t$  and equal to  $\underline{P}$ . Consequently, this matrix is also well-suited for machine computations, and even for deviations from the hemispherical shape, the condition number will remain within reasonable limits.

Now the expansion coefficients  $b_j(t)$  follow from  $\phi_k(t)$  by performing the following two calculations.

(i) The coefficients  $b_j^*(t)$  are calculated with the matrix equation:

$$\phi_k(t) = \sum_{j=0}^{N-1} [\underline{Q}^*(t)]_{kj} b_j^*(t), \quad (3.2.22)$$

(ii) From the calculated values of  $b_j^*(t)$ ,  $b_j(t)$  is determined as follows:

$$b_j(t) = R^*(t)^{2j+1} b^*(t) . \quad (3.2.23)$$

Combination of the expressions for  $dR_k(t)/dt$  and  $d\phi_k(t)/dt$ , obtained by the collocation method discussed above, results in a system of non-linear, coupled, first-order ordinary differential equations. In short-hand notation these equations can be written as:

$$\frac{d}{dt} \begin{pmatrix} R_k \\ \phi_k \end{pmatrix} = F \{ (R_m, \phi_m)_{m=0}^{N-1} \} . \quad (3.2.24)$$

The set of equations (3.2.24) can be solved by computer, using a standard routine for the solution of a set of first-order ordinary differential equations. For every timestep, the matrix equations (3.2.15) and (3.2.17) must be solved; this can also be performed by standard routine.

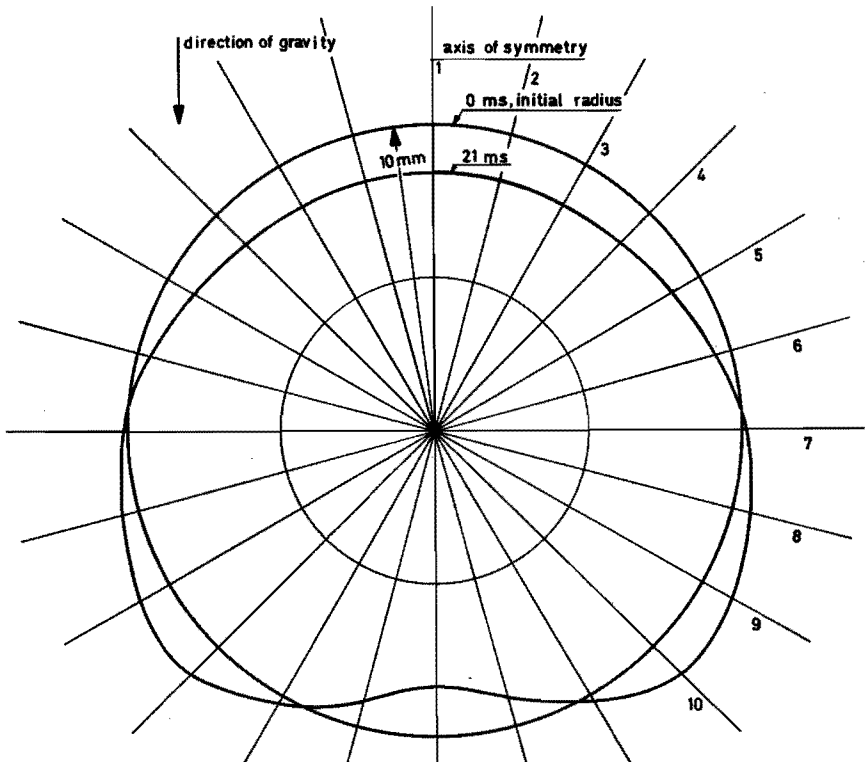


Fig. 3.1. Initial acceleration of an air bubble in water

The advantage of the numerical method described above is that, even for a few collocation points, reasonable results can be obtained. When only one collocation point is used, and when the term  $gR \cos \theta$  in (3.2.5) is omitted, the Rayleigh equation (2.2.10), without the term  $4\eta\dot{R}/\rho R$ , is obtained from (3.2.24).

Finally, two results will be shown in this Section.

Fig. 3.1 shows a gas bubble which is formed at  $t = 0$ , with initial velocity zero. The circle represents the initially spherical bubble with radius  $R = 1$  cm. The wavy line represents the bubble shape after 21 ms. From the displacement of the centre of the bubble, it follows that the initial acceleration is  $20 \text{ m/s}^2 = 2g$ . After a longer time, the calculations show that tongue formation occurs. The results agree with those of Walters and Davidson (1963).

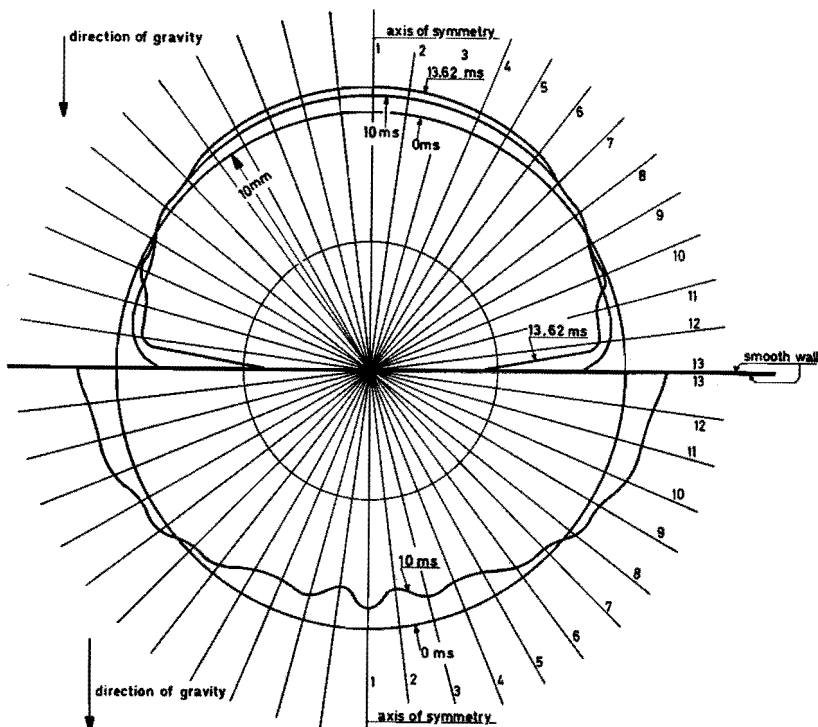


Fig. 3.2. Air bubbles in water adhering to a horizontal wall. One bubble is above and one bubble is beneath the wall.

Fig. 3.2 shows the adherence of two gas bubbles at a smooth wall; one bubble is above, and one bubble is beneath the wall. At time  $t = 0$ , the bubbles are formed with a hemispherical shape, and a radius  $R = 1$  cm. It is observed that the bubble foot of the upper bubble contracts; this effect ultimately leads to departure. The lower bubble is flattened somewhat and shows an extension along the wall.

### 3.2.3. Convergence of orthogonal collocation.

In this Section, the question will be investigated whether the collocation method, described in Section 3.2.2, converges to the exact solution for  $N \rightarrow \infty$ . For this purpose, the equations (3.2.12) and (3.2.5) will be represented in short-hand notation in the following way:

$$\frac{dR}{dt} - G(R, \phi) = 0 \quad , \quad (3.2.25)$$

$$\left\{ \frac{d\phi}{dt} - H(R, \phi) \right\}_{r=R} = 0 \quad . \quad (3.2.26)$$

In (3.2.25, 26),  $R$  and  $\phi$  represent the exact solutions.

To find an approximate solution, the functions  $\tilde{R}$  and  $\tilde{\phi}$ , obtained by cutting the series (3.2.3) and (3.2.1) respectively, are introduced in the following way:

$$\tilde{R}(\mu, t) = \sum_{j=0}^{N-1} \tilde{\alpha}_j(t) P_j(\mu) \quad , \quad (3.2.27)$$

$$\tilde{\phi}(r, \mu, t) = \sum_{j=0}^{N-1} \tilde{\beta}_j(t) \frac{P_j(\mu)}{r^{j+1}} \quad , \quad (3.2.28)$$

where  $\mu = \cos \theta$ .

In (3.2.27, 28),  $\tilde{\alpha}_j(t)$ ,  $\tilde{\beta}_j(t)$  may be considered as approximations of the exact expansion coefficients  $\alpha_j(t)$ ,  $\beta_j(t)$ .



When, instead of the exact solutions, the approximate solutions (3.2.27, 28) are substituted in the left-hand sides of equations (3.2.25, 26), the right-hand sides of these equations will generally not be equal to zero. Let the right-hand sides of (3.2.25,26) be denoted by  $R_G$  and  $R_H$  respectively, defined in the following way:

$$\frac{d\tilde{R}}{dt} - G(\tilde{R}, \tilde{\phi}) = R_G\{\mu, \tilde{\alpha}_j(t), \tilde{\beta}_j(t)\} \quad , \quad (3.2.29)$$

$$\left. \left\{ \frac{d\tilde{\phi}}{dt} - H(\tilde{R}, \tilde{\phi}) \right\} \right|_{r=R} = R_H\{\mu, \tilde{\alpha}_j(t), \tilde{\beta}_j(t)\} \quad . \quad (3.2.30.)$$

In the following discussion, the functionals  $R_G$  and  $R_H$  will be referred to as the residuals. If one wants to find a good approximation, these residuals must be "small" in some sense. The residuals  $R_G$  and  $R_H$ , or shortly  $R$ , will be considered as a function of  $\mu$ , i.e.  $R = R(\mu)$ , since the dependence on  $\tilde{\alpha}_j(t), \tilde{\beta}_j(t)$  is unimportant for the subsequent discussion.

Following the procedure discussed when introducing the collocation method in Section 3.2.2,  $N$  collocation cosines  $\mu_k, k = 0, 1, \dots, N-1$ , will be chosen. The residuals  $R(\mu)$  can be expanded in a series of Lagrange polynomials, with expansion coefficients  $\lambda_k = R(\mu_k)$ , cf. e.g. Fox and Parker (1968):

$$R(\mu) = \sum_{k=0}^{N-1} \lambda_k L_k(\mu) + R^*(\mu) \quad , \quad (3.2.31)$$

$$\lambda_k = R(\mu_k) \quad . \quad (3.2.32)$$

In (3.2.31), the Lagrange polynomial  $L_k(\mu)$  is defined as:

$$L_k(\mu) = \frac{(\mu - \mu_0) \dots (\mu - \mu_{k-1}) (\mu - \mu_{k+1}) \dots (\mu - \mu_{N-1})}{(\mu_k - \mu_0) \dots (\mu_k - \mu_{k-1}) (\mu_k - \mu_{k+1}) \dots (\mu_k - \mu_{N-1})} \quad , \quad (3.2.33)$$

and when  $R(\mu)$  can be differentiated  $N$  times,  $R^*(\mu)$  equals:

$$R^*(\mu) = \frac{(\mu - \mu_0) (\mu - \mu_1) \dots (\mu - \mu_{N-1})}{N!} \left( \frac{d^N R(\mu)}{d\mu^N} \right)_{\mu=\mu'} \quad , \quad (3.2.34)$$

where  $\mu'$  is a  $\mu$ -value in the interval  $-1 \leq \mu \leq 1$ .

In the collocation approximation, the equations (3.2.25, 26) are satisfied at the collocation points  $\mu_k$ , which is equivalent to taking  $R_G(\mu_k) = R_H(\mu_k) = 0$ . From (3.2.32), it follows that this means that  $\lambda_k = 0$  in (3.2.31). Consequently, the residual is given by equation (3.2.34), i.e.  $R(\mu) = R^*(\mu)$ . In this way, the linear relationships (3.2.15, 17) are found from (3.2.27, 28).

From interpolation theory (cf. e.g. Fox and Parker (1968)), it is well-known that  $R^*(\mu)$  tends to zero for  $N \rightarrow \infty$ , only when the values of  $\mu_k$  are chosen in a specific way.

Here interpolation is performed by equating  $\mu_k$  to the zeros of a Legendre polynomial of degree  $N$ . In that case, the maximum absolute value of  $R^*(\mu)$  for  $N \rightarrow \infty$  becomes:

$$|R^*(\mu)| \leq \max_{-1 \leq \mu' \leq 1} \frac{(\pi N)^{\frac{1}{2}}}{2^N N!} \left| \frac{d^N R(\mu)}{d\mu^N} \right|_{\mu=\mu'} \quad (3.2.35)$$

From (2.3.25), it is concluded that for  $N \rightarrow \infty$   $R^*(\mu) \rightarrow 0$ , provided that the  $N$ th derivative of  $R(\mu)$  is bounded.

In this way, the approximated equations (3.2.29, 30) converge to the exact equations (3.2.25, 26), and the approximations  $\hat{R}$  and  $\hat{\phi}$  converge to the exact solutions  $R$  and  $\phi$  as well.

The present method is called the orthogonal collocation method; cf. Finlayson (1972).

### 3.3. Departure of water vapour bubbles under low pressure

#### 3.3.1. Introduction

When the application of the collocation method, described in Section 3.2, is extended to the case of a growing vapour bubble adhering at a superheated conducting wall, the complication arises that the pressure of the vapour in the bubble is coupled to the temperature of the liquid at the bubble boundary. Consequently, the temperature field around the bubble must be solved simultaneously with the flow field.

An accurate local description of the evolution in time of the temperature field is difficult compared to the relative ease of obtaining a solution for the hydrodynamic equations. Also, as will be demonstrated in Section 3.3.2, the solution of the temperature field is very sensitive to changes in the initial temperature field which exists just prior to the start of bubble growth. This initial temperature field will be derived from experiment (cf. Section 3.3.3), and it is to be noted that the initial temperature field can only be determined in an approximate way.

As a matter of course, calculations of the evolution of the temperature with an accuracy greater than that of the initial data will not make sense. For that reason, a relatively simple approach will be presented here, giving a sufficiently accurate estimate of the pressure in the bubble. From this point-of-view, the description of the temperature field around the bubble will be treated as an auxiliary procedure, whilst finding the flow field remains the main purpose of our investigation.

### 3.3.2. *The thermal equations*

First, evaporation of the liquid microlayer will be considered. Since the liquid in this layer is almost at rest, the following expression holds provided that temperature gradients in the radial direction may be neglected; cf. Section 2.4.1.

$$q_M = \begin{cases} 0 & t < t_r \\ -\rho c k^{\frac{1}{2}} t_r^{\frac{1}{2}} D_t^{\frac{1}{2}} \{T_M(t) - T_w\} & t > t_r \end{cases}, \quad (3.3.1)$$

where  $t_r D_t^{\frac{1}{2}}$  represents the generalized Riemann-Liouville operator; cf. Appendix B.

In (3.3.1),  $t_r$  represents the time elapsed after start of bubble growth, at which the bubble contact radius is  $r$ :

$$R_c(t_r) = r. \quad (3.3.2)$$

Like equation (2.4.3) , equation (3.3.1) only holds for a sufficiently thick microlayer.

From expression (3.3.1) , the total heat flowing per unit time to the vapour-liquid interface can be calculated by integration of (3.3.1) over the microlayer, which is assumed to extend from  $r=0$  to  $r=R_c$ :

$$\Phi_M = -2\pi\rho c\kappa^{\frac{1}{2}} \int_{r=0}^{R_c(t)} r t_r D_t^{\frac{1}{2}} \{T_M(t) - T_w\} dr . \quad (3.3.3)$$

When  $\dot{R}_c > 0$ , i.e. when the microlayer is extending in the radial direction, equations (3.3.2) and (3.3.3) can be combined, resulting in:

$$\Phi_M = -2\pi\rho c\kappa^{\frac{1}{2}} \int_{t_r=0}^t R_c(t_r) \dot{R}_c(t_r) t_r D_t^{-\frac{1}{2}} \{T_M(t) - T_w\} dt_r . \quad (3.3.4)$$

As has been discussed in Section 2.4.1 , the heat flux  $\Phi_M$  causes evaporation of the liquid microlayer. As a result, the bubble volume increases by a factor  $(\rho/\rho_1)(\Phi_M/\ell)$  per unit of time. Consequently, the following expression for the volumetric flow rate of vapour at the interface is obtained from (3.3.4) :

$$\dot{V}_M = -\pi \frac{\rho c}{\rho_1 \ell} \kappa^{\frac{1}{2}} \int_{t_r=0}^t \frac{dR_c}{dt_r} t_r D_t^{\frac{1}{2}} \{T_M(t) - T_w\} dt_r . \quad (3.3.5)$$

$R_c(t)$  is known from the solution of the hydrodynamic equations. Let it also be assumed that  $\dot{V}_M$  is prescribed, then the unknown temperature  $T_M(t)$  of the vapour at the vapour-liquid interface of the microlayer follows from equation (3.3.5). An approximate method for solving  $T_M(t)$  will now be introduced.

It was argued in Section 2.4.1 that the most important contribution to vapour production comes from the outer edge of the microlayer; i.e. during a short time interval  $t_r < t < t_r + \Delta t_r$ . During this time interval, the vapour temperature is assumed to be constant when the Riemann-Liouville operator in (3.3.5) is evaluated.

With the aid of equations (2.2.18, 25), the following expression is

then derived from (3.3.5):

$$\dot{V}_M = -\pi \frac{\rho c}{\rho_1 l} \kappa^{\frac{1}{2}} {}_0D_t^{-\frac{1}{2}} \left[ \{T_M(t) - T_W\} \frac{dR_c^2}{dt} \right]. \quad (3.3.6)$$

As a second approximation, it is assumed that the change of  $R_c^2$  with time is dominant as compared to the variation of  $T_M(t) - T_W$  in time. It follows from the numerical results shown in Section 3.3.3 that this assumption is acceptable. Therefore, equation (3.3.6) may be approximated by:

$$\dot{V}_M = -\pi \frac{\rho c}{\rho_1 l} \kappa^{\frac{1}{2}} {}_0D_t^{-\frac{1}{2}} \frac{d}{dt} \left[ \{T_M(t) - T_W\} R_c^2 \right]. \quad (3.3.7)$$

With the aid of the rule of the exponents (B5), and with  $T_M(0) - T_W = 0$ , equation (3.3.7) results in:

$$\dot{V}_M = -\pi \frac{\rho c}{\rho_1 l} \kappa^{\frac{1}{2}} {}_0D_t^{\frac{1}{2}} \left[ \{T_M(t) - T_W\} R_c^2 \right]. \quad (3.3.8)$$

Making use of composition rule (B6), one obtains:

$$T_M(t) - T_W = -\frac{\rho_1 l}{\rho c \kappa^{\frac{1}{2}}} \frac{1}{\pi R_c^2} {}_0D_t^{-\frac{1}{2}} \dot{V}_M. \quad (3.3.9)$$

For reasons which will become clear later, equation (3.3.9) will be further evaluated for a special case. When it is assumed that, during adherence times where microlayer evaporation is important (i.e. at times before contraction of the bubble foot starts),  $\dot{V}_M \propto t^m$  and  $R_c^2 \propto t^n$ , with  $m$  and  $n$  independent of time, then equation (3.3.9) results in:

$$T_M(t) - T_W = -\beta' \frac{\rho_1 l}{\rho c \kappa^{\frac{1}{2}}} {}_0D_t^{-\frac{1}{2}} \frac{\dot{V}_M}{\pi R_c^2}. \quad (3.3.10)$$

In (3.3.10), the coefficient  $\beta'$  is given by:

$$\beta' = \frac{\Gamma(m+1)\Gamma(m-n+3/2)}{\Gamma(m+3/2)\Gamma(m-n+1)}. \quad (3.3.11)$$

When  $n=0$ , i.e. when contraction of the bubble foot sets in, then  $\beta'=1$ . Initially, during a short time after nucleation, inertia-controlled growth dominates, resulting in  $m=2$  and  $n=2$ ; cf. Section 2.2.3.

In that case,  $\beta' = 8/15 \approx 1/2$ . When, at a later stage, diffusion-controlled growth occurs, without contraction of the bubble foot, then  $m = 1/2$  and  $n = 1$ ; cf. Section 2.2.2. In that case,  $\beta' = 1/2$ . Since initial time intervals, where contraction of the bubble foot does not yet take place, are most important for microlayer evaporation,  $\beta' = 1/2$  will further be used as an approximation.

We now turn our attention to evaporation at the bubble dome. Because in the liquid around the bubble dome both conduction and convection play a part, and since there is no spherical symmetry, the calculation of the temperature field is more difficult in this case than the calculation of the temperature field in the microlayer. For that reason, simplifications will be introduced, similar to those discussed in Chapter 2.

In Section 2.2.3, it has been shown that equation (2.2.35) represents a good approximation when bubble growth is considered. Furthermore, it has been shown in Section 2.5 that equation (2.2.35) can adequately describe the response to disturbances in the bubble growth rate. In the present situation, the bubble growth rate may be disturbed because, more-or-less suddenly, the bubble comes into contact with colder liquid, once it has grown to a sufficient size.

Application of equation (2.2.35) results in the following expression for the heat flux  $q_R$  at the bubble dome:

$$q_R(t) = -3^{\frac{1}{2}} \rho c \kappa^{\frac{1}{2}} D^{\frac{1}{2}} \left\{ T_R(t) - T_{\infty} \right\}, \quad (3.3.12)$$

where it is assumed that heat fluxes tangential to the bubble boundary are negligible. In principle, equation (3.3.12) only holds when  $T_{\infty}$  is independent of  $t$ ; however, as an approximation, the use of equation (3.3.12) will be extended to cases where  $T_{\infty} = T_{\infty}(t)$ , as discussed previously in Section 2.4.2.

From expression (3.3.12), the total heat flow to the vapour-liquid interface can be calculated by integration over the surface of the bubble dome:

$$\dot{\Phi}_R(t) = -\pi \rho c (3\kappa)^{\frac{1}{2}} \int_{\theta=0}^{\pi/2} R^2(\theta, t) \sin\theta \circ D_t^{\frac{1}{2}} \{T_R(t) - T_\infty(\theta, t)\} d\theta . \quad (3.3.13)$$

From (3.3.13), the volumetric flow rate at the bubble cap  $\dot{V}_R$  follows from the heat requirement  $\dot{\Phi}_R = \rho_1 \ell \dot{V}_R$ .

As shown in Section 2.4.2, the order of integration, and application of the  $\circ D_t^{\frac{1}{2}}$  operator, may be reversed when the decrease in the apparent contact angle is sufficiently slow. This results in:

$$\frac{\dot{V}_R(t)}{A(t)} = -(3\kappa)^{\frac{1}{2}} \frac{\rho c}{\rho_1 \ell} \circ D_t^{\frac{1}{2}} \{T_R(t) - \bar{T}_\infty(t)\} , \quad (3.3.14)$$

where the mean temperature  $\bar{T}_\infty(t)$  is given by:

$$\bar{T}_\infty(t) = \frac{2\pi}{A(t)} \int_{\theta=0}^{\pi/2} R^2(\theta, t) \sin\theta T_\infty(\theta, t) d\theta , \quad (3.3.15)$$

and  $A(t)$  represents the surface area of the bubble cap:

$$A(t) = 2\pi \int_{\theta=0}^{\pi/2} R^2(\theta, t) \sin\theta d\theta . \quad (3.3.16)$$

Inversion of expression (3.3.14) results in:

$$T_R - \bar{T}_\infty = \frac{\rho_1 \ell}{3^{\frac{1}{2}} \rho c \kappa^{\frac{1}{2}}} \circ D_t^{-\frac{1}{2}} \frac{\dot{V}_R}{A} . \quad (3.3.17)$$

The two equations (3.3.10, 17) must be combined with the following two expressions:

$$T_R(t) = T_M(t) = T_1(t) , \quad (3.3.18)$$

and

$$\dot{V} = \dot{V}_R + \dot{V}_M . \quad (3.3.19)$$

From (3.3.10, 17, 18, 19), the following simple expression for  $T_1$  is derived:

$$T_1(t) - \bar{T}_\infty = \frac{\rho_1 \ell}{\rho c \kappa^{\frac{1}{2}}} \circ D_t^{-\frac{1}{2}} \left\{ \frac{\dot{V}}{3^{\frac{1}{2}} A + 2\pi R_c^2} \right\} , \quad (3.3.20)$$

where  $\bar{T}_\infty$  is defined as:

$$\bar{T}_\infty = \frac{3^{\frac{1}{2}} A \bar{T}_\infty + 2\pi R_c^2 T_w}{3^{\frac{1}{2}} A + 2\pi R_c^2} \quad (3.3.21)$$

In (3.3.20), it has been assumed that  $R_c^2/A$  is independent of time, which is a reasonable assumption when contraction does not yet take place.

The set of equations (3.2.24), describing the flow field and the location of the vapour-liquid interface, has to be solved simultaneously with equation (3.3.20).

For that purpose, (3.3.20) will be transformed in such a way that it can be used in a standard routine for numerical integration of sets of coupled ordinary differential equations. To achieve this, the variables  $x$  and  $y$  are introduced in the following way:

$$x(t) = \frac{\dot{V}}{3^{\frac{1}{2}} A + 2\pi R_c^2} \quad (3.3.22)$$

$$y(t) = \left( \frac{T_1(t) - \bar{T}_\infty(t)}{T_w} \right)^2 \quad (3.3.23)$$

By squaring equation (3.3.20) and then differentiating with respect to time, the following differential equation for  $y$  is obtained:

$$\frac{dy}{dt} = \frac{1}{2\kappa Ja} {}_0 D_t^{-\frac{1}{2}} x {}_0 D_t^{\frac{1}{2}} x \quad (3.3.24)$$

The Riemann-Liouville operators in (3.3.24) will be approximated by the Grünwald series (B9), where  $N$  is taken to be finite.

In this way, (3.3.24) results in:

$$\frac{dy}{dt} = \frac{1}{2\kappa Ja} (x+s^+)(x-s^-) \quad (3.3.25)$$

where

$$s^+ = \frac{1}{\pi^{\frac{1}{2}}} \sum_{j=1}^{N-1} \frac{\Gamma(j+\frac{1}{2})}{\Gamma(j+1)} x(t-j\frac{t}{N}) \quad (3.3.26)$$

and



$$s^{-} = \frac{1}{2\pi^{\frac{1}{2}}} \sum_{j=1}^{N-1} \frac{\Gamma(j-\frac{1}{2})}{\Gamma(j+1)} x(t-j\frac{t}{N}) \quad (3.3.27)$$

For the numerical computation of the series (3.3.26, 27) representing the memory effects, it is essential that the values of  $x$  are stored at equal time intervals  $\Delta t$ . However, the integration of (3.3.25) from  $t$  to  $t+\Delta t$  may be performed with any subdivision of this fixed interval that is required for the numerical integration procedure.

The only unknown which has still to be determined is the temperature  $T_{\infty}(\theta, t)$  at the edge of the thermal boundary layer surrounding the bubble dome.

If the vapour produced at the vapour-liquid interface of the micro-layer is homogeneously distributed over the bubble cap, then the corresponding vapour velocity equals  $\dot{V}_M/A$ . In this way, the local heat requirement at  $r=R(\theta, t)$  is  $q_R = \rho_1 \ell \{(\underline{u} \cdot \underline{n})_{r=R} \dot{V}_M/A\}$ , and the heat flux in the liquid is given by:

$$q(r') = \left(\frac{3}{\pi\kappa}\right)^{\frac{1}{2}} \frac{T_w}{Ja} \int_{t'=0}^t \frac{\exp\left\{-\frac{(r')^2}{4\kappa(t'-t)}\right\}}{(t'-t)^{\frac{1}{2}}} q_R(t') dt' \quad (3.3.28)$$

where  $r' = r - R > 0$ ; cf. Carslaw and Jaeger (1967).

$\dot{V}_M/A$  can be determined by expression (3.3.9), and  $(\underline{u} \cdot \underline{n})_{r=R}$  follows from the solution of the flow field. The thickness  $r' = \delta(\theta, t)$ , where  $q(r')/q_R = 5\%$ , can be determined numerically, and the bulk temperature at that location is taken as  $T_{\infty}(\theta, t)$ .

Finally, the evolution in time of the bulk temperature will be discussed. Temperature gradients are small in the bulk liquid outside the thermal boundary layer, and heat transport is considered to take place by convection only. Thus equation (2.1.4) simplifies to:

$$\left(\frac{\partial}{\partial t} + u_r \frac{\partial}{\partial r} + \frac{u_{\theta}}{r} \frac{\partial}{\partial \theta}\right) T = 0 \quad (3.3.29)$$

Equation (3.3.31) expresses that the temperature does not change along a streamline. Consequently, when the initial temperature distribution is prescribed, the temperature field for  $t > 0$  can

easily be determined when the flow field in the liquid around the bubble is known.

3.3.3. *Example of growth and departure of a bubble in a non-homogeneous temperature field.*

The experiments were carried out in a boiling vessel described by Van Stralen, Cole, Sluyter and Sohal (1975).

Initial temperature fields were measured in the absence of a bubble. The temperature in the thermal boundary layer was determined by a thin thermocouple which could be moved in a vertical direction, while the temperature of the bulk liquid was determined by three fixed thermocouples. A result is plotted in Fig. 3.3, and it is seen that the profile is almost linear. For that reason, the initial temperature field in the calculations has been chosen as:

$$T_{\infty}(z,0) = \begin{cases} T_w + \frac{z}{H}(T_B - T_w) , & z \leq H \\ T_B & z \geq H \end{cases} \quad (3.3.30)$$

In (3.3.30),  $T_B = T_s + \Delta\theta^0$  and  $T_w = T_s + \theta^0$ , where  $\theta^0$  is the wall superheating, and  $\Delta\theta^0$  is the bulk superheating.

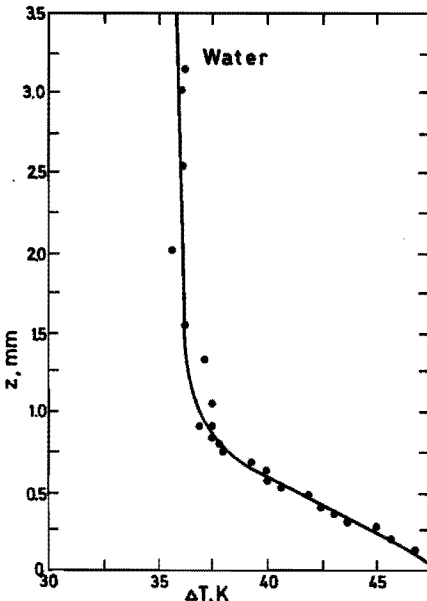


Fig. 3.3. Temperature profile above heated wall in water without bubbles

Further initial conditions are that the liquid is at rest, i.e.  $\phi(r, \theta, 0) = 0$ , and the initial bubble radius has been chosen as  $2R_e$ ; cf. equation (2.2.11).

As an illustration of the application of the numerical procedure described above, the example of water boiling at a subatmospheric pressure of 10 kPa is considered. The numerical results are compared with experimental ones.

Fig. 3.4 shows photographs taken from a high-speed film of a water vapour bubble at a pressure  $p_\infty$  of 10 kPa; the temperature of the superheated wall was 342K, and the corresponding saturation temperature  $T_g$  is 319 K. Hence, the initial wall superheating  $\theta^0$  is 23 K. The Jakob number belonging to this situation is 580. The bulk superheating  $\Delta\theta^0$  was small and could not be measured with the required accuracy because of pressure variations. For the calculations, the value  $\Delta\theta^0 = 0.1$  K has been chosen. In view of the data presented in Fig. 3.3,  $H$  was taken as 0.8 mm.

Fig. 3.5 shows the calculated bubble shapes; the solid lines at 6, 15, 30 and 40 ms represent the values calculated by the procedure described in this Chapter. The dotted lines represent the correction for microlayer formation, cf. Section 4.1, where also a plot of the microlayer thickness will be shown. The qualitative agreement of the bubble shapes obtained by theory and experiment is good.

Comparison of the theoretically and experimentally determined equivalent bubble radii, defined by  $R_{eq} = (3V/4\pi)^{1/3}$ , is presented in Fig. 3.6; the calculated values of  $R_{eq}$  are about 15% lower than the experimental values. By choosing somewhat higher values of  $H$  and  $\Delta\theta_0$ , it is possible to obtain a better agreement. Fig. 3.7 compares the theoretical and experimental values of the contact radius. It is observed that the contact radius, after an initial time interval of growth, decreases and becomes zero after 110 ms; at that time, the bubble leaves the wall. The calculated temperature of the bubble boundary is presented in Fig. 3.8; experimental data for the vapour temperature were not determined. It is to be noted that the calculated vapour temperature can even decrease below the saturation temperature.

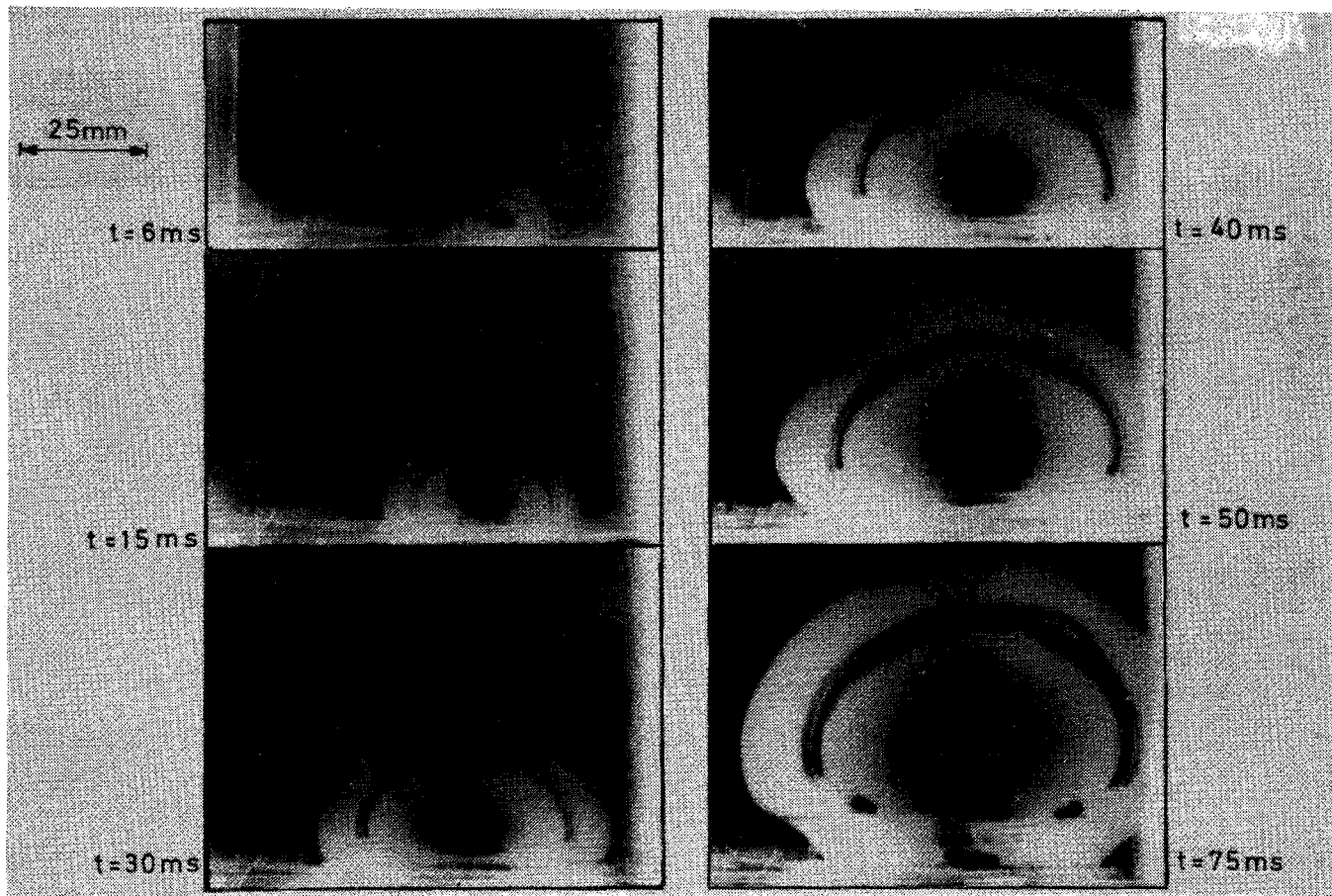


Fig. 3.4. Water boiling at 10 kPa; photographs from high-speed film

The initial growth of the bubble is shown in Fig. 3.9, where also the corresponding displacement of isotherms in the bulk liquid is shown. Fig. 3.10 represents the accompanying equivalent bubble radius and vapour temperature. Here also, no comparison with experiment can be given because of the short times involved.

Fig. 3.11 shows the hypothetical case where evaporation of the microlayer is not taken into account. As a result, the bubble size is decreased considerably. Also, when the initial wall superheating is decreased to 7 K, the bubble size is decreased, as is shown in Fig. 3.12.

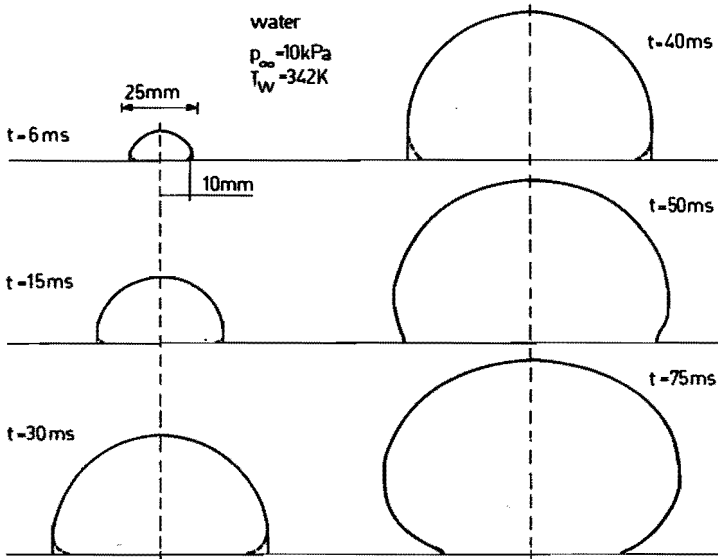


Fig. 3.5. Water boiling at 10 kPa;  
 numerically determined bubble shapes  
 of bubble shown in Fig. 3.4,  
 number of collocation points = 5,  
 maximum number of terms in (3.3.26, 27) = 30

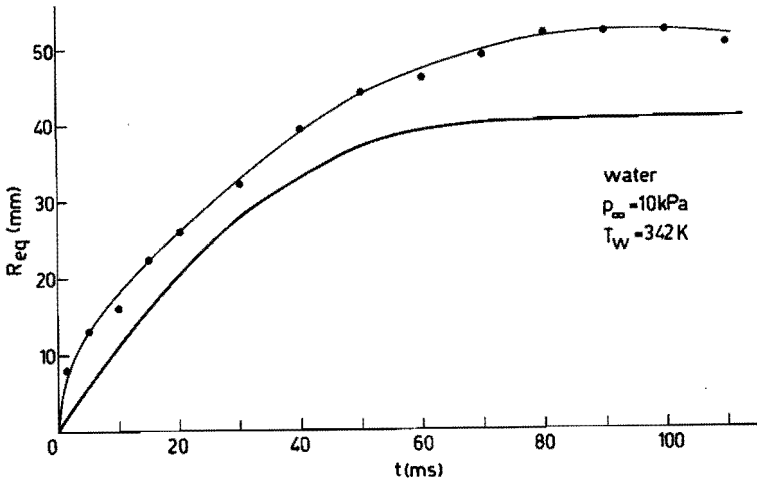


Fig. 3.6. Water boiling at 10 kPa;  
 equivalent bubble radius of bubble shown in Figs. 3.4, 5,  
 (•—•—•) experimental data  
 (—) numerically calculated values

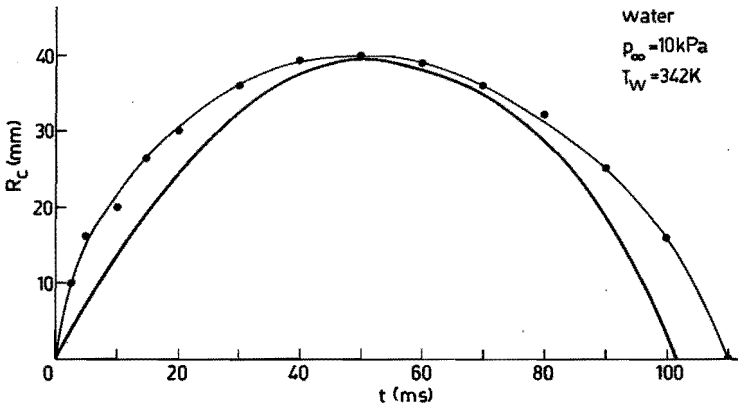


Fig. 3.7. Water boiling at 10 kPa;  
 contact radius of bubble shown in Figs. 3.4, 5, 6,  
 (•—•—•) experimental data  
 (—) numerically calculated values

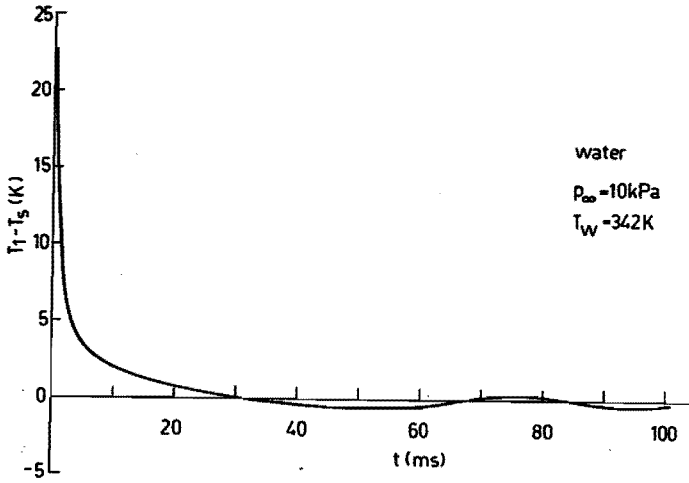


Fig. 3.8. Water boiling at 10 kPa;  
 calculated vapour temperature of bubble shown in Figs. 3.4, 5, 6, 7

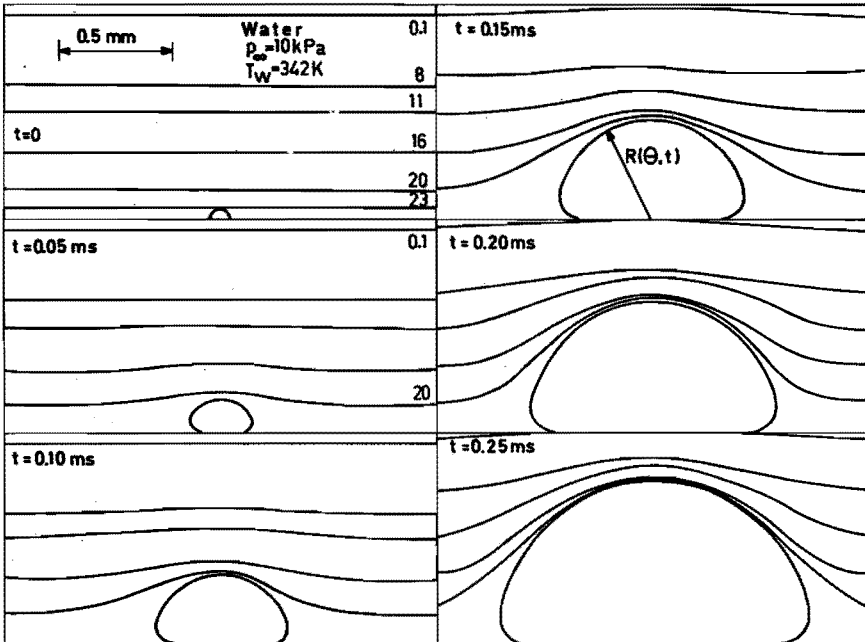


Fig. 3.9. Water boiling at 10 kPa;  
 calculated initial bubble shapes and isotherms  
 of bubble shown in Figs. 3.4, 5, 6, 7, 8

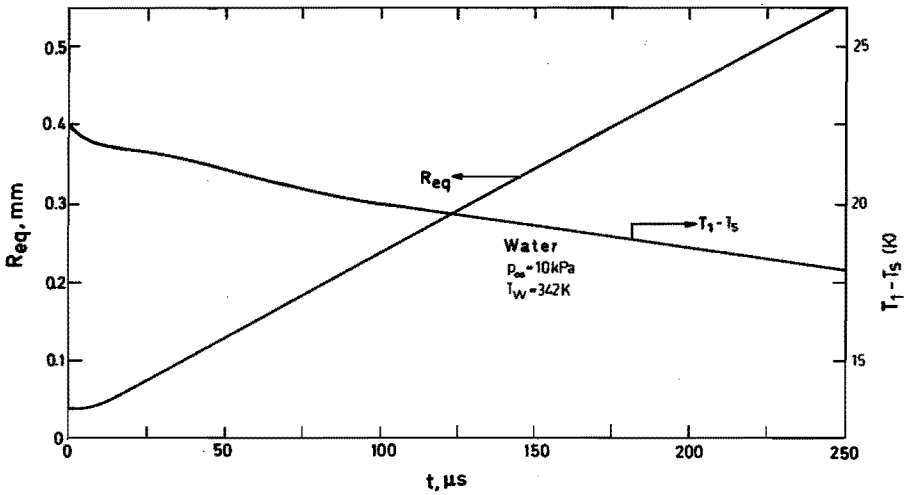


Fig. 3.10. Water boiling at 10 kPa; calculated initial equivalent bubble radius and vapour temperature of bubble shown in Figs. 3.4, 5, 6, 7, 8, 9

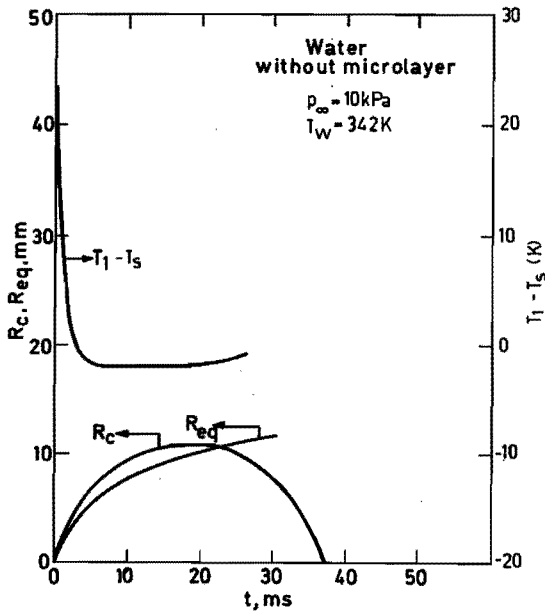


Fig. 3.11. Water boiling at 10 kPa; bubble shown in previous Figures, however, the effect of micro-layer evaporation has been neglected in the calculation



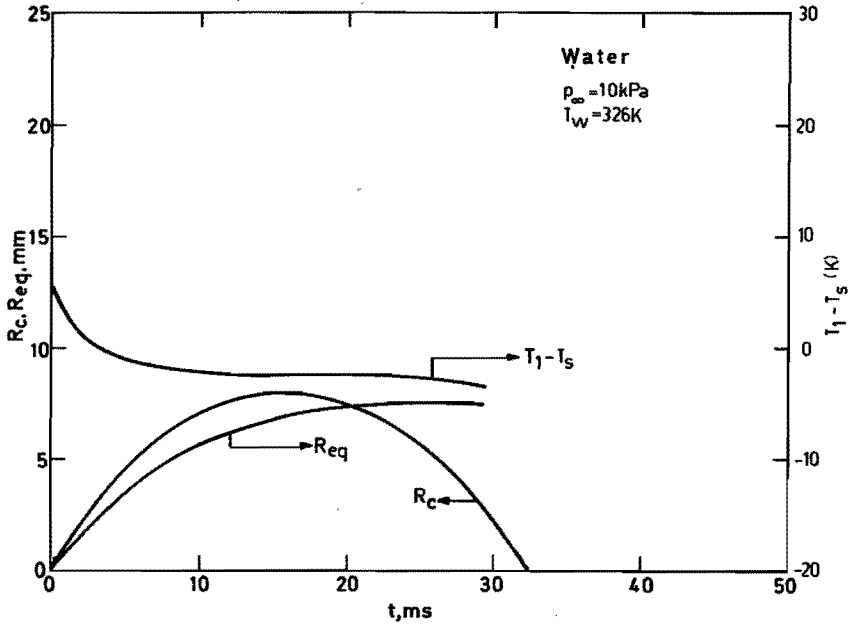


Fig. 3.12. Water boiling at 10 kPa;  
 bubble shown in previous Figures,  
 however, the wall superheating is 70% lower

From this example, the following conclusions can be drawn:

- i) The calculations presented in this Chapter agree qualitatively with the phenomena observed under experimental conditions; the calculations also represent a good explanation of the hydrodynamic mechanism of bubble departure.
- ii) The agreement between theory and experiment can be made quantitative by fitting of the parameters characterizing the initial temperature field in the calculations.
- iii) Better agreement can be obtained when more accurate local measurements of the temperature field are applied; in the latter case, also the calculation of the temperature field needs refinement.

CHAPTER 4

THIN LIQUID LAYERS IN RELATION TO BUBBLES GROWING AT A WALL

4.1. The thickness of formation of the liquid microlayer

4.1.1. Creeping flow in the meniscus region

When the gas-liquid interface is a single-valued function of  $r$ , the equation for the position of this moving surface in cylindrical coordinates  $(r,z)$  is written as, cf. Fig. 4.1 :

$$F(r,z,t) = z - h(r,t) = 0 \quad , \quad (4.1.1)$$

where again symmetry with respect to the  $z$ -axis is assumed.

From the general expression for the normal unit vector at this interface,  $\underline{n} = \nabla F / |\nabla F|$ , it is derived that the normal component of the rate of displacement of the interface is given by:

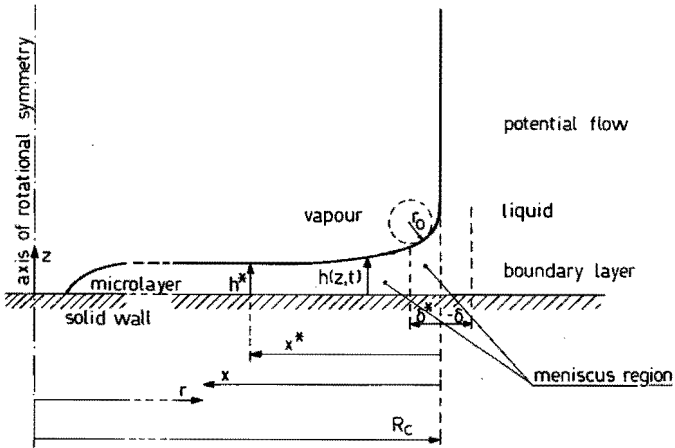


Fig.4.1. Flow regions of the liquid microlayer

$$\underline{n} \frac{\partial}{\partial t} (r, z)_h = \frac{\frac{\partial h}{\partial t}}{\left\{1 + \left(\frac{\partial h}{\partial r}\right)^2\right\}^{\frac{1}{2}}} . \quad (4.1.2)$$

The normal component of the liquid velocity at the interface is given by:

$$(\underline{u} \cdot \underline{n})_h = \frac{-u_h \frac{\partial h}{\partial r} + w_h}{\left\{1 + \left(\frac{\partial h}{\partial r}\right)^2\right\}^{\frac{1}{2}}} . \quad (4.1.3)$$

By analogy with the boundary conditions (2.2.3, 12), it can be found from equations (4.1.2, 3) that, when  $\rho_1 \ll \rho$  and heat conduction in the gaseous phase is negligible, then:

$$\frac{\partial h}{\partial t} + u_h \frac{\partial h}{\partial r} - w_h = -\frac{q_h \cdot \underline{n}}{\rho l} \left\{1 + \left(\frac{\partial h}{\partial r}\right)^2\right\}^{\frac{1}{2}} \approx -\frac{q_h}{\rho l} . \quad (4.1.4)$$

Here,  $(\rho_1/\rho)u_{1h}$  is not small with respect to  $u_h$ .

Equation (4.1.4) represents the kinematic boundary condition for a liquid layer.

When the lubrication approximation is made (i.e. when quasi steady Stokes flow is assumed, with  $\partial p/\partial z + \rho g = 0$  and  $|\partial(r\partial u/\partial r)/\partial r|/r \ll |\partial^2 u/\partial z^2|$ ), the momentum equation in the r-direction simplifies to:

$$\eta \frac{\partial^2 u}{\partial z^2} = \frac{\partial p}{\partial r} . \quad (4.1.5)$$

Since, in the lubrication approximation, the normal viscous stress is negligible with respect to the pressure differences, the discontinuity of normal stress over the gas-liquid interface leads to:

$$p = p_1 - \rho g(z-h) - \sigma \frac{\partial^2 h}{\partial r^2} - \frac{\sigma}{r} \frac{\partial h}{\partial r} . \quad (4.1.6)$$

In expression (4.1.6) it is assumed that  $(\partial h/\partial r)^2 \ll 1$  so that the expressions for the principal radii of curvature simplify.

The boundary condition for the tangential stress at the gas-liquid interface becomes:

$$\eta \left( \frac{\partial u}{\partial z} \right)_h = \left( \frac{\partial \sigma}{\partial r}, \frac{\partial \sigma}{\partial z} \right) \cdot \underline{t} \sim \frac{\partial \sigma}{\partial r} \quad (4.1.7)$$

Equation (4.1.7) represents the so-called Marangoni-Gibbs boundary condition; cf. Traykov and Ivanov (1977).

Surface tension gradients are caused by gradients in temperature, by gradients in concentration of surface impurities, or by gradients in electrical charge densities along the gas-liquid interface.

Use of the Marangoni-Gibbs boundary condition (4.1.7), in combination with the no-slip or adherence boundary condition  $u(r,0,t) = 0$  at the solid wall results, after integration of (4.1.5), in the following expression:

$$u = -\frac{1}{\eta} \frac{\partial p}{\partial r} z \left( \frac{1}{2} z - h \right) + \frac{z}{\eta} \frac{\partial \sigma}{\partial r} \quad (4.1.8)$$

The continuity equation reads:

$$\frac{\partial u}{\partial r} + \frac{u}{r} + \frac{\partial w}{\partial z} = 0 \quad (4.1.9)$$

From (4.1.8, 9), the following expression is derived:

$$w = -\frac{z^2}{2\eta} \left( \frac{\partial^2 p}{\partial r^2} + \frac{1}{r} \frac{\partial p}{\partial r} \right) + \frac{z^2}{2\eta} \frac{\partial p}{\partial r} \frac{\partial h}{\partial r} - \frac{z^2}{2\eta} \left( \frac{\partial^2 \sigma}{\partial r^2} + \frac{1}{r} \frac{\partial \sigma}{\partial r} \right) \quad (4.1.10)$$

Substitution of (4.1.8, 10) in the boundary condition (4.1.4) results in:

$$\frac{\partial h}{\partial t} + \frac{1}{r} \frac{\partial}{\partial r} \left\{ r \left( -\frac{h^3}{3\eta} \frac{\partial p}{\partial r} + \frac{h^2}{2\eta} \frac{\partial \sigma}{\partial r} \right) \right\} = -\frac{q_h}{\rho \ell} \quad (4.1.11)$$

The volumetric flow rate in the r-direction,  $\dot{\Gamma}$ , can be found by integration of (4.1.8) over the layer thickness, resulting in:

$$\dot{\Gamma} = 2\pi r \left( -\frac{h^3}{3\eta} \frac{\partial p}{\partial r} + \frac{h^2}{2\eta} \frac{\partial \sigma}{\partial r} \right) \quad (4.1.12)$$

From (4.1.12), it is observed that (4.1.11) may be interpreted as a global continuity equation; cf. Whitham (1974) and Section C5.

In the most important cases where surface tension gradients occur, these gradients are caused by variations of concentration of surfactants along the interface. For quasi-steady diffusion of impurities present in the liquid layer, Traykov and Ivanov (1977) derived the following expression for  $\partial\sigma/\partial r$ :

$$\frac{\partial\sigma}{\partial r} = \frac{\partial\sigma}{\partial C} \frac{\Gamma_s u_h}{\kappa h} \quad (4.1.13)$$

where  $\Gamma_s$  represents the surface concentration,  $C$  represents the bulk concentration and  $\kappa$  represents the diffusion coefficient.

Combination of (4.1.13) with (4.1.8) results in:

$$\frac{\partial\sigma}{\partial r} = -\frac{h}{2} \frac{\partial p}{\partial r} \frac{\frac{\partial\sigma}{\partial C} \frac{\Gamma_s}{\eta\kappa}}{1 - \frac{\partial\sigma}{\partial C} \frac{\Gamma_s}{\eta\kappa}} \quad (4.1.14)$$

Substitution of (4.1.14) into (4.1.12) results in:

$$\dot{\Gamma} = -\frac{2\pi r h^3}{3\beta_s \eta} \frac{\partial p}{\partial r} \quad (4.1.15)$$

where

$$\frac{1}{\beta_s} = \frac{1 - \frac{1}{4} \frac{\partial\sigma}{\partial C} \frac{\Gamma_s}{\eta\kappa}}{1 - \frac{\partial\sigma}{\partial C} \frac{\Gamma_s}{\eta\kappa}} \quad (4.1.16)$$

When there is no surface concentration, then  $\beta_s = 1$ ; however, as has been discussed by Groenveld (1970a), in many cases it is better to suppose that  $|\partial\sigma/\partial C| \Gamma_s / \eta\kappa \gg 1$ . In the latter case,  $\beta_s$  tends to 4 and this case is equivalent to the situation where  $u_h = 0$  at the interface. Impurities present in the gaseous phase do not influence the flow pattern in the liquid layer, as has been shown by Traykov and Ivanov (1977).

In the following treatment, it will be assumed that the term  $\sigma(\partial h/\partial r)/r$  in (4.1.6) is negligible with respect to the term  $\sigma \partial^2 h/\partial r^2$ ; cf. also Fig. 4.1. Also, since  $\rho g r_0^2/\sigma \ll 1$ , the term  $\rho g(z-h)$  in (4.1.6) is negligible with respect to the second order term. In this way,

equation (4.1.11) combined with (4.1.12, 15) simplifies to:

$$\frac{\partial h}{\partial t} + \frac{1}{r} \frac{\partial}{\partial r} \left( \frac{r \sigma h^3}{3\beta_s \eta} \frac{\partial^3 h}{\partial r^3} \right) = - \frac{q_h}{\rho \ell} . \quad (4.1.17)$$

During the growth process, microlayer formation only takes place in a region close to  $r = R_c$ ; consequently,  $r$  may be approximated by  $R_c$  in equation (4.1.17). In this way, (4.1.17) simplifies to the global continuity equation for a quasi one-dimensional layer:

$$\frac{\partial h}{\partial t} + \frac{\partial}{\partial r} \left( \frac{\sigma h^3}{3\beta_s \eta} \frac{\partial^3 h}{\partial r^3} \right) = - \frac{q_h}{\rho \ell} . \quad (4.1.18)$$

It is convenient to consider the process of microlayer formation in a coordinate system moving with the bubble contact radius  $R_c$ . For that reason, a coordinate transform  $x = R_c - r$  is introduced; cf. Fig. 4.1. The transformed equation (4.1.18) then becomes:

$$\frac{\partial h}{\partial t} + \frac{\partial}{\partial x} (R_c \dot{h} + \frac{\sigma h^3}{3\beta_s \eta} \frac{\partial^3 h}{\partial x^3}) = - \frac{q_h}{\rho \ell} . \quad (4.1.19)$$

Integration of (4.1.19) over the length of the layer from  $x$  to a value  $x^*$  outside the meniscus region, where  $\partial^3 h / \partial x^3 \rightarrow 0$ , results in:

$$\frac{\partial^3 h}{\partial x^3} = \frac{3\beta_s \eta R_c}{\sigma} \frac{h^* - h}{h^3} + \frac{3\beta_s \eta}{\sigma h^3} \int_x^{x^*} \left( \frac{\partial h}{\partial t} + \frac{q_h}{\rho \ell} \right) dx' , \quad (4.1.20)$$

where  $h = h^*$  at  $x = x^*$ .

For most cases of importance, the second term in the right-hand side of (4.1.20) is negligible, and the following dimensionless equation is obtained:

$$\frac{\partial^3 L}{\partial \lambda^3} = \frac{1-L}{L^3} , \quad (4.1.21)$$

where

$$L = \frac{h}{h^*} , \quad (4.1.22)$$

and

$$\lambda = \frac{x}{h^*} \left( \frac{3\beta_s \eta R_c}{\sigma} \right)^{1/3} . \quad (4.1.23)$$

It is now assumed that  $\lambda = \lambda^*$  is the location where the liquid microlayer becomes plane and parallel to the wall. Consequently, (4.1.21) must be solved with the following boundary conditions:

$$\begin{aligned} \lambda = \lambda^* : \quad L &\rightarrow 1 , \\ \partial L / \partial \lambda &\rightarrow 0 , \\ \partial^2 L / \partial \lambda^2 &\rightarrow 0 . \end{aligned} \quad (4.1.24)$$

In the region where  $\lambda \rightarrow 0$ , the dimensionless thickness  $L$  of the microlayer will be large compared to the minimum thickness  $L^* = 1$  at  $\lambda = \lambda^*$ . Consequently, following Landau and Levich (1942), the radius of curvature of the liquid layer when tending to  $\lambda \rightarrow 0$  may be approximated by:

$$r_0 = \lim_{L \rightarrow \infty} h^* \left( \frac{\sigma}{3\beta_s \eta R_c} \right)^{2/3} \left( \frac{\partial^2 L}{\partial \lambda^2} \right)^{-1} = \lim_{h \rightarrow \infty} \left( \frac{\partial^2 h}{\partial x^2} \right)^{-1} \quad (4.1.25)$$

Since, in addition,  $\lambda^*$  is large compared to  $L^* = 1$ , the boundary conditions (4.1.24) may be applied at  $\lambda = \lambda^* \rightarrow \infty$ .

Following Landau and Levich, a new variable is introduced:

$$\xi = \left( \frac{\partial L}{\partial \lambda} \right)^2 . \quad (4.1.26)$$

Combination of (4.1.21) with (4.1.26) results in a second order equation for  $\xi$  as a function of  $L$ :

$$\frac{\partial^2 \xi}{\partial L^2} = \frac{2(1-L)}{\xi^{1/2} L^3} . \quad (4.1.27)$$

With the aid of equation (4.1.21), Landau and Levich (1942) investigated in more detail the character of the behaviour of the derivatives  $\partial L / \partial \lambda$  and  $\partial^2 L / \partial \lambda^2$  for  $\lambda$  increasing to infinity. In this way, they derived the following boundary conditions for equation (4.1.27):

$$\lambda = \lambda^* \rightarrow \infty : \xi \rightarrow (1-L) , \quad \frac{\partial \xi}{\partial L} \rightarrow 2(L-1) . \quad (4.1.28)$$

To determine  $(\partial^2 L / \partial \lambda^2)_{L \rightarrow \infty} = \frac{1}{2} (\partial \xi / \partial L)_{L \rightarrow \infty}$ , Landau and Levich obtained a solution for the dimensionless equation (4.1.27) with boundary conditions (4.1.28). Their final result, substituted in (4.1.25), is:

$$h^* = f' \left( \frac{\beta_s \eta \dot{R}_c}{\sigma} \right)^{2/3} r_0 , \quad (4.1.29)$$

where  $f'$  was found by numerical integration.

In their original paper, Landau and Levich gave  $f' = 2.29 \times \sqrt{2}$ . However, this was due to a typographical error; Levich (1962) quotes  $f' = 0.93 \times \sqrt{2} = 1.315$ . Groenveld (1970a) introduced  $f' = 4/3$ , which will be used subsequently.

The importance of Landau and Levich's equation (4.1.29) is that it describes the thickness of microlayer formation when the minimum radius of curvature  $r_0$  in the meniscus region is known.

#### 4.1.2. Inertia effects in the meniscus region

To calculate the pressure in the potential flow region, cf. Fig. 4.1, the bubble is approximated by a hemisphere with radius  $R_c(t) = R(t)$ . Linearization of momentum equation (2.2.6) for  $0 \geq x = R_c - r > -\delta$ , with  $\delta/R_c \ll 1$ , then results in:

$$p_\phi(x, t) = p_\infty + \rho(R_c \ddot{R}_c + \frac{3}{2} \dot{R}_c^2) + \rho \{ \ddot{R}_c x - 3 \left( \frac{\dot{R}_c}{R_c} \right)^2 x^2 + O(x^3) \} . \quad (4.1.30)$$

According to the Rayleigh equation (2.2.10) where viscous effects have been neglected, the following expression relates the vapour pressure  $p_1(t)$  to the pressure  $p_\infty$  far away from the bubble:

$$p_\infty = p_1(t) - \rho \left( R_c \ddot{R}_c + \frac{3}{2} \dot{R}_c^2 \right) - \frac{2\sigma}{R_c} .$$



In the following treatment, terms of the order of magnitude  $\sigma/R_c$  will be neglected; cf. also Section 2.2.3.

Thus, it is found that:

$$p_\phi(x,t) = p_1(t) + \rho \left\{ \ddot{R}_c x - 3 \left( \frac{\dot{R}_c}{R_c} \right)^2 x^2 \right\}, \quad 0 \leq x < -\delta. \quad (4.1.31)$$

It is now assumed that expression (4.1.31) also holds in the meniscus region  $0 \leq x < \delta^*$ , with  $\delta^*/R_c \ll 1$ . This means, inter alia, that at  $x = 0$ , i.e. at  $r = R_c$ , the values of  $p$ ,  $\partial p/\partial x$  and  $\partial^2 p/\partial x^2$  are continuous.

On the other hand, from the boundary layer approximation  $\partial p_m/\partial z = 0$ , it follows for the pressure  $p_m(x,t)$  in the microlayer that:

$$p_m(x,t) = p_1(t) - \sigma \left( \frac{1}{R_1} + \frac{1}{R_2} \right),$$

where

$$\frac{1}{R_1} = \frac{\frac{\partial^2 h}{\partial x^2}}{\left\{ 1 + \left( \frac{\partial h}{\partial x} \right)^2 \right\}^{3/2}},$$

and  $R_2 \approx R_c$ . Consequently, when neglecting  $\sigma/R_c$ , the following expression holds:

$$p_m(x,t) = p_1(t) - \frac{\sigma \frac{\partial^2 h}{\partial x^2}}{\left\{ 1 + \left( \frac{\partial h}{\partial x} \right)^2 \right\}^{3/2}}, \quad x \geq 0. \quad (4.1.32)$$

Equating (4.1.31) to (4.1.32) results in:

$$\rho \left\{ \ddot{R}_c x - 3 \left( \frac{\dot{R}_c}{R_c} \right)^2 x^2 \right\} = - \frac{\sigma \frac{\partial^2 h}{\partial x^2}}{\left\{ 1 + \left( \frac{\partial h}{\partial x} \right)^2 \right\}^{3/2}}, \quad 0 \leq x < \delta^*. \quad (4.1.33)$$

After integration of (4.1.33) over  $x$ , between the boundaries  $0$  and  $x < \delta^*$ , the following expression results:

$$\sigma \left[ \frac{\frac{\partial h}{\partial x}}{\left\{ 1 + \left( \frac{\partial h}{\partial x} \right)^2 \right\}^{1/2}} + 1 \right] = - \frac{1}{2} \rho \left\{ \ddot{R}_c x^2 - 2 \left( \frac{\dot{R}_c}{R_c} \right)^2 x^3 \right\}, \quad 0 \leq x < \delta^*. \quad (4.1.34)$$

In (4.1.34), the integration constant has been determined with the condition that, at  $x = 0$ ,  $\partial h / \partial x \rightarrow -\infty$ .

Following Landau and Levich (1942),  $\delta^*$  is chosen in such a way that  $|\partial h / \partial x| \ll 1$  at  $x = \delta^*$ . The expression between square brackets in (4.1.34) can then be approximated by 1, and  $\delta^*$  is found as a root of the following third order polynomial :

$$ax^3 + bx^2 - c = 0 \quad , \quad (4.1.35)$$

where  $a = 2(\dot{R}_c / R_c)^2 \geq 0$ ,  $b = -\ddot{R}_c \geq 0$ , and  $c = 2\sigma/\rho \geq 0$ .

The real, positive solution which is continuous in  $a$ ,  $b$  and  $c$ , can be expressed in the following way:

$$\delta^* = f(a,b,c) = \begin{cases} f_1(a,b,c) & \text{if } 4b^3/27a^2c \leq 1 \quad , \\ f_2(a,b,c) & \text{if } 4b^3/27a^2c \geq 1 \quad . \end{cases} \quad (4.1.36)$$

In (4.1.36),  $f_1$  and  $f_2$  are defined as:

$$f_1 = -\frac{b}{3a} + \left(\frac{c}{a}\right)^{1/3} \left\{ \frac{1}{2} - \frac{b^3}{27a^2c} + \left( \frac{1}{2} - \frac{b^3}{27a^2c} \right)^{1/2} \right\}^{1/3} + \left(\frac{c}{a}\right)^{1/3} \left\{ \frac{1}{2} - \frac{b^3}{27a^2c} - \left( \frac{1}{2} - \frac{b^3}{27a^2c} \right)^{1/2} \right\}^{1/3} \quad , \quad (4.1.37)$$

$$f_2 = -\frac{b}{3a} + \frac{b}{3a} \cos \left\{ \frac{1}{3} \arccos \left( 1 - \frac{27a^2c}{2b^3} \right) \right\} + \frac{b\sqrt{3}}{3a} \sin \left\{ \frac{1}{3} \arccos \left( 1 - \frac{27a^2c}{2b^3} \right) \right\} \quad . \quad (4.1.38)$$

It is noted that, when  $4b^3/27a^2c = 1$ ,  $\delta^* = (c/4a)^{1/3} = (3c/4b)^{1/2} = b/3a$ .

The meniscus radius  $r_0$  at  $x = \delta^*$  is found by substitution of (4.1.36) in (4.1.33), and is given by:

$$\frac{1}{r_0} = \left( \frac{\partial^2 h}{\partial r^2} \right)_{x=\delta^*} = \frac{f}{c} (3af + 2b) \quad . \quad (4.1.39)$$

### 4.1.3. Thickness of microlayer formation

To elucidate the rather complex expression (4.1.39), some limiting cases will be considered first.

$$(i) \underline{4b^3 \ll 27a^2 c}$$

This is the case where  $-\rho R_c^4 R_c^3 \ll 54\sigma R_c^4$ , and it applies both during initial growth, where  $R_c \dot{R}_c \rightarrow 0$  and  $R_c \rightarrow 0$ , and during asymptotic, diffusion-controlled growth for sufficiently small Ja. In these cases, equation (4.1.39) for the meniscus radius simplifies with  $f_1 = (c/a)^{1/3}$  to:

$$r_o = \frac{1}{3} \left( \frac{\sigma}{\rho} \right)^{1/3} \left( \frac{R_c}{\dot{R}_c} \right)^{2/3}. \quad (4.1.40)$$

Following Landau and Levich (1942), the condition for matching solution (4.1.29) of the creeping flow region with solution (4.1.39) of the region where inertia effects play a part, is that the two values of  $r_o$  are the same.

In this way, the following result for the thickness of formation of the microlayer is obtained:

$$h^* = \frac{4}{9} \left( \frac{nv}{\sigma} \right)^{1/3} (\beta_s R_c)^{2/3}. \quad (4.1.41)$$

$$(ii) \underline{27a^2 c \ll 4b^3}$$

This is the case where  $54\sigma R_c^4 \ll -\rho R_c^4 R_c^3$ , and it applies during diffusion-controlled growth for sufficiently large Jakob number, and during contraction of the bubble foot when  $\dot{R}_c \rightarrow 0$ ; cf. Section 3.3.3. In this case, equation (4.1.39) simplifies with  $f_2 = (c/b)^{1/2}$  to:

$$r_o = \left( \frac{-\sigma}{2\rho \dot{R}_c} \right)^{1/2}. \quad (4.1.42)$$

With the aid of Landau and Levich's equation (4.1.29), the following expression for  $h^*$  is obtained using the matching procedure described in (i):

$$h^* = \frac{4}{3} \beta_s^{2/3} \left( \frac{\eta \dot{R}_c}{\sigma} \right)^{1/6} \left( \frac{-v \dot{R}_c}{2 \ddot{R}_c} \right)^{1/2} \quad (4.1.43)$$

It should be noted that the theory presented here was used by Landau and Levich (1942) to calculate the thickness of a liquid film, covering a solid plate which is withdrawn vertically from a liquid. In that case,  $-\ddot{R}_c$  in equation (4.1.42) has to be replaced by the gravitational acceleration  $g$ . For that case, experimental verification of equation (4.1.43) has been presented by Spiers, Subbaraman and Wilkinson (1974), and White and Tallmadge (1965) for  $\beta_s = 1$ , and by Groenveld (1970 a,b,c) for  $\beta_s = 1$  and  $\beta_s = 4$ . Levich (1962) also presents comparisons with experiment.

For a vapour bubble in the diffusion-controlled mode of growth, during times which are small with respect to the departure time, the radius of the bubble base  $R_c$  grows according to equations (2.2.34) and (2.3.8) like:

$$R_c(t) = \gamma(\kappa t)^{1/2} \quad (4.1.44)$$

Substitution of (4.1.44) in (4.1.41) and (4.1.43) results, for a pure solvent where  $\beta_s = 1$ , in:

$$\frac{h^*(t)}{(vt)^{1/2}} = \left( \frac{2}{3} \right)^2 \gamma^{2/3} Pr^{1/6} \left( \frac{\rho \kappa}{\sigma} \right)^{1/3} \left( \frac{\kappa}{t} \right)^{1/6}, \quad (4.1.45)$$

$$\text{when } \gamma^3 \ll \frac{3^6}{2} \frac{\sigma}{\rho \kappa} \left( \frac{t}{\kappa} \right)^{1/2},$$

and

$$\frac{h^*(t)}{(vt)^{1/2}} = \frac{2^{11/6}}{3} \gamma^{1/6} Pr^{1/6} \left( \frac{\rho \kappa}{\sigma} \right)^{1/6} \left( \frac{\kappa}{t} \right)^{1/12}, \quad (4.1.46)$$

$$\text{when } \gamma^3 \gg \frac{3^6}{2} \frac{\sigma}{\rho \kappa} \left( \frac{t}{\kappa} \right)^{1/2}.$$

The transitional case  $\gamma^3 \simeq (3^6 \sigma / 2 \rho \kappa) (t / \kappa)^{1/2}$  follows from the general equations (4.1.29, 39). A plot of  $h^*$  obtained in this way for the example treated in Chapter 3 is presented in Fig. 4.2.

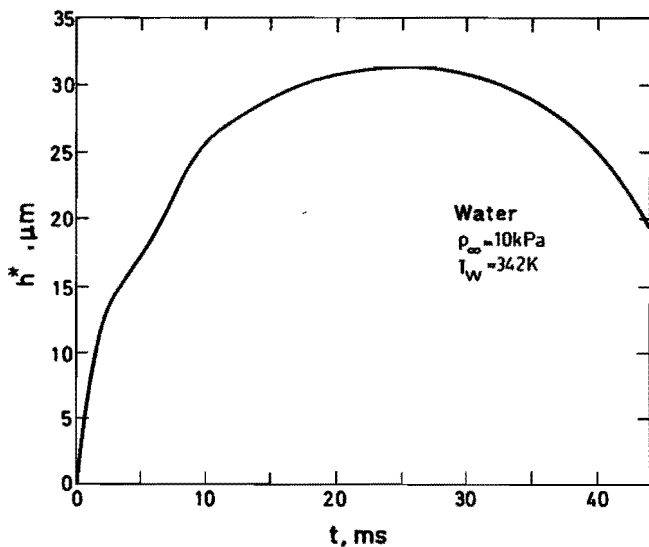


Fig. 4.2. Theoretical thickness of microlayer formation for the bubble shown in Chapter 3, Figs. 3.4, 5, 6, 7, 8, 9, 10

In the following discussion, more insight will be obtained from the limiting cases (4.1.45, 46).

For the case of diffusion-controlled growth during short times after nucleation, Van Ouwerkerk (1970, 1971) theoretically determined the displacement thickness  $z_o(t)$  of the hydrodynamic boundary layer at  $r = R_c(t)$ . His result reads:

$$z_{oD} = \frac{z_o(t)}{(vt)^{1/2}} = 1.27 \quad (4.1.47)$$

When  $h^* < z_o$ , not all the liquid of the hydrodynamic boundary layer is incorporated in the microlayer; consequently, an upward-directed flow along the bubble cap will be observed. Similarly, when  $h^* > z_o$ , there is a downward-directed flow. Such flow patterns have been observed experimentally by Baranenko, Chichkan, Nikolaev and Smirnov (1974), using an interferometric technique. These authors, however, explained the flows on the basis of the existence of surface tension

gradients which, as becomes clear from the foregoing discussion, are only partly responsible for these effects.

It has been suggested by Cooper and Lloyd (1969) that the thickness of microlayer formation can be taken as the displacement thickness of the hydrodynamic boundary layer. Many authors have followed this line of thought. However, in the same paper, Cooper and Lloyd already express their doubts concerning this assumption by remarking that the dependence on surface tension cannot be accounted for. Also, the effect of surface impurities, as expressed by the factor  $\beta_s$ , cannot be accounted for in this way.

Katto and Shoji (1970) and Katto, Takahashi and Yokoya (1973) also ventured criticism. On the basis of measurements of liquid microlayers in the case of air bubbles growing between two rigid walls, the latter authors proposed an empirical expression for  $h^*(t)$  in pool boiling under low pressures.

Before discussing these latter results, it will be elucidating to consider an interesting experimental study undertaken by Pike (1977); cf. also Cooper, Judd and Pike (1978). A test vessel was brought under free-fall conditions in a drop tower, thus introducing a zero gravity environment for the bubble. In the latter case, equation (4.1.45) holds during the complete adherence time. The method of measuring the microlayer thickness was similar to that described by Cooper and Lloyd (1969). To compare Pike's data with the theory presented here, a dimensionless time  $t_D$  will be introduced in the following way:

$$t_D = \frac{t}{2^{1/2} \frac{\gamma}{\rho} \text{Pr}^{1/4} \kappa^{3/2} / 3^{1/2} \sigma^2} \quad (4.1.48)$$

In this way, the dimensionless microlayer thickness  $h_D = h^*/(\nu t)^{1/2}$ , given by equation (4.1.45) reads:

$$h_D = t_D^{-1/6} \quad (4.1.49)$$

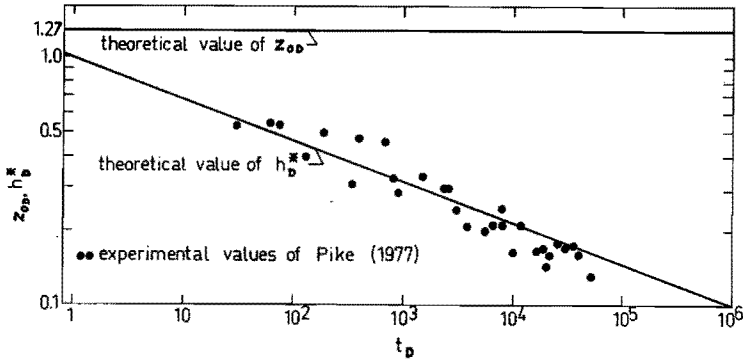


Fig. 4.3. Comparison of equation (4.1.45) with experimental values of Pike (1977).

A plot of equation (4.1.49) has been presented in Fig. 4.3, where comparison has been made with experimental data of Pike (1977). The agreement shows that the experiments are better described by the theory presented here than by the original suggestion  $h^* = z_o$ .

The other extreme case, represented by equation (4.1.46), has been investigated by Katto, Takahashi and Yokoya (1973), who considered pool boiling under low pressure. Since, in the latter case, the growth of the bubble base is not exactly represented by equation (4.1.44), the authors interpreted their results with the aid of the following expression:

$$R_c(t) = \gamma_s (\kappa t)^s. \quad (4.1.50)$$

In their experiments,  $s$  varied from 0.721 to 0.561 for different bubbles. The equivalent of equation (4.1.46) in this case becomes:

$$\frac{h^*(t)}{(\gamma t)^{1/2}} = \frac{4}{3} \frac{s^{1/6}}{(2-2s)^{1/2}} \gamma_s^{1/6} \text{Pr}^{1/6} \left(\frac{\rho \kappa}{\sigma}\right)^{1/6} \left(\frac{\kappa^s}{t^{1-s}}\right)^{1/6}. \quad (4.1.51)$$

When  $s = 1/2$ ,  $\gamma_s = \gamma$  and equation (4.1.51) reduces to (4.1.46).

Katto, Takahashi and Yokaya showed that their experimental data could be represented by:

$$\frac{h^*(t)}{(\nu t)^{1/2}} = \frac{4}{3} \frac{\gamma_s^{1/6} Pr^{1/6}}{s^{1/3}} \left(\frac{\rho K}{\sigma}\right)^{1/6} \left(\frac{\kappa^s}{t^{1-s}}\right)^{1/6} . \quad (4.1.52)$$

Equation (4.1.52) has been proposed on the basis of dimensional analysis, combined with the results of the study of flattened air bubbles between two parallel discs mentioned earlier. For  $s = 2/3 = 0.67$  the agreement with (4.1.51) is exact, and the agreement remains reasonable within the range of  $s$ -values considered.

Finally, the radius of curvature of the vapour-liquid interface in the meniscus region will be discussed.

Experimental observation of this radius is relatively easy, and it is therefore surprising that no attention has been paid to this subject in literature. Since Cooper and Lloyd's assumption  $h^* = z_0$  does not take into account the normal and tangential stress conditions in the meniscus region, their analysis cannot be applied to determine the radius of curvature in the meniscus region.

In an elucidating paper by Groenveld (1970a), it has been shown that the mean radius of curvature in the meniscus region,  $\bar{r}_0$ , is three times the minimum radius of curvature  $r_0$ , i.e.:

$$\bar{r}_0 = 3r_0 . \quad (4.1.53)$$

When restriction is again made to the asymptotic, diffusion-controlled mode of growth, the following expressions for  $\bar{r}_0$  follow from (4.1.40, 42):

$$\frac{\bar{r}_0(t)}{(\nu t)^{1/2}} = \frac{4^{1/3}}{Pr^{1/2}} \left(\frac{\sigma}{\rho K}\right)^{1/3} \left(\frac{t}{\kappa}\right)^{1/6} , \quad (4.1.54)$$

$$\text{when } \gamma^3 \ll \frac{3^6}{2} \frac{\sigma}{\rho K} \left(\frac{t}{\kappa}\right)^{1/2} ,$$

and

$$\frac{\bar{r}_0(t)}{(\nu t)^{1/2}} = \frac{3.2^{1/4}}{\gamma^{1/2} Pr^{1/2}} \left(\frac{\sigma}{\rho K}\right)^{1/2} \left(\frac{t}{\kappa}\right)^{1/4} , \quad (4.1.55)$$



when  $\gamma^3 \gg \frac{3^6}{2} \frac{\sigma}{\rho\kappa} \left(\frac{t}{\kappa}\right)^{1/2}$ .

Since  $Pr = \nu/\kappa$ , it is observed from (4.1.54, 55) that  $\bar{r}_0(t)$  does not depend on viscosity. This is in agreement with experimental observations of Cooper, Judd, Malcotsis and Pike (1975) and Cooper, Judd and Pike (1978) who state that viscosity has little effect on the bubble shape. Agreement between  $\bar{r}_0(t)$ -values calculated from equation (4.1.39) with experimental results is reasonable; cf. Fig. 3.4 compared to Fig. 3.5, cf. also Fig. 3.9.

#### 4.2. *The growth rate of a dry area*

##### 4.2.1. *Formation of an adsorption layer. Contact angle between the adsorption layer and the microlayer*

In the microlayer, a dry spot with radius  $R_d(t)$  may grow; cf. Fig. 1.2. Growth of the microlayer is caused by two mechanisms: (i) evaporation, resulting in so-called dry-out, and (ii) capillary effects. Since dry area growth by evaporation has been treated extensively in the literature, cf. e.g. Van Ouwerkerk (1970, 1971), here only dry area growth by capillary effects will be treated. Dry area growth in liquid films under isothermal conditions has applications beyond the field of microlayer behaviour, and the theory developed here will be used to explain the growth of the contact perimeter of a gas bubble on a wall in Section 4.3.

Under isothermal conditions, a completely *dry* area will not be formed, since it would be a violation of the adherence or no-slip condition at the solid wall. Instead, a thin microscopic liquid film, the so-called adsorption layer, remains at the wall. Since such a liquid film hardly evaporates, the name dry area for the part of the solid wall covered by the adsorption layer is acceptable. Since the surface tension of the adsorption layer is smaller than the surface tension of the microlayer (or bulk layer), a contact angle  $\Theta_0$  will be formed between the adsorption layer with thickness  $h_s$  and the bulk layer; cf. De Feijter and Vrij (1972), and cf. Fig. 4.4.

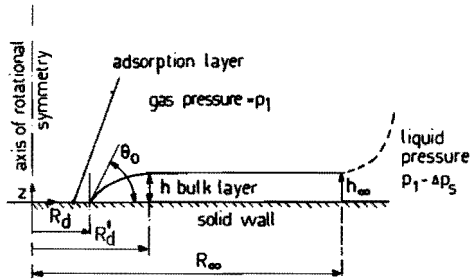


Fig. 4.4. Thin liquid layer adhering to a horizontal solid wall

In conclusion, it follows that:

$$\text{at } h = h_s, \quad \frac{\partial h}{\partial r} = \tan \theta_0. \quad (4.2.1)$$

For the rate of thinning of the bulk layer, the following equation can be obtained by combining equations (C53, 58, 62) from Appendix C:

$$\frac{\partial h}{\partial t} = \frac{2h^3}{3\eta r^2} \left[ \frac{\sigma \frac{\partial^2 h}{\partial r^2}}{\left\{1 + \left(\frac{\partial h}{\partial r}\right)^2\right\}^{\frac{3}{2}}} + \frac{\sigma \frac{\partial h}{\partial r}}{r \left\{1 + \left(\frac{\partial h}{\partial r}\right)^2\right\}^{\frac{1}{2}}} - \rho g(h - h_\infty) \right] - \frac{4h^3 \Delta p_s}{3\eta (R_\infty^2 - R_d^2)} \ln \frac{R_\infty}{R_d} - \frac{q_h}{\rho \ell}. \quad (4.2.2)$$

For the meaning of the symbols in equation (4.2.2) cf. also Fig. 4.4.

When, for a sufficiently large value of  $R_d$ , gravity, suction and evaporation are neglected, the rate of thinning of the liquid layer under the influence of capillary forces is given by the following equation:

$$\frac{\partial h}{\partial t} = \frac{2\sigma h^3}{3\eta r^2 \left\{1 + \left(\frac{\partial h}{\partial r}\right)^2\right\}^{\frac{3}{2}}} \frac{\partial^2 h}{\partial r^2}. \quad (4.2.3)$$

From (4.2.3), it is observed that for  $h = 0$ ,  $\frac{\partial h}{\partial t} = 0$ ; consequently, complete drying by capillary forces cannot occur in the present case.

However, as is discussed above, a 'dry' area is formed when a certain thickness,  $h_s$ , is reached by thinning; consequently, the condition (4.2.1) must be applied at the dry area radius  $r = R_d(t)$ . In this way, the evolution in time of  $R_d(t)$  can be determined with the aid of equation (4.2.3). Since it is customary to speak about 'slip' over the wall by the contact perimeter  $R_d(t)$ , the thickness  $h_s$  will further be referred to as the slip thickness.

It is a well-known phenomenon in surface chemistry that the contact angle is not a constant, but depends on the sign and magnitude of the velocity  $\dot{R}_d$ ; cf. Elliott and Riddiford (1967). Here,  $R_d > 0$ , and the so-called dynamic-receding contact angle must be used. In the following analysis this angle will be considered as constant.

#### 4.2.2. Dry area growth under the influence of surface tension

In this Section, the rate of expansion of a capillary-induced dry area will be investigated for liquid layers, which are sufficiently thin for gravity effects to be neglected. In that case, equation (4.2.3) must be solved with the boundary condition (4.2.1) applied at  $r = R_d$ .

It is convenient to consider the process of film thinning, and the resulting dry area growth or adsorption layer formation, in a coordinate system moving with the dry area radius  $R_d(t)$ . For that reason, a new coordinate  $x = r - R_d$  is introduced and the transformed equation (4.2.3) becomes:

$$\frac{\partial h}{\partial t} - \dot{R}_d \frac{\partial h}{\partial x} = \frac{2\sigma h^3}{3\eta(x+R_d)^2} \frac{\frac{\partial^2 h}{\partial x^2}}{\left\{1 + \left(\frac{\partial h}{\partial x}\right)^2\right\}^{\frac{3}{2}}}. \quad (4.2.4)$$

After some time, the influence of the initial conditions  $h(r,0)$  has disappeared, and the process of asymptotic dry area growth may be considered as quasi-steady; i.e. the term  $\partial h/\partial t$  in (4.2.4) may be neglected. Thus, integration of (4.2.4), with use of the boundary layer approximation  $x \ll R_d$ , results in:

$$\dot{R}_d \left( \frac{1}{h^2} - \frac{1}{h_\infty^2} \right) = \frac{4\sigma}{3\eta R_d^2} \frac{\frac{\partial h}{\partial x}}{\left[ 1 + \left( \frac{\partial h}{\partial x} \right)^2 \right]^{\frac{1}{2}}} . \quad (4.2.5)$$

In (4.2.5), the integration constant has been determined so that for  $h = h_\infty$ ,  $\partial h / \partial x = 0$ .

Substitution of condition (4.2.1) into (4.2.5) results in:

$$R_d^2 \dot{R}_d = \frac{4\sigma h_s^2 \sin \theta_o}{3\eta} . \quad (4.2.6)$$

Integration of (4.2.6), under the assumption that  $h_s$  and  $\theta_o$  are independent of time, results in:

$$R_d(t) = \left\{ R_{d_o}^3 + \frac{4\sigma h_s^2 \sin \theta_o}{\eta} (t - t_o) \right\}^{\frac{1}{3}} , \quad (4.2.7)$$

where  $R_{d_o}$  is the dry area radius at  $t = t_o$ .

To check equation (4.2.7), the following simple experiment was performed. A horizontal glass plate was covered with a thin layer of water. The thickness of the layer was 1.5 mm, and the layer was coloured with blue ink, so that it was clearly visible. At time  $t = 0$ , a drop of 1-Pentanol (amyl-alcohol) was allowed to fall upon the layer of coloured water. Since the 1-Pentanol has a surface tension which is much lower than that of water, a contact angle is formed between the 1-Pentanol and the water. As a consequence, the situation as shown in Fig. 4.4 is obtained, however, with a thin layer of 1-Pentanol instead of the adsorption layer. In a similar way as described above, the surface tension of the water will drive the liquid aside, and the area where a thin layer of 1-Pentanol is present will grow. The growth of this thin layer with radius  $R_d(t)$  was observed by high-speed cinematography. The result of one such experiment is shown in Fig. 4.5. A linear relationship between  $R_d^3$  and  $t$  holds indeed during a certain time interval.

Next, a numerical example of dry area growth by capillary effects in a microlayer of a water vapour bubble will be considered.

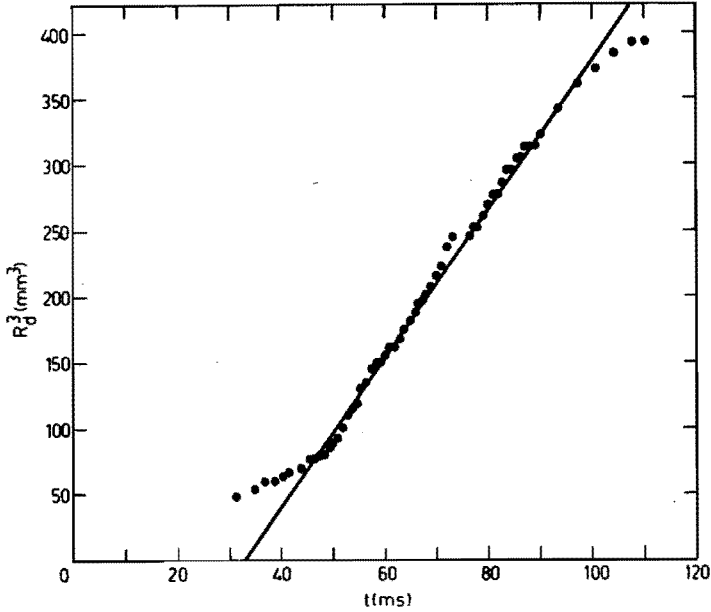


Fig. 4.5. Experimental data for the radius vs. time of a thin layer of 1-Pentanol driving aside a layer of water

For water, at  $T = 373 \text{ K}$ ,  $\sigma = 0.06 \text{ N/m}$  and  $\eta = 3 \times 10^{-4} \text{ Pa.s}$ . A value of  $\theta_0 = \pi/6$  is chosen, whilst  $h_s = 0.1 \text{ }\mu\text{m}$  may be considered as an acceptable value; cf. Ludviksson and Lightfoot (1968). Thus,  $4\sigma h_s^2 \sin \theta_0 / \eta = 4 \times 10^{-12} \text{ m}^3/\text{s}$ . In this example,  $R_{d0}$  is the radius of the cavity where the bubble is nucleated, and its magnitude will be chosen as  $1 \text{ }\mu\text{m}$ . Thus, it follows from equation (4.2.7) that, after  $5 \text{ ms}$ ,  $R_d$  has grown from  $1 \text{ }\mu\text{m}$  to  $27 \text{ }\mu\text{m}$ .

It has been found by several authors, among which Van Ouwerkerk (1970, 1971), that, in that time interval, evaporation may cause the dry area radius to grow to a value of several millimeters; consequently, in water under ordinary boiling conditions, the effect of capillary on dry area formation is of the order of a few percents.

### 4.3. Gas bubble departure as governed by the growth of the bubble contact perimeter

In this Section, the theory for the description of dry area formation in a thin liquid film under the action of capillary forces, will be extended to the description of growth of the contact area between a gas bubble and the wall to which it adheres.

When gas bubbles are considered, the process of bubble departure cannot be described by the theory presented in Chapter 3, upon which the simple model of Section 2.3.1 is based, because for gas bubbles  $Ja \ll 1$ , and the bubbles grow relatively slowly, i.e.,  $\gamma \ll 1$ . Furthermore, the Schmidt number  $Sc = \kappa/\nu$  is also small with respect to one; cf. the numerical example in Section 2.2.2. It then follows from equations (4.1.44) and (4.1.45) that the thickness of formation of the microlayer is much larger than the bubble dimensions. Consequently, the theory of microlayer formation, presented in Section 4.1, does not apply in this case, and a microlayer is not formed. Instead, the bubble makes contact with the wall at the perimeter of the adsorption layer, or 'dry' area, i.e.  $R_d = R_c$ ; cf. Fig. 1.1. The bubble adheres as long as the upward buoyancy force is smaller than the downward force of adhesion.

After nucleation, cf. Figs.4.6a,b, the bubble radius is approximately equal to the radius  $R_0$  of the cavity where the bubble is formed. At that time, the apparent contact angle is about  $\frac{1}{2}\pi$ . As the bubble grows, the bubble contact radius also spreads beyond the cavity, as will be explained subsequently.

During growth, the apparent contact angle,  $\theta_a$ , cannot immediately be equal to the natural contact angle  $\theta_0$ , cf. Fig. 4.6c. Consequently, a liquid 'layer' extending only over the short distance from  $R_c$  to  $R_\infty$ , may be supposed to exist near the bubble contact perimeter, cf. Fig. 4.6d.

As has been illustrated in Fig. 4.6, initially, when the bubble contact radius starts growing beyond the cavity radius,  $\theta_a/\theta_0 \gg 1$ . For this latter case, it will be shown that the bubble contact

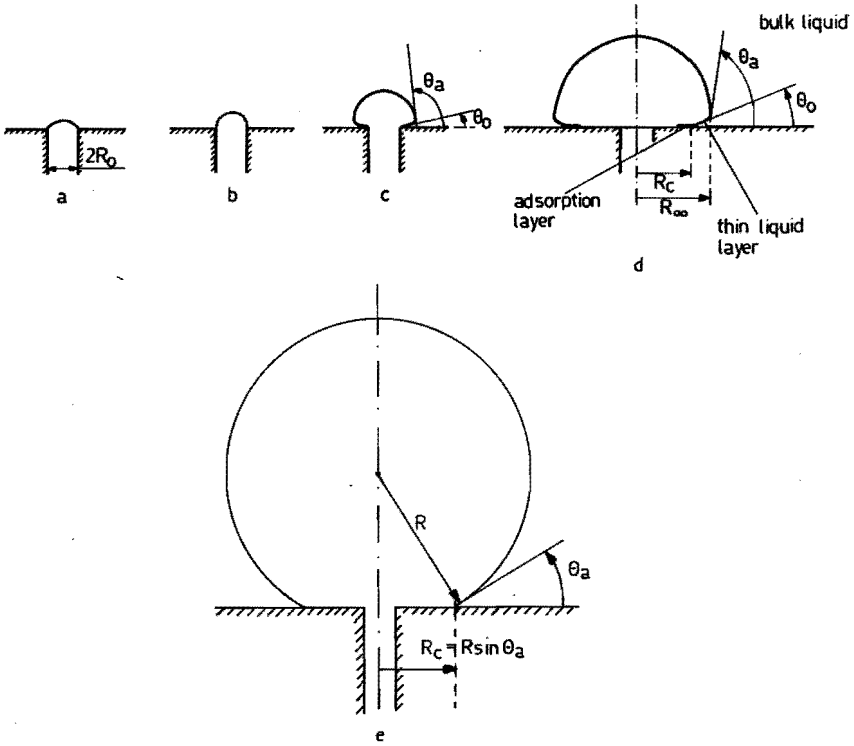


Fig. 4.6. Nucleation and growth of a gas bubble at a horizontal wall

perimeter can grow indeed. First, the extreme case where the rate of growth of the actual contact radius,  $\dot{R}_c$ , is lagging behind the component of the bubble growth rate parallel to the wall,  $\dot{R} \sin \theta_a$ , will be considered, i.e.  $\dot{R}_c \ll \dot{R} \sin \theta_a$ , or  $\dot{\theta}_a < 0$ ; cf. Fig. 4.6e.

Assume that, in that case, the curvature of the gas-liquid interface in the region  $R_c < r < R_\infty$  may be neglected with respect to the curvature of the bubble boundary  $1/R(t)$ . Then surface tension forces are negligible with respect to the suction pressure in equation (4.2.2).

Also, since the layer extends over a relatively short distance, it may be assumed that  $R_\infty \approx R_c = R_d$  in equation (4.2.2). Consequently, the rate of thinning is governed by the following equation:

$$\frac{\partial h}{\partial t} = - \frac{4\sigma h^3}{3\eta R_c^2 R}, \quad (4.3.1)$$

where  $\Delta p_s = 2\sigma/R$ .

In the same way as in the discussion presented in Section 4.2.2, it is assumed that the process of film thinning is almost steady in a coordinate system moving with the velocity of the contact radius  $R_c(t)$ . In this way, the following expression is derived from (4.3.1):

$$\dot{R}_c \frac{\partial h}{\partial r} = \frac{4\sigma h^3}{3\eta R_c^2 R}. \quad (4.3.2)$$

At  $r = R_c$ ,  $h = h_s$ , and  $\partial h/\partial r = \tan \Theta_o$ . Substitution of the latter conditions in (4.3.2) results in:

$$\frac{dR_c^3}{dt} = \frac{4\sigma h_s^3}{\eta \tan \Theta_o R}. \quad (4.3.3)$$

Under the assumption that  $h_s$  and  $\Theta_o$  are constant, it follows with  $R = \gamma(\kappa t)^{\frac{1}{2}}$  that:

$$R_c = [R_{c0}^3 + \frac{8\sigma h_s^3}{\eta \gamma \kappa^{\frac{1}{2}} \tan \Theta_o} (t^{\frac{1}{2}} - t_0^{\frac{1}{2}})]^{\frac{1}{3}}. \quad (4.3.4)$$

In many cases, however, the growth rate  $\dot{R}_c$  predicted by equation (4.3.4) is not small with respect to  $\dot{R} \sin \Theta_a$ . In that case, the assumption of negligible curvature in the liquid layer no longer holds. When the principal radii of curvature  $1/R_1$  and  $1/R_2$  in the region  $R_c < r < R_\infty$  are no longer negligible, equation (4.2.2) reads:

$$\frac{\partial h}{\partial t} = \frac{2\sigma h^3}{3\eta R_c^2} \left( \frac{1}{R_1} + \frac{1}{R_2} - \frac{2}{R} \right), \quad (4.3.5)$$

where again  $\Delta p_s = 2\sigma/R$ .

In the limit  $R_1 \rightarrow R$ ,  $R_2 \rightarrow R$ ,  $\partial h/\partial t \rightarrow 0$ ; i.e. the rate of thinning decreases when the gas-liquid interface in the region  $R_c < r < R_\infty$  is curved. This explains why the growth rate of the bubble contact



radius will not exceed the value  $\dot{R} \sin \theta_a$ , and consequently  $\dot{\theta}_a \leq 0$ .

During adherence, the apparent contact angle  $\theta_a$  may gradually decrease and, at a certain time,  $\theta_a = \theta_o$ . When this situation is reached, again two possibilities arise:

- (i) the growth rate of the bubble contact radius lags behind  $\dot{R} \sin \theta_o$ , i.e. the situation  $\theta_a \ll \theta_o$  will occur. In this case, the curvature in the region  $R_c < r < R_\infty$  may be assumed to be large with respect to  $1/R(t)$ ; cf. Fig. 1.1. Consequently, the growth of  $R_c$  must be described by equation (4.2.7).
- (ii) As previously discussed, the second possibility is that the growth rate of the contact area follows the growth of the bubble radius, and  $\theta_a \approx \theta_o$ . In the literature, it is often assumed that  $\theta_a = \theta_o$ , i.e. that  $\dot{R}_c = \dot{R} \sin \theta_o$  and, consequently, that the bubble foot moves smoothly over the wall when the bubble grows. For the latter case, Fritz's equation (2.4.28) for the departure diameter holds.

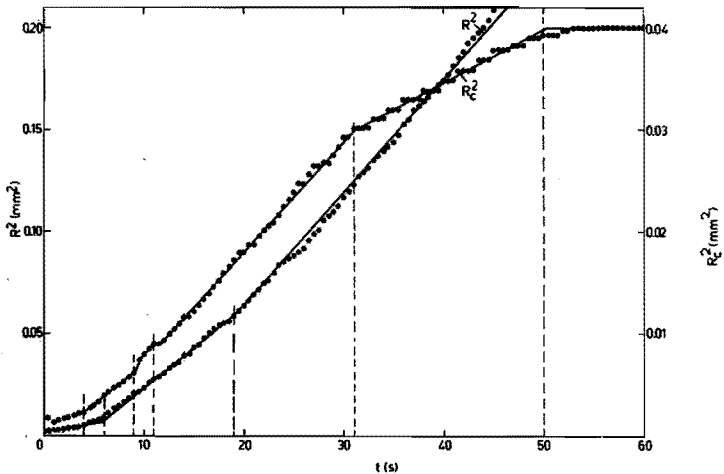


Fig. 4.7. Experimentally determined radii vs. time of a  $\text{CO}_2$ -bubble in beer

In the previous discussion, an explanation is given of the hydrodynamics of the growth of the bubble foot. Now, as an illustration, results of a simple experiment will be reported. Fig. 4.7 shows  $R^2$  and  $R_c^2$  vs.  $t$  for a  $\text{CO}_2$ -bubble growing in beer. The bubble adheres to a brass wall. It is observed that, during the first 31 s of bubble growth, the growth rate of the bubble foot does not lag behind  $\dot{R} \sin \theta_a$ . Hence equations (4.3.4) and (4.2.7) cannot be applied in this time interval and they predict too high a value for  $\dot{R}_c$ .

However, it is observed that, after  $t = 31$  s, the bubble foot is lagging behind the bubble radius and, at  $t = 50$  s, a constant value  $R_c = 0.2$  mm is reached. It was seen from the experimental results that the maximum value of  $R_c$  is not reproducible very well and, consequently, since the departure radius of gas bubbles strongly depends on  $R_c$ , it is not possible to predict accurately the departure radius in this case.

#### 4.4. Conclusions

In this Chapter, the hydrodynamic aspects of the phenomena occurring between the bubble and the horizontal solid wall have been investigated.

In Section 4.1, a theory has been developed for the description of the thickness of formation of the liquid micro-layer between a rapidly-growing vapour bubble and a wall. The theory has been compared with experimental results of Pike (1977) and Katto, Takahashi and Yokoya (1973). The agreement shows that the experiments are better described by the theory presented here than by previous theories found in the literature.

In Section 4.2, the growth of a dry area in the microlayer is considered. Since in the literature dry area formation caused by evaporation has been treated extensively, here dry area formation by capillary effects is treated only. The physical model is described

in Appendix C, and an approximate equation for the rate of dry area growth has been derived. It is shown that, for water vapour bubbles under ordinary boiling conditions, capillary effects only contribute a few percents to dry area growth; this constitutes a theoretical verification of the assumption made in the literature, that capillary effects may be neglected with respect to evaporation.

In Section 4.3, the theory developed in Section 4.2 is used to show that the base of a slowly-growing gas bubble can grow beyond the cavity where it was nucleated. It is explained that, during a certain time interval, the apparent contact angle of the bubble may be constant. On this latter assumption, the well-known Fritz equation (2.4.28) for bubble departure is based. However, after a sufficiently long time of bubble growth, the apparent contact angle decreases and, consequently, Fritz's equation cannot be used. These theoretical results are also illustrated by an experimental example.

APPENDIX A

*Equations of motion for potential flow around spherical bubbles*

When the flow field is not spherically symmetric, the Rayleigh equation (2.2.10) does not hold. However, when rotational symmetry is assumed around a spherical bubble, the equations of motion can be derived easily by using potential flow theory. In order to show the validity of certain equations for single bubbles, and for the purpose of an order of magnitude estimation (cf. Section 2.3.3), the equations of motion of two neighbouring bubbles will be considered here; cf. Fig. A1.

The general solution of the potential equation (2.1.15) for flow around two bubbles is given by:

$$\phi(\underline{r}, t) = \sum_{i=0}^{\infty} \frac{a_i(t)}{r(t)^{i+1}} P_i\{\cos \Theta(t)\} + \sum_{i=0}^{\infty} \frac{a_i^*(t)}{r^*(t)^{i+1}} P_i\{\cos \Theta^*(t)\}. \quad (A1)$$

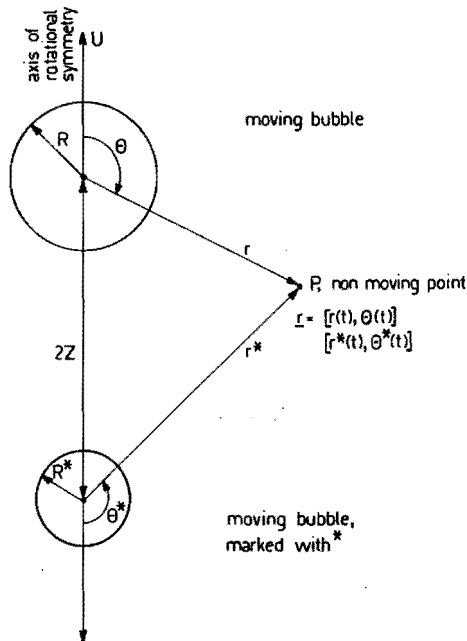


Fig. A1. Configuration of two spherical bubbles

The spherical coordinate systems  $\{r(t), \theta(t)\}$  and  $\{r^*(t), \theta^*(t)\}$  are fixed with respect to the two moving bubbles. The quantities for one of the bubbles are distinguished from those of the other bubble by the superscript \*. In (A1)  $\theta$  represents the azimuthal angle.

For our purpose, it is sufficient to consider the influence of *growth* of one spherical bubble on the growth and translation of another spherical bubble. In that case, the result must be correct up to order  $(R/z)^2$  and  $(R^*/z)^2$ , and only the monopole and dipole terms of expression (A1) play a part; cf. e.g. Isenberg and Sideman (1971). Consequently, expression (A1) simplifies to:

$$\phi(\underline{r}, t) = \frac{a_0}{r} + \frac{a_1}{r^2} \cos \theta + \frac{a_0^*}{r^*} + \frac{a_1^*}{(r^*)^2} \cos \theta^*. \quad (\text{A2})$$

The coordinate  $r^*$  can be determined from  $r$ ,  $z$  and  $\cos \theta$  with the aid of the cosine rule:

$$r^* = (r^2 + 4rz \cos \theta + 4z^2)^{\frac{1}{2}}. \quad (\text{A3})$$

By making use of the Poisson formula, cf. e.g. Butkov (1973), one obtains:

$$\frac{2z}{r^*} = \frac{1}{\left\{1 + \frac{r}{z} \cos \theta + \left(\frac{r}{2z}\right)^2\right\}^{\frac{1}{2}}} = \sum_{i=0}^{\infty} (-1)^i \left(\frac{r}{2z}\right)^i P_i(\cos \theta). \quad (\text{A4})$$

In the following treatment, the flow field in the neighbourhood of the upper bubble will be considered; i.e. the point P in the flow field is chosen near  $r = R$ ; cf. Fig. A1. Consequently, expression (A4) simplifies to:

$$\frac{1}{r^*} = \frac{1}{2z} - \frac{r \cos \theta}{4z^2}. \quad (\text{A5})$$

From the cosine rule  $r = \{(r^*)^2 + 4r^*z \cos \theta + 4z^2\}^{\frac{1}{2}}$ , combined with (A5), one obtains:

$$\cos \theta^* = -1 + \frac{1}{8} \left(\frac{r}{z}\right)^2. \quad (\text{A6})$$

Substitution of (A5,6) into (A2) results in:

$$\phi(\underline{r},t) = \frac{a_0}{r} + \frac{a_0^*}{2z} - \frac{a_1^*}{4z^2} + \left( \frac{a_1}{r^2} - \frac{a_0^* r}{4z^2} \right) \cos \theta. \quad (A7)$$

For a translating spherical bubble, the equivalent of the kinematic boundary condition (2.2.4) becomes:

$$\left( \underline{u}_r \right)_{r=R} = \dot{R} + U \cos \theta. \quad (A8)$$

Making use of equation (2.1.15), i.e. of  $\underline{u} = \nabla\phi$ , it is easily seen from (A7,8) that the following expressions hold:

$$a_0 = -R^2 \dot{R}, \quad (A9)$$

$$a_1 = -\frac{1}{2}R^3 U - \frac{a_0^* R^3}{8z^2}. \quad (A10)$$

In a similar way, it can also be derived that:

$$a_0^* = -(R^*)^2 \dot{R}^*, \quad (A11)$$

$$a_1^* = -\frac{1}{2}(R^*)^3 U^* - \frac{a_0 (R^*)^3}{8z^2}. \quad (A12)$$

Substitution of (A11) into (A10) results in:

$$a_1 = -\frac{1}{2}R^3 U + \frac{1}{8} \left( \frac{RR^*}{z} \right)^2 RR^*. \quad (A13)$$

Similarly, it is found that:

$$a_1^* = -\frac{1}{2}(R^*)^3 U^* + \frac{1}{8} \left( \frac{RR^*}{z} \right)^2 R^* \dot{R}^*. \quad (A14)$$

It is remarked here, that substitution of (A9,11,13,14) into (A2) gives the same result as obtained from an exact expression for  $\phi$  derived by Isenberg and Sideman (1971), when terms of order  $(R/z)^3$  and higher orders are neglected.

With the aid of expressions (A9,11,13,14), the expression  $(\nabla\phi)^2$  in the Bernoulli equation (2.1.16) at  $r = R$  can be expressed in  $R, \dot{R}, U, R^*, \dot{R}^*$  and  $U^*$ . In the latter expression, terms in  $U^2 \cos 2\theta$  also occur due to its non-linear character. The occurrence of terms in  $\cos 2\theta$  indicate that a translating spherical bubble cannot exactly satisfy the dynamic boundary condition equivalent to (2.2.7); i.e. a deviation from the spherical shape will occur. However, in the following treatment, cases where  $U \ll \dot{R}$  will be considered only, so that terms in  $\cos 2\theta$  are sufficiently small.

Also the term  $(\partial\phi/\partial t)_{r=R}$ , occurring in the Bernoulli equation, can be expressed in  $R, \dot{R}, U, R^*, \dot{R}^*$ , and  $U^*$ . When evaluating this term, expressions for  $\dot{r}, \dot{r}^*, \dot{\theta}$  and  $\dot{\theta}^*$  are needed. For spherical bubbles the following expressions are easily obtained:

$$\dot{r} = -U \cos \theta, \quad \dot{r}^* = -U^* \cos \theta^*, \quad (\text{A15})$$

$$\dot{\theta} = \frac{U}{r} \sin \theta, \quad \dot{\theta}^* = \frac{U^*}{r^*} \sin \theta^*. \quad (\text{A16})$$

Further, it will be assumed that the surface tension along the vapour-liquid interfaces changes with  $\theta$  in the following way:

$$\sigma = \sigma_0 + \sigma' \cos \theta, \quad \sigma^* = \sigma_0^* + (\sigma')^* \cos \theta^*. \quad (\text{A17})$$

With the expression for the normal viscous stress  $\tau_n = 2\eta\partial u_r/\partial r$ , the following two expressions are found by application of the Bernoulli equation (2.1.16) at the vapour-liquid interface  $r = R$ :

$$\begin{aligned} & RR\dot{R} + \frac{3}{2} \dot{R}^2 - \left(\frac{U}{4}\right)^2 + \frac{R^*}{z} \left( \frac{R^* \dot{R}^*}{2} + (\dot{R}^*)^2 \right) - \frac{1}{8} \left(\frac{R^*}{z}\right)^2 (R^* \dot{U}^* + 5\dot{R}^* U^* - \frac{\dot{R}^* U^*}{4}) = \\ & = \frac{p_R - p_\infty}{\rho} - \frac{2\sigma_0}{R} - \frac{4\eta\dot{R}}{\rho R}, \end{aligned} \quad (\text{A18})$$

$$\begin{aligned} & R\dot{U} + 3\dot{R}U - \frac{3}{4} \left(\frac{R^*}{z}\right)^2 (R\dot{R}^* + \dot{R}\dot{R}^*) - \frac{3}{2} \frac{RR^*}{z^2} (\dot{R}^*)^2 = \\ & = 2gR - \frac{4\sigma'}{\rho R} - \frac{12\eta U}{\rho R} + \frac{3\eta}{\rho} \left(\frac{R^*}{z}\right)^2 \frac{\dot{R}^*}{R}. \end{aligned} \quad (\text{A19})$$

As has been discussed above, in (A18,19) terms of order  $(R^*/z)^3$  and higher orders have been neglected, and it is observed from (A19) that, in this approximation, only the *growth* of the lower bubble influences the translation of the upper bubble. In (A18) the term  $(U/4)^2$  has formally been included; however, it is stressed again that, when  $U$  is not small with respect to  $\dot{R}$ , the bubble deviates from the spherical shape and is somewhat flattened.

The coupled set of equations (A18,19) also describes one bubble at a distance  $z$  away from a solid wall where the normal component of the velocity vanishes. The latter boundary condition can be satisfied by considering the lower bubble as a 'mirror' bubble with  $U^* = U$  and  $R^* = R$ . In this way, equation (2.3.17) has been obtained with  $\dot{z} = U$ .

For a free bubble, equations (2.3.1,2) are obtained by taking the limit  $z \rightarrow \infty$ .

Finally, it is stressed that equations (A18,19), based on the assumption of potential flow, are valid only when the vorticity produced by the tangential stress boundary condition at the vapour-liquid interface has not yet been transported far away from the bubble.

## APPENDIX B

### *Product rules for the generalised Riemann-Liouville operator*

This Appendix provides an introduction to the mathematics used in Sections 2.2, 2.5 and in Section 3.3.2. Proofs of the equations stated here will not be given since these can be found in the book by Oldham and Spanier (1974).

According to a classical formula due to Dirichlet, cf. Ross (1973), the Riemann-Liouville integral defined by equation (2.2.18) is equivalent to an  $n$ -fold integral when  $-v = n$  is an integer  $\geq 1$ :



$$\begin{aligned}
{}_c D_t^{-n} f(t) &= \frac{1}{\Gamma(n)} \int_c^t \frac{f(t')}{(t-t')^{1-n}} dt' = \\
&= \int_c^t dt_{n-1} \int_c^{t_{n-1}} dt_{n-2} \dots \int_c^{t_2} dt_1 \int_c^{t_1} f(t_0) dt_0.
\end{aligned} \tag{B1}$$

In the following discussion, the meaning of  ${}_c D_t^n f(t)$ ,  $n$  is integer  $\geq 0$ , will be investigated. As can be seen when differentiating equation (2.2.18) of Chapter 2, the following expression holds:

$$\frac{d^n}{dt^n} {}_c D_t^v f(t) = {}_c D_t^{n+v} f(t), \quad n+v < 0. \tag{B2}$$

Expression (B2) can be used to extend the definition of the Riemann-Liouville operator to values  $v \geq 0$  in the following way:

$${}_c D_t^v f(t) = \frac{d^n}{dt^n} {}_c D_t^{-n+v} f(t), \quad -n+v < 0, \quad v \geq 0. \tag{B3}$$

As a consequence of (B3), composition rule or product rule (B2) is valid for every real  $v$ . From definition (B3) it also follows that:

$${}_c D_t^n f(t) = \frac{d^n f(t)}{dt^n}, \tag{B4}$$

independent of  $c$ , which has been omitted in the notation in this case.

From equations (B1) and (B3), it is seen that the generalized Riemann-Liouville operator  ${}_c D_t^v$ ,  $-\infty < v < \infty$ , has the character of a fractional ' $v$ -fold' integration or ' $v$ -fold' differentiation. Euler's rule (2.2.25) for fractional differentiation of powers of  $t$  has also the same form as the ordinary rule for differentiation. For these reasons, the notation  $d^v f(t)/d(t-c)^v$  is frequently used to stress the similarity between fractional and ordinary differentiation.

Equation (B2) represents one of the product rules for fractional differentiation, namely  ${}_c D_t^n {}_c D_t^v = {}_c D_t^{n+v}$ ,  $n$  integer  $\geq 0$ ,  $-\infty < v < \infty$ . In the following presentation, the other product rules will be

mentioned without proof. These rules represent the main advantage of using fractional derivatives rather than the original integrals. The inverse of equation (B2) is given by:

$${}_c D_t^v D_t^n f(t) = {}_c D_t^{n+v} f(t) - \sum_{j=0}^{n-1} \frac{t^{j-n-v}}{\Gamma(j-n-v+1)} \left( \frac{d^j f}{dt^j} \right)_{t=c}. \quad (B5)$$

Another very important rule is:

$${}_c D_t^{-v} {}_c D_t^v f(t) = f(t) + \sum_{j=1}^m C_j t^{v-j}. \quad (B6)$$

In (B6),  $m=0$  for  $v \leq 0$ . For  $v \leq 1$ ,  $C_1 = 0$  when  $f(c) = 0$ . For  $v > 0$ ,  $v \leq m < v+1$ ; the determination of the coefficients  $C_j$  has been treated by Oldham and Spanier (1974).

Finally, the general 'law of exponents' is given as:

$${}_c D_t^u {}_c D_t^v f(t) = {}_c D_t^{u+v} f(t), \quad (B7)$$

and holds for all  $u$  when  $v$  has such a value that the series in the right-hand side of (B6) vanishes.

The composition rules (B2, B5, B6) have been used in Section 2.5. Oldham and Spanier (1974) have tabulated useful rules and fractional derivatives of many functions, especially for  $v = \pm \frac{1}{2}$ . One of these standard results, used in the derivation of equation (2.2.46) from equation (2.2.44) reads:

$${}_0 D_t^{-\frac{1}{2}} \exp(t) \operatorname{erfc}(t^{\frac{1}{2}}) = 1 - \exp(t) \operatorname{erfc}(t^{\frac{1}{2}}). \quad (B8)$$

Also, the so-called Grünwald rule, used in Section 3.3.2, is recalled here:

$${}_c D_t^v f(t) = \lim_{N \rightarrow \infty} \frac{\left( \frac{t-c}{N} \right)^{-v}}{\Gamma(-v)} \sum_{j=0}^{N-1} \frac{\Gamma(j-v)}{\Gamma(j+1)} f \left( t - j \frac{t-c}{N} \right). \quad (B9)$$

The latter series expansion is often used as a definition of fractional derivatives.

## APPENDIX C

*The equations of motion of the gas-liquid interface of a thin liquid layer at a horizontal wall under the influence of forces normal to that interface*

### *C1. Division of the flow field in finite elements*

To obtain a solution of the flow field in the thin liquid layer shown in Fig. 4.4, the following equation of the biharmonic type must be satisfied:

$$D^4 \psi = D^2 (D^2 \psi) = \left( \frac{\partial^2}{\partial r^2} - \frac{1}{r} \frac{\partial}{\partial r} + \frac{\partial^2}{\partial z^2} \right)^2 \psi = 0 \quad . \quad (C1)$$

Equation (C1) is presented in cylindrically symmetric cylinder coordinates; this equation has been derived in a way which is similar to the derivation of equation (2.1.9) in cylindrically symmetric spherical coordinates. Only quasi steady, low Reynolds number flow will be considered, so that the inertia terms of the left-hand side of (2.1.9) vanish.

Equation (C1) must be complemented by two boundary conditions at a boundary enclosing the flow field. At the solid wall, these conditions are that the normal and tangential components of the velocity vanish. At the gas-liquid interface, a condition for the normal and tangential stress must be satisfied. When, in addition, conditions at the beginning and end of the layer are prescribed, the flow field can be determined in principle. From this solution of the flow field, an expression for the normal velocity component at the gas-liquid interface follows. From this expression, the evolution in time of the gas-liquid interface can be determined. Since it is not possible to match analytically the boundary conditions to the general solution of (C1), because the gas-liquid interface has an irregular shape and is not known beforehand, the flow field is divided into  $N+1$  finite elements with vertical boundaries; cf. Fig. C1. Each boundary between the elements is characterized by an integer  $i$ ,  $i = 0, 1, \dots, N$ . An element bounded by boundaries  $i$  and  $i + 1$ , or  $i - 1$  and  $i$ , is denoted

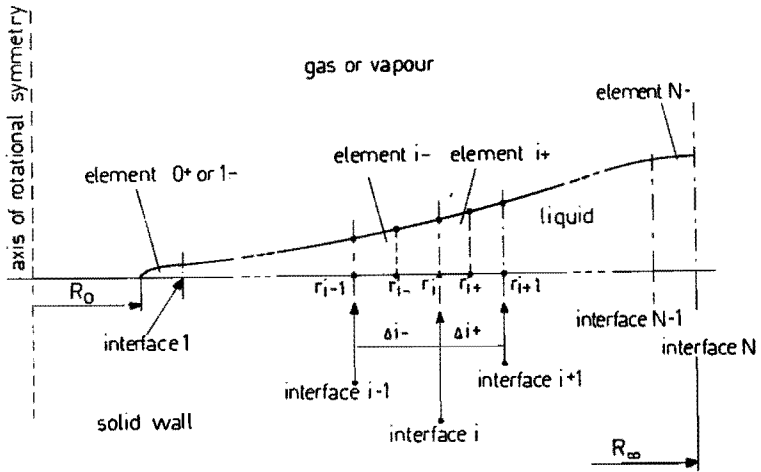


Fig. C1. Division of the flow field in finite elements

by element  $i + \frac{1}{2}$ , or  $i - \frac{1}{2}$ , respectively. In short-hand notation, these elements will be denoted by  $i+$  and  $i-$ . The distance between interfaces  $i$  and  $i + 1$ , or  $i - 1$  and  $i$ , is denoted by  $\Delta_{i+}$ , or  $\Delta_{i-}$ , respectively. Consequently, the equation:

$$r_i = \sum_{j=0}^i \Delta_{j+} = \sum_{j=1}^{i+1} \Delta_{j-} \quad , \quad (C2)$$

gives the position of interface  $i$ .

The radius  $(r_i + r_{i+1})/2$ , situated in the middle of the interval for which  $r_i \leq r \leq r_{i+1}$ , will be denoted by  $r_{i+1/2}$ , or shortly by  $r_{i+}$ . In this way, the distance between to neighbouring radii  $r_{i-}$  and  $r_{i+}$  equals  $\Delta_i = (\Delta_{i-} + \Delta_{i+})/2$ .

In each element  $i+$ , the following solution satisfies equation (C1):

$$\psi_{i+}(r, z, t) = a_{i+} z^2 + b_{i+} z^3 + c_{i+} r^2 z^2 + d_{i+} r^2 z^3 \quad . \quad (C3)$$

In (C3), the coefficients  $a_{i+}$ ,  $b_{i+}$ ,  $c_{i+}$  and  $d_{i+}$  are independent of  $r$  and  $z$ ; however, they are functions of time.

With expressions for the velocity components, which are similar to expressions (2.1.7, 8), namely:

$$(u,w) = \frac{1}{r} \left( -\frac{\partial}{\partial z}, \frac{\partial}{\partial r} \right) \psi \quad , \quad (C4)$$

the following expressions follow from (C3):

$$u_{i+}(r,z,t) = -2a_{i+} \frac{z}{r} - 3b_{i+} \frac{z^2}{r} - 2c_{i+} rz - 3d_{i+} rz^2 \quad , \quad (C5)$$

$$w_{i+}(r,z,t) = 2c_{i+} z^2 + 2d_{i+} z^3 \quad . \quad (C6)$$

From (C5) and (C6) it is noted that, at the solid wall  $z = 0$ , the conditions of impermeability  $w = 0$  and the adherence or no-slip condition  $u = 0$  have already been satisfied.

The solution defined by equation (C3) is not a general solution, since it cannot be matched to the boundary conditions everywhere. Furthermore, also continuity conditions are required to connect one element to another. The expansion coefficients  $a_{i+}(t)$ , ...  $d_{i+}(t)$  will be determined in such a way that the boundary and continuity conditions are approximately satisfied. The four coefficients can be determined when, in addition to the two boundary conditions, two continuity conditions are prescribed.

From a physical point of view, the most obvious continuity conditions to be satisfied are: (i) continuity of volumetric flow rate  $\dot{\Gamma} = -2\pi\psi_n$  from one element to another, and (ii) continuity of velocity in the  $z$ -direction  $w_n = (\partial\psi/\partial r)_n/r$  at the gas-liquid interface.

By way of approximation, only these two continuity conditions will be satisfied. Consequently, step-functions,  $\delta$ -functions, and derivatives of  $\delta$ -functions occur in  $D^4\psi$  at the boundaries between two adjacent elements. Therefore, in the limit of zero discretization interval, it is no longer guaranteed that equation (C1) is satisfied. However, in Section C6 it will be shown that the error introduced in this way is sufficiently small.

Another approximation will be that the normal and tangential stress boundary conditions at the gas-liquid interface are satisfied at  $r = r_{i+}$  only, i.e. in the middle of each fluid element. The latter points are the so-called collocation points, and the approximation method proposed in this way is the so-called local collocation method; cf. Finlayson (1972).

In the next part of this Section, expressions will be derived for the normal and tangential stresses at the gas-liquid interface, and for the volumetric flow rate.

From the general expression for the stress tensor  $\underline{\tau}$ , the following expressions can be derived for the tangential and normal stresses at the gas-liquid interface  $z = h$ :

$$\tau_t = \eta \left( \frac{\partial u}{\partial z} + \frac{\partial w}{\partial r} - \frac{w}{r} \right)_h \frac{1 - \left( \frac{\partial h}{\partial r} \right)^2}{1 + \left( \frac{\partial h}{\partial r} \right)^2} - 2\eta \left( \frac{\partial u}{\partial r} - \frac{u}{r} - \frac{\partial w}{\partial z} \right)_h \frac{\frac{\partial h}{\partial r}}{1 + \left( \frac{\partial h}{\partial r} \right)^2}, \quad (C7)$$

$$\tau_n = -p + 2\eta \left( \frac{\partial w}{\partial z} \right)_h - 2\eta \left( \frac{\partial u}{\partial z} + \frac{\partial w}{\partial r} - \frac{w}{r} \right)_h \frac{\frac{\partial h}{\partial r}}{1 + \left( \frac{\partial h}{\partial r} \right)^2} + 2\eta \left( \frac{\partial u}{\partial r} - \frac{u}{r} \right)_h \frac{\left( \frac{\partial h}{\partial r} \right)^2}{1 + \left( \frac{\partial h}{\partial r} \right)^2}. \quad (C8)$$

In the following treatment, it will be assumed that  $|\partial h / \partial r|$  is sufficiently small to neglect the second term in the right-hand side of (C7) and the second and third terms in the right-hand side of (C8).

Under these assumptions, (C7) simplifies to:

$$\tau_{ti+}(r, h, t) = -2\eta \left( a_{i+} \frac{1}{r} + 3b_{i+} \frac{h}{r} + c_{i+} \left( r + \frac{h^2}{r} \right) + d_{i+} \left( 3rh + \frac{h^3}{r} \right) \right) \frac{1 - \left( \frac{\partial h}{\partial r} \right)^2}{1 + \left( \frac{\partial h}{\partial r} \right)^2}. \quad (C9)$$

In the following treatment, restriction will always be made to the case  $z \leq h \ll r$ . This assumption will lead to considerable simplification and there will be no explicit indication where it

has been used in the following discussion. In this way, the interesting case  $r = 0$  has been excluded from the discussion; cf. also Section C6. Thus equation (C9) further simplifies to:

$$\tau_{ti+}(r, h, t) = -2\eta(a_{i+} \frac{1}{r} + 3b_{i+} \frac{h}{r} + c_{i+}r + 3d_{i+}rh) \frac{1 - (\frac{\partial h}{\partial r})^2}{1 + (\frac{\partial h}{\partial r})^2} . \quad (C10)$$

Since a simple algebraic expression (C3) has been proposed for the solution, the pressure in the layer can easily be expressed as a function of the expansion coefficients by integration of the two momentum equations for Stokes flow:

$$\frac{\partial p}{\partial r} = -\frac{\eta}{r} \frac{\partial}{\partial z} D^2 \psi , \quad (C11)$$

$$\frac{\partial p}{\partial z} = \frac{\eta}{r} \frac{\partial}{\partial r} D^2 \psi - \rho g . \quad (C12)$$

Substitution of (C3) into (C11,12) results in:

$$\left(\frac{\partial p}{\partial r}\right)_{i+} = -6\eta(b_{i+} \frac{1}{r} + d_{i+}r) , \quad (C13)$$

$$\left(\frac{\partial p}{\partial z}\right)_{i+} = 4\eta(c_{i+} + 3d_{i+}z) - \rho g . \quad (C14)$$

Since  $\partial p/\partial r$  turns out to be a function of  $r$  only, and similarly  $\partial p/\partial z$  is a function of  $z$  only, expressions (C13, 14) can easily be integrated, resulting in:

$$p_{i+}(r, z, t) = \eta\{-6b_{i+} \ln \frac{r}{r_{i+}} + 4c_{i+}z + 3d_{i+}(2z^2 - r^2)\} - \rho gz + p_{oi+} , \quad (C15)$$

where  $p_{oi+}$  is an integration constant which will be specified subsequently.

In the following discussion, the relatively slowly varying logarithmic term in (C15) will be neglected with respect to variations of the term in  $r^2$ . In this way, equation (C15) simplifies to:

$$p_{i+}(r, z, t) - p_l = \eta(4c_{i+}z - 3d_{i+}r^2) - \rho g(z - h_\infty) - \Delta p_s . \quad (C16)$$

In (C16) the choice of the integration constant  $p_{oi+} = \rho g h_{\infty} - \Delta p_s$  needs some clarification. When there is no liquid motion, all expansion coefficients in (C3) are zero and, at thickness  $h = h_{\infty}$ , the pressure difference over the horizontal gas-liquid interface equals  $p_{\infty} - p_l = -\Delta p_s$ , where  $\Delta p_s$  represents an applied suction pressure; cf. Fig. 4.4.

Provided that  $|\partial h/\partial r|$  is sufficiently small, the following expression for the normal stress at the gas-liquid interface results from substitution of (C16) into (C8):

$$\tau_{ni+}(r, h, t) + p_l = \eta(4c_{i+}h + 3d_{i+}r^2) + \rho g(h - h_{\infty}) + \Delta p_s \quad (C17)$$

Finally, from equation (C4) the following expression is derived for the volumetric flow rate  $\dot{V}$  parallel to the wall:

$$\begin{aligned} \dot{V}_{i+}(r, t) &= 2\pi r \int_0^h u_{i+}(r, z, t) dz = -2\pi \psi_{i+}(r, h, t) = \\ &= -2\pi(a_{i+}h^2 + b_{i+}h^3 + c_{i+}r^2h^2 + d_{i+}r^2h^3) \quad (C18) \end{aligned}$$

## C2. Normal stress and normal velocity conditions

According to the well-known Laplace-Kelvin equation, the difference in normal stress over the gas-liquid interface is related to its curvature by:

$$\tau_n + p_l = \frac{\sigma \frac{\partial^2 h}{\partial r^2}}{\{1 + (\frac{\partial h}{\partial r})^2\}^{3/2}} + \frac{\sigma \frac{\partial h}{\partial r}}{r\{1 + (\frac{\partial h}{\partial r})^2\}^{1/2}} = f_{\sigma} \quad (C19)$$

Substitution of (C19) into (C17) at the collocation point  $(r_{i+}, h_{i+})$  results in the following expression for  $d_{i+}$ :



$$d_{i+} = -\frac{4}{3} c_{i+} \frac{h_{i+}}{r_{i+}^2} + \frac{1}{3\eta} \frac{f_{i+}}{r_{i+}^2} . \quad (C20)$$

In (C20),  $f$  is defined by:

$$f = f_{\sigma} - \rho g(h-h_{\infty}) - \Delta p_s = f_{\sigma} - f_g - \Delta p_s . \quad (C21)$$

Substitution of expression (C20) into equation (C6) results in the following expression for  $w_{i+}$ :

$$w_{i+}(r, z, t) = 2c_{i+} z^2 + \frac{2}{3\eta} \frac{f_{i+}}{r_{i+}^2} z^3 . \quad (C22)$$

In the same way, a similar expression can be derived for  $w_{i-}$ :

$$w_{i-}(r, z, t) = 2c_{i-} z^2 + \frac{2}{3\eta} \frac{f_{i-}}{r_{i-}^2} z^3 . \quad (C23)$$

The requirement of continuity of velocity in the  $z$ -direction at the gas-liquid interface, at the place where fluid element  $i-$  borders on fluid element  $i+$ , is given by:

$$w_{i-}\{r_i, h(r_i, t), t\} = w_{i+}\{r_i, h(r_i, t), t\} . \quad (C24)$$

Substitution of (C22, 23) into (C24) results in:

$$c_{i+} - c_{i-} = \frac{1}{3\eta} h_i \left( \frac{f_{i-}}{r_{i-}^2} - \frac{f_{i+}}{r_{i+}^2} \right) . \quad (C25)$$

By means of the following Taylor series expansions:

$$\frac{1}{r_{i\pm}^2} = \frac{1}{r_i^2} \mp \frac{\Delta_{i\pm}}{r_i^3} + 0(\Delta_{i\pm})^2 , \quad (C26)$$

$$f_{i\pm} = f_i \mp \frac{1}{2} \Delta_{i\pm} \left( \frac{\partial f}{\partial r} \right)_i + 0(\Delta_{i\pm})^2 , \quad (C27)$$

the following expression results from (C25):

$$\frac{c_{i+\frac{1}{2}} - c_{i-\frac{1}{2}}}{\Delta_i} = \frac{2h_i}{3\eta r_i^2} \left\{ f_i - \frac{r_i}{2} \left( \frac{\partial f}{\partial r} \right)_i \right\} + 0(\Delta_i) . \quad (C28)$$

In the limit  $\Delta_i \rightarrow 0$ , equation (C28) becomes:

$$\frac{\partial c}{\partial r} = \frac{2h}{3\eta r^3} \left( f - \frac{r}{2} \frac{\partial f}{\partial r} \right) \quad (C29)$$

In (C29)  $c$  is a function of  $r$ , which is in contrast to what was stated in Section (C1) where the expansion coefficients were introduced as functions of time only. Consequently, when (C29) is used, it is no longer guaranteed that equation (C1) is satisfied. However, in Section C6 it will be shown that the error involved in satisfying (C1) is sufficiently small.

### *C3. Tangential stress and volumetric flux conditions*

In addition to the normal component of the surface tension force at the gas-liquid interface, a tangential component may also be the cause of liquid motion. A gradient in the surface tension results in a tangential stress in the liquid adjacent to the gas-liquid interface, expressed by the Marangoni-Gibbs equation:

$$\tau_t = \frac{\frac{\partial \sigma}{\partial r} + \frac{\partial \sigma}{\partial z} \frac{\partial h}{\partial r}}{\left\{ 1 + \left( \frac{\partial h}{\partial r} \right)^2 \right\}^{1/2}}, \quad z = h. \quad (C30)$$

Combining (C30) with expression (C9) for the tangential stress at the collocation point  $r_{i+}$  results in the following expression for  $b_{i+}$ :

$$b_{i+} = -\frac{a_{i+}}{3} \frac{1}{h_{i+}} - \frac{c_{i+}}{3} \frac{r_{i+}^2}{h_{i+}} - d_{i+} r_{i+}^2 - \frac{1}{6\eta} \frac{r_{i+} s_{i+}}{h_{i+}} \quad (C31)$$

In (C31)  $s$  is defined by:

$$s = \frac{\frac{\partial \sigma}{\partial r} + \frac{\partial \sigma}{\partial z} \frac{\partial h}{\partial r}}{\left\{ 1 + \left( \frac{\partial h}{\partial r} \right)^2 \right\}^{-1/2} \left\{ 1 - \left( \frac{\partial h}{\partial r} \right)^2 \right\}} \approx \frac{\partial \sigma}{\partial r} \quad (C32)$$

Substitution of equation (C20) for  $d_{i+}$  into (C31) results in:

$$b_{i+} = -\frac{a_{i+}}{3} \frac{l}{h_{i+}} - \frac{c_{i+}}{3} \frac{r_{i+}^2}{h_{i+}} - \frac{l}{3\eta} f_{i+} - \frac{l}{6\eta} \frac{r_{i+} s_{i+}}{h_{i+}} \quad (C33)$$

Substitution of expressions (C20) and (C33) for  $d_{i+}$  and  $b_{i+}$  respectively into equation (C18) for the volumetric flow rate  $\dot{\Gamma}$  results in:

$$\begin{aligned} -\frac{\dot{\Gamma}_{i+}(r,t)}{2\pi} &= a_{i+} h^2 \left(1 - \frac{h}{3h_{i+}}\right) + c_{i+} r^2 h^2 \left(1 - \frac{r_{i+}^2 h}{3r^2 h_{i+}}\right) + \\ &-\frac{f_{i+} h^3}{3\eta} \left(1 - \frac{r^2}{r_{i+}^2}\right) - \frac{r_{i+} s_{i+} h^3}{6\eta h_{i+}} \quad (C34) \end{aligned}$$

A similar expression can be obtained in element  $i-$ :

$$\begin{aligned} -\frac{\dot{\Gamma}_{i-}(r,t)}{2\pi} &= a_{i-} h^2 \left(1 - \frac{h}{3h_{i-}}\right) + c_{i-} r^2 h^2 \left(1 - \frac{r_{i-}^2 h}{3r^2 h_{i-}}\right) + \\ &-\frac{f_{i-} h^3}{3\eta} \left(1 - \frac{r^2}{r_{i-}^2}\right) - \frac{r_{i-} s_{i-} h^3}{6\eta h_{i-}} \quad (C35) \end{aligned}$$

The requirement of continuity of volumetric flow rate across the boundaries of the fluid elements is given by:

$$\dot{\Gamma}_{i+}(r_i, t) = \dot{\Gamma}_{i-}(r_i, t) \quad (C36)$$

Substitution of expressions (C34, 35) into (C36) results in:

$$\begin{aligned} (a_{i+} - a_{i-}) - \frac{h_i}{3} \left(\frac{a_{i+}}{h_{i+}} - \frac{a_{i-}}{h_{i-}}\right) &= - (c_{i+} - c_{i-}) r_i^2 + \\ + \frac{h_i}{3} \left(\frac{c_{i+} r_{i+}^2}{h_{i+}} - \frac{c_{i-} r_{i-}^2}{h_{i-}}\right) + \frac{f_{i+} - f_{i-}}{3\eta} h_i - \left(\frac{f_{i+}}{r_{i+}^2} - \frac{f_{i-}}{r_{i-}^2}\right) \frac{r_i^2 h_i}{3\eta} + \\ + \frac{h_i}{6\eta} \left(\frac{r_{i+} s_{i+}}{h_{i+}} - \frac{r_{i-} s_{i-}}{h_{i-}}\right) \quad (C37) \end{aligned}$$

In the same way as in Section C2, the quantities at  $i+$  and  $i-$  are expressed as quantities at  $i$  with the aid of Taylor series expansions. Thus equation (C37) becomes:

$$\frac{a_{i+\frac{1}{2}} - a_{i-\frac{1}{2}}}{\Delta i} = - \frac{c_{i+\frac{1}{2}} - c_{i-\frac{1}{2}}}{\Delta i} r_i^2 + \frac{h_i f_i}{\eta r_i} + \frac{1}{4\eta} \left( \frac{\partial \sigma}{\partial r} \right)_i - \frac{r_i s_i}{4\eta h_i} \left( \frac{\partial h}{\partial r} \right)_i + \frac{r_i}{4\eta} \left( \frac{\partial s}{\partial r} \right)_i + 0(\Delta i) . \quad (C38)$$

Substitution of equation (C28) into equation (C38) results in:

$$\frac{a_{i+\frac{1}{2}} - a_{i-\frac{1}{2}}}{\Delta_i} = \frac{h_i}{3\eta r_i} \left\{ f_i - r_i \left( \frac{\partial f}{\partial r} \right)_i \right\} + \frac{s'}{4\eta} + 0(\Delta_i) , \quad (C39)$$

or in the limit  $\Delta_i \rightarrow 0$ :

$$\frac{\partial a}{\partial r} = \frac{h}{3\eta r} \left( f - r \frac{\partial f}{\partial r} \right) + \frac{s'}{4\eta} . \quad (C40)$$

In (C39, 40)  $s'$  represents the effect of surface tension gradients, and is defined by:

$$s' = \frac{\partial}{\partial r} (rs) - \frac{rs}{h} \frac{\partial h}{\partial r} . \quad (C41)$$

#### *C4. Conditions at the triple interfacial line and at the place of outflow*

Expressions (C20, 29, 33, 40) make it possible to determine the complete flow field in the layer when one value for  $a_{i+}$  and one value for  $c_{i+}$  are prescribed. For that reason, it is assumed that at the place  $r = R_0$  the tangential stress vanishes. From equation (C10) it follows that this condition results in:

$$a_0 + c_0 R_0^2 = 0 . \quad (C42)$$

At  $r = R_\infty$  it follows that:

$$a_N + c_N R_\infty^2 = - \frac{3\Gamma_\infty}{4\pi h_\infty^2} + \frac{R_\infty s_\infty}{4\eta} . \quad (C43)$$

The coefficients  $a_N$ ,  $c_N$  can be expressed in  $a_o$ ,  $c_o$  with the aid of expressions (C29, 40), which respectively yield for  $a(r)$  and  $c(r)$ :

$$a(r) = a_o + \frac{1}{3\eta} \int_{R_o}^r \left( \frac{hf}{r} - h \frac{\partial f}{\partial r} \right) dr + \frac{1}{4\eta} \int_{R_o}^r s' dr, \quad (C44)$$

$$c(r) = c_o + \frac{2}{3\eta} \int_{R_o}^r \left( \frac{hf}{r^3} - \frac{1}{2r^2} \frac{\partial f}{\partial r} \right) dr. \quad (C45)$$

Substitution of (C44, 45) at  $r = R_\infty$  into (C43) and combination of (C42) with (C43), results in the following expression for  $c_o$ :

$$c_o (R_\infty^2 - R_o^2) = - \frac{3\dot{\Gamma}_\infty}{4\pi h_\infty^2} + \frac{R_\infty s_\infty}{4\eta} - \frac{1}{4\eta} \int_{R_o}^{R_\infty} s' dr - \frac{1}{3\eta} \int_{R_o}^{R_\infty} \left( \frac{hf}{r} - h \frac{\partial f}{\partial r} \right) dr - \frac{2R_\infty^2}{3\eta} \int_{R_o}^{R_\infty} \left( \frac{hf}{r^3} - \frac{1}{2r^2} \frac{\partial f}{\partial r} \right) dr. \quad (C46)$$

A similar expression can also be found for  $a_o$ .

Application of equations (C5, 18) at  $r = R_o$  results, in a similar way as equation (C43) in:

$$\frac{a_o}{R_o} + c_o R_o = - \frac{u_o}{h_o} + \frac{s_o}{2\eta} = - \frac{3\dot{\Gamma}_o}{4\pi R_o h_o^2} + \frac{s_o}{4\eta}. \quad (C47)$$

When it is assumed that  $s_o = 0$  at  $r = R_o$ , it follows from (C42, 47) that also  $u_o = \dot{\Gamma}_o = 0$  at  $r = R_o$ .

### *C5. Kinematic boundary condition and global continuity*

The kinematic boundary condition at the gas-liquid interface reads, cf. equation (4.1.4) :

$$\frac{\partial h}{\partial t} + u_h \frac{\partial h}{\partial r} = w_h - \frac{q_h}{\rho l}. \quad (C48)$$

As has been described in Section 4.1.1, integration of (C48) should result in the following global equation, expressing conservation of mass:

$$\dot{\Gamma}(r,t) = -2\pi \int_{R_0}^r \left( \frac{\partial h}{\partial t} + \frac{q_h}{\rho l} \right) r \, dr. \quad (C49)$$

When  $\dot{\Gamma}$  is known, the velocity in the r-direction at the interface,  $u_h$ , can be determined from the following equation derived from (C5) and (C18):

$$u_h(r,h,t) = \frac{3\dot{\Gamma}}{4\pi rh} + \frac{hs}{4\eta}. \quad (C50)$$

From equations (C6, 20) it follows that the following expression holds for the velocity in the z-direction at the interface:

$$w_h = 2ch^2 + \frac{2fh^3}{3\eta r^2}. \quad (C51)$$

From equations (C45, 46) an expression for  $c(r)$  can be found; substitution of that expression into (C51) results in:

$$\begin{aligned} \frac{\partial h}{\partial t} + u_h \frac{\partial h}{\partial r} &= \frac{2h^3 f}{3\eta r^2} + \frac{4h^2}{3\eta} \int_{R_0}^r \left( \frac{hf}{r^3} - \frac{h}{2r^2} \frac{\partial f}{\partial r} \right) dr - \frac{4h^2 R_\infty^2}{3\eta(R_\infty^2 - R_0^2)} \times \\ &+ \frac{h^2}{2\eta(R_\infty^2 - R_0^2)} \left( s_\infty R_\infty - \int_{R_0}^{R_\infty} s' dr \right) - \frac{2h^2}{3\eta(R_\infty^2 - R_0^2)} \int_{R_0}^{R_\infty} \left( \frac{hf}{r} - h \frac{\partial f}{\partial r} \right) dr + \\ &+ \frac{h^2}{2\eta(R_\infty^2 - R_0^2)} \left( s_\infty R_\infty - \int_{R_0}^{R_\infty} s' dr \right) - \frac{3\dot{\Gamma}_\infty h^2}{2\pi h_\infty^2 (R_\infty^2 - R_0^2)} - \frac{q_h}{\rho l}. \end{aligned} \quad (C52)$$

Equation (C52) expresses the rate of thinning  $-\partial h/\partial t$  of the layer as a function of the pressures acting normally at the gas-liquid interface, and as a function of the volumetric flux  $\dot{\Gamma}_\infty$  flowing out of the layer at  $r = R_\infty$ . Of course, there is a relationship between these normal forces and the rate of outflow, and the relationship can be determined with the aid of the global continuity equation (C49).

First, equation (C52) will be simplified by considering only the cases where the fifth term in the right-hand side, i.e. the surface tension gradient term, vanishes.

With the above approximation, the rate of thinning  $-\partial h/\partial t$  and the accompanying rate of outflow  $\dot{\Gamma}_\infty$  is composed of three parts, cf. also (C21):

- (i) The rate of thinning  $-\partial h_1/\partial t$  caused by evaporation; the accompanying outflow equals zero, and  $f_1 = 0$ .
- (ii) The rate of thinning  $-\partial h_2/\partial t$  caused by suction; the accompanying outflow will be denoted by  $\dot{\Gamma}_{\infty 2}$ , and  $f_2 = -\Delta p_s$ .
- (iii) The rate of thinning  $-\partial h_3/\partial t$  caused both by capillary effects and differences in hydrostatic pressure; the corresponding outflow will be denoted by  $\dot{\Gamma}_{\infty 3}$ , and  $f_3 = f_\sigma - f_g$ .

When it may be assumed that  $|\partial h/\partial t| \gg |u_h \partial h/\partial r|$ , equation (C53) can be decomposed into three parts, each part representing one of the causes of motion of the gas-liquid interface:

$$\frac{\partial h_1}{\partial t} = -\frac{\dot{q}_h}{\rho l} \quad , \quad (C53)$$

$$\begin{aligned} \frac{\partial h_2}{\partial t} = & -\frac{2h^3 \Delta p_s}{3\eta r^2} - \frac{4h^2 \Delta p_s}{3\eta} \int_{R_0}^r \frac{h dr}{r^3} + \frac{4h^2 R_\infty^2 \Delta p_s}{3\eta (R_\infty^2 - R_0^2)} \int_{R_0}^{R_\infty} \frac{h dr}{r^3} + \\ & + \frac{2h^2 \Delta p_s}{3\eta (R_\infty^2 - R_0^2)} \int_{R_0}^{R_\infty} \frac{h dr}{r} - \frac{3\dot{\Gamma}_{\infty 2} h^2}{2\pi h_\infty^2 (R_\infty^2 - R_0^2)} \quad , \quad (C54) \end{aligned}$$

$$\frac{\partial h_3}{\partial t} = \frac{2h^3 f_3}{3\eta r^2} + \frac{4h^2}{3\eta} \int_{R_0}^r \left( \frac{h f_3}{r^3} - \frac{h}{2r^2} \frac{\partial f_3}{\partial r} \right) dr - \frac{4h^2 R_\infty^2}{3\eta (R_\infty^2 - R_0^2)} \times$$

$$\begin{aligned} & \int_{R_0}^{R_\infty} \left( \frac{h f_3}{r^3} - \frac{h}{2r^2} \frac{\partial f_3}{\partial r} \right) dr - \frac{2h^2}{3\eta (R_\infty^2 - R_0^2)} \int_{R_0}^{R_\infty} \left( \frac{h f_3}{r} - h \frac{\partial f_3}{\partial r} \right) dr + \\ & - \frac{3\dot{\Gamma}_{\infty 3} h^2}{2\pi h_\infty^2 (R_\infty^2 - R_0^2)} \quad . \quad (C55) \end{aligned}$$

Equation (C54) will be applied to the case where  $h_2 = h$  is independent of  $r$ . In that case, equation (C54) simplifies to:

$$\frac{dh_2}{dt} = \frac{2h_2^3 \Delta p_s}{3\eta(R_\infty^2 - R_0^2)} \ln \frac{R_\infty}{R_0} - \frac{3\dot{\Gamma}_{\infty 2}}{2\pi(R_\infty^2 - R_0^2)} \quad (C56)$$

For a horizontal interface, the flux flowing out of the layer can easily be determined from equation (C49). It equals:

$$\dot{\Gamma}_{\infty 2} = - \frac{dh_2}{dt} \pi(R_\infty^2 - R_0^2) \quad (C57)$$

Substitution of (C57) into (C56) results in:

$$\frac{dh_2}{dt} = - \frac{4h_2^3 \Delta p_s}{3\eta(R_\infty + R_0)R_0} \frac{\ln \frac{R_\infty}{R_0}}{\frac{R_\infty}{R_0} - 1} \quad (C58)$$

In the limit  $R_\infty \rightarrow R_0 = R_c$ , (C58) results in:

$$\frac{dh_2}{dt} = - \frac{2h_2^3 \Delta p_s}{3\eta R_c^2}, \quad R_0 = R_\infty = R_c \quad (C59)$$

It is stressed here that the derivation of (C58) has been made under the assumption  $h \ll r$ , consequently, expression (C58) loses its validity for the case  $R_0 \rightarrow 0$ ,  $h_2 \neq 0$ .

Next, equation (C55) will be considered. First it is assumed that:

$$\dot{\Gamma}_{\infty 3} = - \frac{4\pi}{3\eta} \int_{R_0}^R \frac{h_3^3 f_3}{r} dr \quad (C60)$$

In the following discussion, it will be shown that this choice is, under some limiting assumptions, in agreement with the global continuity equation (C49).

Substitution of (C60) into (C55) for the case  $h_3 = h$  results, for sufficiently large value of  $R_\infty$ , in:



$$\frac{\partial h_3}{\partial t} = \frac{2h^3 f_3}{3\eta r^2} - \frac{4h^2}{3\eta} \int_r^{R_\infty} \left( \frac{hf_3}{r^3} - \frac{h}{2r^2} \frac{\partial f_3}{\partial r} \right) dr. \quad (C61)$$

Only over a relatively small interval  $R_0 \leq r < R'_0$ , where  $R'_0 \ll R_\infty$ , deviations from the horizontal shape are appreciable; cf. also Fig. 4.4 where  $R_0$  is replaced by  $R'_0$ . Consequently, the second term in the right-hand side of (C61) represents a substantial contribution only in the region  $R_0 \leq r < R'_0$ , and its maximal absolute value is obtained when  $r = R_0$ .

Thus, the first term in the integrand results in a contribution to  $\partial h_3 / \partial t$  which is an order  $|R'_0 - R_0| / R_0$  smaller than the first term in the right-hand side of (C61), and may, consequently, be neglected. Partial integration shows that the second term of the integrand has a negligible contribution when  $|\partial h / \partial r| \ll h / (R'_0 - R_0)$ .

In this way, equations (C60,61) have been simplified to:

$$\frac{\partial h_3}{\partial t} = \frac{2h_3^3}{3\eta r^2} \{f_\sigma - \rho g(h_3 - h_\infty)\}, \quad (C62)$$

$$\dot{\Gamma}_{\infty 3} = -\frac{4\pi}{3} \int_{R_0}^{R_\infty} \frac{R_\infty h_3^3}{r} \{f_\sigma - \rho g(h_3 - h_\infty)\} dr = -2\pi \int_{R_0}^{R_\infty} r \frac{\partial h_3}{\partial t} dr. \quad (C63)$$

From (C63) it can be seen that equation (C62) is in agreement with global continuity condition (C49).

### C6. Discussion

From equation (C58) it follows that the rate of thinning of a horizontal layer under the action of suction is given by:

$$\frac{1}{h^2} - \frac{1}{h_0^2} = \frac{8\Delta p_s \ln(R_\infty / R_0)}{3\eta (R_\infty - R_0)^2} (t - t_0) \quad (C64)$$

An approximation for the rate of thinning of a thin layer between two solid walls with  $R_0 = 0$  has been derived by Reynolds (1886) with

the aid of the lubrication approximation equation. That approximation makes it impossible to satisfy the normal stress condition locally and, for that reason, the normal stress condition was only satisfied in an integral sense. An extension of Reynolds' result to the case where gradients in surface tension, characterized by  $\beta_s$ , play a part is given by:

$$\frac{1}{h^2} - \frac{1}{h_0^2} = \frac{16\Delta p_s}{3\beta_s \eta R_\infty^2} (t - t_0). \quad (C65)$$

An extension of Reynolds' expression to cases where  $R_0 \neq 0$  is, however, impossible when the lubrication approximation is used.

Scheludko (1957) experimentally verified equation (C65), and he also investigated the case  $R_0 \neq 0$ . The relationship  $1/h^2 - 1/h_0^2 \propto t - t_0$  was found indeed.

After all this lengthy analysis, the hydrodynamic interpretation of the final equations of motion (C58) and (C62) is quite simple. Equations (C58, 62) express that the interface is set in motion, under the influence of a force normal to that interface, in the direction of that force. The factor of proportionality  $2h^3/3\eta r^2$  in (C62)) represents the viscous resistance against motion of the liquid adhering at the solid wall. In the layer, the normal motion is transformed into tangential motion. For the case of a horizontal interface, with  $R_0 = 0$ , this tangential motion can reasonably well be described by the lubrication approximation, as has been done by Reynolds (1886). However, the explanation of this motion, and the extension to situations where  $R_0 \neq 0$  and where the interface is curved, can only be given when both normal and tangential gradients in pressure are accounted for, as in this Appendix.

Finally, it is investigated whether equation (C1) is satisfied. First, the case described by equations (C62, 63) will be considered.

From equation (C49) it follows that  $\psi_h = -\dot{\Gamma}/(2\pi)$  is given by:

$$\psi_h(r, t) = \frac{2}{3\eta} \int_{R_0}^r \frac{h^3 f_3}{r} dr. \quad (C66)$$

On the basis of (C66), it will now be assumed that:

$$\psi(r, z, t) = \frac{2z^3}{3\eta} \int_{R_0}^r \frac{f_3 dr}{r}. \quad (C67)$$

In the region  $r > R'_0$ , this is a reasonable assumption since there the interface is almost horizontal. With the aid of equation (C12), it follows from (C67) that:

$$\eta D^4 \psi = -4 \left( \frac{\partial p}{\partial z} + \rho g \right) + \frac{4z}{r} \frac{\partial f_3}{\partial r} + \frac{2z^2}{r} \frac{\partial^2 f_3}{\partial r^2}. \quad (C68)$$

For  $r > R'_0$ , the last two terms in the right-hand side of (C68) are small since the interface is almost horizontal. Also  $|\partial p / \partial z + \rho g| \ll |\partial p / \partial r|$ , and the error in satisfying (C1) can be compared with the error introduced when the lubrication approximation (where  $\partial p / \partial z + \rho g = 0$ ) is applied.

For the case described by equation (C58), the expansion coefficients can easily be determined from equations (C20, 33, 42, 44, 45, 46). Substitution of the values obtained in this way into equation (C2), and making use of (C12), shows that equation (C68) is found again, however, with  $\partial f_3 / \partial r = 0$ ,  $\partial^2 f_3 / \partial r^2 = 0$ . Consequently, it is shown that the error in satisfying equation (C1) is sufficiently small in this case too.

LIST OF SYMBOLS

$a$	: = $2(\dot{R}_c/R_c)^2$ , cf. eq. (4.1.35)	$[s^{-2}]$
$a_i$	: expansion coefficient, cf. App. A	$[m^{i+3}]$
$a_{i+}$	: expansion coefficient, cf. App. C	$[ms^{-1}]$
$a_j$	: expansion coefficient, cf. Ch. 3	$[m]$
$A$	: surface area of bubble cap	$[m^2]$
$A_o$	: amplitude, cf. eq. (2.5.9)	$[m]$
$b$	: = $-\dot{R}_c$ , cf. eq. (4.1.35)	$[ms^{-2}]$
$b_{i+}$	: expansion coefficient, cf. App. C	$[s^{-1}]$
$b_j$	: expansion coefficient, cf. Ch. 3	$[m^{i+3}]$
$B_o$	: amplitude, cf. eq. (2.5.9)	$[m]$
$c$	: = $2\sigma/\rho$ , cf. eq. (4.1.35), liquid specific heat	$[m^3s^{-2}]$ $[J\ kg^{-1}]$
$c_{i+}$	: expansion coefficient, cf. App. C	$[m^{-1}s^{-1}]$
$c_{1p}$	: vapour specific heat at constant pressure	$[J\ kg^{-1}]$
$c_{1v}$	: vapour specific heat at constant volume	$[J\ kg^{-1}]$
$C$	: concentration of gas dissolved in liquid	$[kg\ m^{-3}]$
$C_R$	: concentration at gas-liquid interface	$[kg\ m^{-3}]$
$C_s$	: saturation concentration	$[kg\ m^{-3}]$
$C_\infty$	: concentration at edge of diffusion boundary layer	$[kg\ m^{-3}]$
$d_{i+}$	: expansion coefficient, cf. App. C	$[m^{-2}s^{-1}]$
$D_o$	: amplitude, cf. eq. (2.5.9)	$[m]$
$D^2$	: differential operator	$[m^{-2}]$
$D^h$	: differential operator	$[m^{-h}]$
$D_c^v$	: Riemann-Liouville operator	$[s^{-v}]$
$f$	: normal force per unit area at gas-liquid interface, cf. App. C	$[Pa]$
$f_g$	: hydrostatic pressure at gas-liquid interface, cf. App. C	$[Pa]$
$f_1$	: cf. eq. (4.1.37), cf. Sect. C5	$[m]$ $[Pa]$
$f_2$	: cf. eq. (4.1.38), = $-\Delta p_g$ , cf. Sect. C5	$[m]$ $[Pa]$
$f_3$	: = $f_\sigma - f_g$ , cf. Sect. C5	$[Pa]$
$f'$	: numerical constant in eq. (4.1.29)	
$f_\sigma$	: normal force per unit area at gas-liquid interface, cf. App. C	$[Pa]$

$F$	: vector function, cf. eq. (3.2.24)	$[m, m^2 s^{-1}]$
$F_d$	: total downward force exerted by wall on bubble	[N]
$F_g$	: upward buoyancy force acting on bubble	[N]
$F_i$	: downward inertia force acting on bubble	[N]
$F_r$	: upward reaction force exerted by wall on bubble	[N]
$F_\sigma$	: downward surface tension force of adhesion acting on bubble	[N]
$g$	: absolute value of gravitational acceleration	$[m s^{-2}]$
$g_r$	: component of gravitational acceleration in r-direction	$[m s^{-2}]$
$g_\theta$	: component of gravitational acceleration in $\theta$ -direction	$[m s^{-2}]$
$G$	: cf. eq. (3.2.25)	$[m s^{-1}]$
$h$	: thickness of thin liquid layer	[m]
$h_s$	: slip thickness of liquid layer	[m]
$h_\infty$	: thickness at end of liquid layer	[m]
$h^*$	: thickness of formation of microlayer	[m]
$h_D^*$	: dimensionless thickness of formation of microlayer	
$H$	: cf. eq. (3.2.26), initial thickness of thermal boundary layer above wall	$[m^2 s^{-2}]$ [m]
$Ja$	: Jakob number	
$k$	: constant in Henri's law	$[Pa m^3 kg^{-1}]$
$\lambda$	: latent heat of evaporation	$[J kg^{-1}]$
$L$	: dimensionless thickness of microlayer	
$N$	: number of collocation points, number of terms in Grünwald series	
$p$	: liquid pressure	[Pa]
$p_m$	: liquid pressure in microlayer	[Pa]
$p_R$	: liquid pressure at bubble cap	[Pa]
$p_{tr}$	: transitional pressure, cf. Sect. 2.4.2.	[Pa]
$p_\phi$	: pressure in potential flow region	[Pa]
$p_1$	: gas or vapour pressure	[Pa]
$p_{1R}$	: gas or vapour pressure at bubble cap	[Pa]
$p_\infty$	: liquid pressure at wall far away from bubble	[Pa]

$\Delta p_s$	: suction pressure	[Pa]
$P_k$	: Legendre polynomial of degree k	
Pr	: Prandtl number	
$[P]_{kj}$	: matrix element, cf. eq. (3.2.15)	
q	: heat flow density	[W m <sup>-2</sup> ]
$q_h$	: heat flow density at vapour-liquid interface of liquid layer, cf. App. C	[W m <sup>-2</sup> ]
$q_M$	: heat flow density at vapour-liquid interface in microlayer	[W m <sup>-2</sup> ]
$q_R$	: heat flow density at vapour-liquid interface of bubble cap	[W m <sup>-2</sup> ]
$[Q]_{kj}$	: matrix element, cf. eq. (3.2.18)	[m <sup>-(2j+1)</sup> ]
$[Q^*]_{kj}$	: dimensionless matrix element $\underline{Q}$	
r	: radial coordinate in spherical and cylindrical coordinate system	[m]
$r_i$	: location of interface between two fluid elements, cf. App. C	[m]
$r_{i+}$	: midpoint of fluid element, cf. App. C	[m]
$r_o$	: minimum radius of curvature in meniscus region	[m]
$r'$	: distance from bubble cap	[m]
$\bar{r}_o$	: mean radius of curvature in meniscus region	[m]
$\Delta r$	: region in liquid microlayer where evaporation is maximal	[m]
R	: bubble radius	[m]
$R_c$	: bubble contact radius, location of microlayer formation	[m]
$R_d$	: dry area radius	[m]
$R_{dep}$	: bubble departure radius	[m]
$R_e$	: equilibrium bubble radius	[m]
$R_{eq}$	: equivalent bubble radius	[m]
$R_i$	: bubble radius at collocation angle $\theta_i$	[m]
$R_o$	: radius of cavity where bubble is formed, location in liquid layer where tangential velocity vanishes, cf. App. C	[m]
$R_\infty$	: undisturbed bubble radius, cf. Sect. 2.5, location in liquid layer where suction pressure is applied, cf. App. C	[m]

$R_1, R_2$	: principal radii of curvature	[m]
$R'_O$	: location of transition between regions of appreciable and negligible curvature of gas-liquid interface, cf. App. C	[m]
$R_G$	: residual, cf. eq. (3.2.29)	[m s <sup>-1</sup> ]
$R_G^*$	: residual, cf. eq. (3.2.31)	[m s <sup>-1</sup> ]
$R_H$	: residual, cf. eq. (3.2.30)	[m <sup>2</sup> s <sup>-2</sup> ]
$R_H^*$	: residual, cf. eq. (3.2.31)	[m <sup>2</sup> s <sup>-2</sup> ]
s	: exponent in bubble growth law, function representing surface tension gradient, cf. App. C	[Pa]
$s^+, s^-$	: functions describing memory effects, cf. eqs. (3.3.28,29)	[m s <sup>-1</sup> ]
Sc	: Schmidt number	
t	: time elapsed after start of bubble growth	[s]
$\underline{t}$	: unit vector tangential to interface	[m]
$t_D$	: dimensionless time, cf. eq. (4.1.48)	
$t_{dep}$	: bubble departure or adherence time	[s]
$t_r$	: time when $R_c = r$	[s]
$t_w$	: waiting time	[s]
$t^*$	: cf. eq. (2.2.30)	[m <sup>h</sup> s]
T	: liquid temperature	[K]
$T_B$	: temperature of bulk liquid	[K]
$T_M$	: temperature of vapour-liquid interface in microlayer	[K]
$T_R$	: liquid temperature at bubble cap	[K]
$T_s$	: saturation temperature at pressure $p_\infty$	[K]
$T_w$	: wall temperature	[K]
$T_1$	: vapour temperature	[K]
$T_{1R}$	: vapour temperature at bubble cap	[K]
$T_\infty$	: temperature at edge of thermal boundary layer surrounding bubble cap	[K]
$\bar{T}_\infty$	: mean value of $T_\infty$ , cf. eq. (2.4.15)	[K]
$\underline{\underline{T}}_\infty$	: mean temperature, cf. eq. (3.3.23)	[K]
$\Delta T$	: liquid temperature	[°C]
u	: velocity in r-direction in cylindrical coordinates	[m s <sup>-1</sup> ]
$u_h$	: velocity in r-direction at gas-liquid interface	[m s <sup>-1</sup> ]

$u_r$	: velocity in r-direction in spherical coordinates	[m s <sup>-1</sup> ]
$u_\theta$	: velocity in $\theta$ -direction in spherical coordinates	[m s <sup>-1</sup> ]
$\underline{u}$	: liquid velocity vector	[m s <sup>-1</sup> ]
$\underline{u}_l$	: gas velocity vector	[m s <sup>-1</sup> ]
$U$	: translation velocity of spherical bubble	[m s <sup>-1</sup> ]
$V$	: bubble volume	[m <sup>3</sup> ]
$V_R$	: volume of vapour originated from bubble cap	[m <sup>3</sup> ]
$V_M$	: volume of vapour originated from microlayer	[m <sup>3</sup> ]
$w$	: velocity in z-direction in cylindrical coordinates	[m s <sup>-1</sup> ]
$w_h$	: velocity in z-direction at gas-liquid interface	[m s <sup>-1</sup> ]
$x$	: coordinate parallel to wall in microlayer, unknown in third order equation (2.4.12), function defined by eq. (3.3.24)	[m] [m s <sup>-1</sup> ]
$x^*$	: place where vapour-liquid interface in microlayer becomes horizontal	[m]
$y$	: function defined by eq. (3.3.25)	
$z$	: coordinate normal to solid wall, half of distance between centres of two spherical bubbles	[m] [m]
$z_o$	: displacement thickness at $R_c$ of hydrodynamic boundary layer	[m]
$z_{oD}$	: dimensionless thickness of hydrodynamic boundary layer	

#### Greek symbols

$\alpha$	: numerical constant in eq. (2.4.25)	
$\alpha_j$	: expansion coefficient, cf. Ch. 3	[m]
$\beta_j$	: expansion coefficient, cf. Ch. 3	[m <sup>j+3</sup> ]
$\beta_s$	: factor characterizing influence of concentration gradient at gas-liquid interface	
$\beta'$	: coefficient, cf. eq. (3.3.11)	
$\gamma$	: bubble growth constant for diffusion - controlled growth	
$\gamma_o$	: bubble growth constant for inertia - controlled growth	[m s <sup>-1</sup> ]



$\gamma_s$	: bubble growth constant, cf. eq. (4.1.50)	$[m^{1-2s}]$
$\gamma'$	: bubble growth constant, cf. eqs. (2.2.31,36)	$[m s^{-s}]$
$\Gamma$	: gamma function	
$\dot{V}$	: volumetric flow rate	$[m^3 s^{-1}]$
$\dot{V}_\infty$	: volumetric flow rate at R, cf. App. C	$[m^3 s^{-1}]$
$\delta$	: thickness of thermal or diffusion boundary layer around bubble cap,	$[m]$
	small distance in potential flow region outside microlayer	$[m]$
$\delta^*$	: small distance in meniscus region of microlayer	
$\Delta_i$	: distance between midpoints, cf. App. C	$[m]$
$\Delta_{i+}$	: distance between interfaces, cf. App. C	$[m]$
$\epsilon$	: disturbance in bubble radius	$[m]$
$\zeta$	: ratio of final to initial thickness of thermal boundary layer above wall	
$\eta$	: liquid dynamic viscosity	$[Pa s]$
$\Theta$	: azimuthal angle in spherical coordinates	
$\Theta_a$	: apparent contact angle	
$\Theta_o$	: natural contact angle	
$\Theta^o$	: wall superheating	$[K]$
$\Delta\Theta^o$	: bulk superheating	$[K]$
$\kappa$	: liquid thermal diffusivity,	$[m^2 s^{-1}]$
	diffusion coefficient of solute in liquid	$[m^2 s^{-1}]$
$\kappa_1$	: thermal diffusivity of gaseous phase	$[m^2 s^{-1}]$
$\lambda$	: liquid coefficient of heat conduction,	$[W k^{-1} m^{-1}]$
	dimensionless coordinate in microlayer	
$\lambda_1$	: coefficient of heat conduction in gaseous phase	$[W k^{-1} m^{-1}]$
$\mu$	: $= \cos \Theta$ , cf. eqs. (3.2.27,28)	
$\nu$	: liquid kinematic viscosity	$[m^2 s^{-1}]$
$\xi$	: cf. eq. (4.1.26)	
$\rho$	: liquid density	$[kg m^{-3}]$
$\rho_1$	: density of gaseous phase	$[kg m^{-3}]$
$\sigma$	: surface tension	$[N m^{-1}]$
$\sigma_o$	: mean surface tension, cf. App. A	$[N m^{-1}]$
$\sigma'$	: variation of surface tension, cf. App. A	$[N m^{-1}]$
$\tau$	: characteristic time for bubble growth	$[s]$

$\tau_n$	: normal stress at gas-liquid interface	[Pa]
$\tau_t$	: tangential stress at gas-liquid interface	[Pa]
$\underline{\underline{\tau}}$	: stress tensor	[Pa]
$\phi$	: velocity potential	[m <sup>2</sup> s <sup>-1</sup> ]
$\phi$	: heat flux	[W]
$\psi$	: stream function	[m <sup>3</sup> s <sup>-1</sup> ]
$\omega$	: component of vorticity vector normal to cross-sectional plane,	[s <sup>-1</sup> ]
	circular frequency of bubble oscillations	[s <sup>-1</sup> ]
$\omega_M$	: Minnaert frequency	[s <sup>-1</sup> ]
$\underline{\underline{\omega}}$	: vorticity vector	[s <sup>-1</sup> ]
$\nabla$	: grad, differential operator	[m <sup>-1</sup> ]
$\nabla^2$	: divgrad, differential operator	[m <sup>-2</sup> ]

## REFERENCES

- Baranenko, V.I., Chichkan, L.A., Nikolaev, G.F., and Smirnov, G.F., (1974). Optical investigation of heat transfer mechanism with boiling. Fifth Int. Heat Transf. Conf., Paper B2.4, Tokyo.
- Bénard, H., (1901). Les tourbillons cellulaires dans une nappe liquide transportant de la chaleur par convection en régime permanent. Ann. Chim. Phys., 7, 23, 62-144.
- Bird, R.B., Steward, W.E., and Lightfoot, E.N., (1960). Transport Phenomena. John Wiley and Sons, New York.
- Birkhoff, G., Margulies, R.S., and Horning, W.A., (1958). Spherical bubble growth. Physics of Fluids, 1, 201-204.
- Bošnjacovič, F., (1930). Verdampfung und Flüssigkeitsüberhitzung. Techn. Mech. Thermo-Dynam., 1, 358-362.
- Butkov, E., (1973). Mathematical physics. Addison-Wesley Publ. Comp., Inc.
- Carslaw, H.S., and Jaeger, J.C., (1967). Conduction of heat in solids. Clarendon Press, Oxford.
- Cho, S.M., and Seban, R.A., (1969). On some aspects of steam bubble collapse. J. Heat Transfer, 91(C), 537-542.
- Cole, R., and Rohsenow, W.M., (1969). Correlations of bubble departure diameters for boiling of saturated liquids. Chem. Engng. Prog. Symp. Ser., Heat Transfer, Philadelphia, 65, 211-217.
- Cole, R., (1974). Boiling nucleation. Adv. Heat Transfer, 10, 85-165.
- Cooper, M.G., and Lloyd, A.J.P., (1969). The microlayer in nucleate pool boiling. Int. J. Heat Mass Transfer, 12, 895-913.
- Cooper, M.G., and Vijuk, R.M., (1970). Bubble growth in nucleate pool boiling. Fourth Intern. Heat Transfer Conf., 5, B.2.1.

Cooper, M.G., and Merry, J.M.D., (1972). Microlayer evaporation in nucleate boiling. 4th all-Union Heat Mass Transfer Conf., Minsk.

Cooper, M.G., and Merry, J.M.D., (1973). A general expression for the rate of evaporation of a layer of liquid on a solid body. Int. J. Heat Mass Transfer, 16, 1811-1815.

Cooper, M.G., Judd, A.M., Malcotsis, G., and Pike, R.A., (1975). Bubble growth under simplified conditions. Letters Heat Mass Transfer, 2(3), 207-212.

Cooper, M.G., Judd, A.M., and Pike, R.A., (1978). Shape and departure of single bubbles growing at a wall. 6th. Int. Heat Transfer Conf., Toronto.

Dalle Donne, M., and Ferranti, M.P., (1975). The growth of vapour bubbles in superheated sodium. Int. J. Heat Mass Transfer 18, 477-493.

De Feijter and Vrij, cf. Feijter.

Diesselhorst, T., Grigull, U., and Hahne, E., (1977). Hydrodynamic and surface effects on the peak heat flux in pool boiling. Heat transfer in boiling, Chapt. 6, Hemisphere Publishing Corp.

Elliott, G.E.P., and Riddiford, A.C., (1967). Dynamic contact angles; the effect of impressed motion. J. Coll. Interface Sci., 23, 389-398.

Epstein, A.S., and Plesset, M.S., (1950). On the stability of gas bubbles in liquid-gas solutions. J. Chem. Phys., 18 (11), 1505-1509.

Feijter, J.A. de, and Vrij, A., (1972). Transition regions, line tensions and contact angles in soap films. J. Electroanal. Chem., 37, 9-22.

Finlayson, B.A., (1972). The method of weighted residuals and variational principles. Academic Press, New York.

Fox, L., and Parker, I.B., (1968). Chebyshev polynomials in numerical analysis. Oxford university press, London.

Fritz, W., (1935). Berechnung des Maximalvolumens von Dampfblasen. Phys. Z., 11, 379-384.

Groenveld, P., (1970 a). High capillary number withdrawal from viscous Newtonian liquids by flat plates. Chem. Engng. Sci., 25, 33-40.

Groenveld, P., (1970 b). Low capillary number withdrawal. Chem. Engng. Sci., 25, 1259-1266.

Groenveld, P., (1970 c). Laminar withdrawal with appreciable inertial forces. Chem. Engng. Sci., 25, 1267-1273.

Han, C.Y., and Griffith, P., (1965). The mechanism of heat transfer in nucleate boiling I: bubble initiation, growth and departure. Int. J. Heat Mass Transfer, 8, 887-914.

Hayes, J.G., (1970). Numerical approximation to functions and data. The Athtone Press, London.

Hermans, W.A.H.J., (1973). On the instability of a translating gas bubble under influence of a pressure step. Ph. D.-thesis, University of Technology, Eindhoven, The Netherlands.

Hsieh, D.Y., (1965). Some analytical aspects of bubble dynamics. J. Basic Engng., A.S.M.E., 87(D), 991-1005.

Isenberg, J., and Sideman, S., (1971). Flow field around collapsing bubble trains: theoretical analysis. Appl. Sci. Res., 24, 53-64.

Jakob, M., (1958). Heat Transfer. John Wiley and Sons, New York.

Kabanow, B., and Frumkin, A., (1933). Ueber die Grösse elektrolytisch entwickelter Gasblasen. Z. Chem., 165, 433-452.

Katto, Y., and Shoji, M., (1970). Principal mechanism of micro-liquid-layer formation on a solid surface with a growing bubble in nucleate boiling. *Int. J. Heat Mass Transfer*, 13, 1299-1311.

Katto, Y., Takahashi, S., and Yokoya, S., (1973). Law of micro-liquid-layer formation between a growing bubble and a solid surface with a special reference to nucleate boiling. *Bull. JSME*, 16 (97), 1066-1075.

Kenning, D.B.R., and Toral, H., (1977). On the assessment of thermocapillary effects in nucleate boiling of pure fluids. The Levich birthday conference on physical chemistry and hydrodynamics, Oxford, July 11-13.

Kiper, A.M., (1971). Minimum bubble departure diameter in nucleate pool boiling. *Int. J. Heat Mass Transfer*, 14, 931-937.

Lamb, H., (1974). *Hydrodynamics*. Cambr. Univ. Press.

Landau, L., and Levich, B., (1942). Dragging of a liquid by a moving plate. *Acta Physicochimica U.R.S.S.*, 17, 42-54.

Levich, B.G., (1962). *Physico-chemical hydrodynamics*. Prentice-Hall, Englewood, N.J.

Ludviksson, V., and Lightfoot, E.N., (1968). Deformation of advancing menisci. *AIChEJ.*, 14, no 4, 674-677.

Manley, D.M.J.P., (1960). Change of size of air bubbles in water containing a small dissolved air content. *Brit. J. Appl. Phys.*, 11, 38-42.

Mathis, D.A., (1976). *Hydrogen technology for energy*. Noyes Data Corp., New Jersey.

Mikic, B.B., Rohsenow, W.M., and Griffith, P., (1970). On bubble growth rates. *Int. J. Heat Mass Transfer*, 13, 657-666.

- Minnaert, M., (1933). On musical air-bubbles and the sounds of running water. *Phil. Mag. (ser. 7)*, 11, 235-248.
- Moalem, D., Zijl, W., and Stralen, S.J.D. van, (1977). Nucleate boiling at a liquid-liquid interface. *Letters Heat Mass Transfer*, 4, 319-329.
- Moore, F.D., and Mesler, R.B., (1961). The measurement of rapid surface temperature fluctuations during nucleate boiling of water. *A.E.Ch.E.J.*, 7, 620-624.
- Oldham, K.B., and Spanier, J., (1970). The replacement of Fick's law by a formulation involving semidifferentiation. *J. Electroanal. Chem.*, 26, 331-341.
- Oldham, K.B., (1973). Diffusive transport to planar, cylindrical and spherical electrodes. *Electroanal. Chem. and Interface Electrochem.* 41, 351-358.
- Oldham, K.B., and Spanier, J., (1974). *The fractional calculus*. Academic Press, New York - London.
- Ouwerkerk, H.J. van, (1970). The role of the evaporating microlayer and dry surface areas in boiling. Ph. D.-thesis, Univ. of Techn. Eindhoven, the Netherlands.
- Ouwerkerk, H.J. van, (1971). The rapid growth of a vapour bubble at a liquid-solid interface. *Int. J. Heat Mass Transfer*, 14, 1415-14 .
- Pike, R.A., (1977). Bubble dynamics in boiling. Ph. D.-thesis, Cambridge University.
- Plesset, M.S., and Zwick, S.A., (1952). A nonsteady heat diffusion problem with spherical symmetry. *J. Appl. Phys.* 23(1), 95-98.
- Plesset, M.S., (1954a). On the stability of fluid flows with spherical symmetry. *J. Appl. Phys.*, 25, 96-98.

Plesset, M.S., and Zwick, S.A. (1954b). The growth of vapour bubbles in superheated liquids. *J. Appl. Phys.* 25, 493-500.

Plesset, M.S., and Zwick, S.A., (1955). On the dynamics of small vapour bubbles in liquids. *J. Math. Phys.*, 33, 308-330.

Plesset, M.S., and Chapman, R.B., (1971). Collapse of an initially spherical vapour cavity in the neighbourhood of a solid boundary. *J. Fluid Mech.*, 47, 283-290.

Plesset, M.S., and Prosperetti, A., (1977). Bubble dynamics and cavitation. *Ann. Rev. Fluid Mech.*, 9, 145-185.

Prosperetti, A., and Plesset, M.S., (1978). Vapour-bubble growth in a superheated liquid. *J. Fluid Mech.*, 85(2), 349-368.

Prüger, W., (1941). Die Verdampfungsgeschwindigkeit von Flüssigkeiten. *Z. Phys.*, 115, 202-244.

Rayleigh, J.W.S., (1906). On convection currents in a horizontal layer of fluid when the higher temperature is on the under side. *Phil. Mag.*, 6, 32, 529-546.

Rayleigh, J.W.S., (1917). On the pressure developed in a liquid during collapse of a spherical cavity. *Phil. Mag.*, 34, 94-98.

Reynolds, O., (1886). On the theory of lubrication and its application to Mr. Béauchamp Tower's experiments, including an experimental determination of the viscosity of olive oil. *Phil. Trans. Royal Soc. London*, 177, 157-234.

Ross, B., (1975). A brief history and exposition of the fundamental theory of fractional calculus. *Lecture notes in mathematics 457*, Springer-Verlag, Berlin.

Sabotin, V.I., Sorokin, D.N., Orechkin, D.M., and Rudryavtsev, A.P., (1972). Heat transfer in boiling metals by natural convection. Israel program for scientific translations, Jerusalem.



Scheludko, A., (1957). Ueber das Ausfliessen der Lösung aus Schaumfilmen. Kolloid Zeitschr. 155, 39-44.

Scheludko, A., Tschaljowska, Sl., and Fabrikant, A., (1970). Contact between a gas bubble and a solid surface and froth flotation. Special discussions of the Faraday Society no. 1. Ac. Press, London.

Schmidt, H., (1977). Bubble formation and heat transfer during dispersion of superheated steam in saturated water I: bubble size and bubble detachment at single orifices. Int. J. Heat Mass Transfer, 20, 635-646.

Scriven, L.E., (1959). On the dynamics of phase growth. Chem. Engng. Sci., 10(1), 1-13.

Siegel, R., and Keshock, E.G., (1964). Effects of reduced gravity on nucleate boiling bubble dynamics in saturated water. A.I.Ch.E. Journal, 10, 4, 509-517.

Sluyter, W.M., (1978). Het gedrag van imploderende gasbellen, theorie en numerieke berekeningen. M.Sc.-thesis, Eindhoven University of Technology, the Netherlands.

Spiers, R.P., Subbaraman, C.V., and Wilkinson, W.L., (1974). Free coating of a Newtonian liquid onto a vertical surface. Chem. Engng. Sci., 29, 389-396.

Stralen, S.J.D. van, (1968). The growth rate of vapour bubbles in superheated pure liquids and binary mixtures, I: theory; II: experimental results. Int. J. Heat Mass Transfer, 11, 1491-1512.

Stralen, S.J.D. van, Cole, R., Sluyter, W.M., and Sohal, M., (1975). Bubble growth rates in nucleate boiling of water at subatmospheric pressures. Int. J. Heat Mass Transfer, 18, 655-669.

Theofanous, T.G., and Patel, P.D., (1976). Universal relations for bubble growth. Int. J. Heat Mass Transfer, 19, 425-429.

Traykov, T.T., and Ivanov, I.B., (1977). Hydrodynamics of thin liquid films; effect of surfactants on the velocity of thinning of emulsion films. *Int. J. Multiphase Flow*, 3, 471-483.

Trividi, G., and Funk, J.E., (1970). Dynamics and stability of electrolytic bubbles: bubble departure diameters. Project Themis Research Rep., 17, U.S.A.

Turner, J.S., (1973). Buoyancy effects in fluids. Cambridge University Press.

Van Ouwerkerk, cf. Ouwerkark.

Van Stralen, cf. Stralen.

Walters, J.K., and Davidson, J.F., (1962). The initial motion of a gas bubble formed in an inviscid liquid I: The two-dimensional bubble. *J. Fluid Mech.*, 12, 408-417.

Walters, J.K., and Davidson, J.F., (1963). The initial motion of a gas bubble formed in an inviscid liquid II: The three-dimensional bubble and the toroidal bubble. *J. Fluid Mech.*, 17, 321-337.

Wayner, P.C.Jr., Kao, Y.K., and La Croix, L.V., (1976). The interline heat-transfer coefficient of an evaporating wetting film. *Int. J. Heat Mass Transfer*, 19, 487-492.

White, D.A., and Tallmadge, J.A., (1965). Theory of drag out of liquids on flat plates. *Chem. Engng. Sci.*, 20, 33-37.

Whitham, G.B., (1974). *Linear and non-linear waves*. Wiley Interscience, New York.

Witze, C.P., Schrock, V.E., and Chambré, P.L., (1968). Flow about a growing sphere in contact with a plane surface. *Int. J. Heat Mass Transfer*, 11, 1637-1652.

Yao, S.C., and Schrock, V.E., (1976). Heat and mass transfer from freely falling drops. J. Heat Transfer A.S.M.E., 98(C), 120-126.

Yeh, H.C., (1967). The dynamics of gas bubbles moving in liquids with pressure gradient. Ph.D.-thesis, University of Michigan, U.S.A.

Yu, C., and Mesler, R., (1977). A study of nucleate boiling near the peak heat flux through measurement of transient surface temperature. Int. J. Heat Mass Transfer, 20, 827-840.

Zijl, W., Moalem, D., and Stralen, S.J.D. van, (1977). Inertia and diffusion controlled bubble growth and implosion in initially uniform pure and binary systems. Letters Heat Mass Transfer, 4, 331-339.

## SUMMARY

In this thesis, the departure of a bubble growing at a horizontal wall has been investigated both theoretically and experimentally. Two kinds of bubbles can be distinguished:

- (i) *Vapour bubbles*. At a superheated wall, these bubbles grow relatively rapidly by means of evaporation. A thin liquid layer, the so-called microlayer, remains between bubble and wall. Evaporation takes place both at the surface of the microlayer and at the bubble cap.
- (ii) *Gas bubbles*. These bubbles grow by accretion of dissolved gas which diffuses from the liquid to the bubble. These bubbles are quasi-static and a microlayer is not formed. However, a very thin adsorption layer is present between the bubble and the wall.

The process of departure is strongly dependent on the bubble growth rate. For quasi-static gas bubbles, the rate of growth of the adsorption layer, or so-called 'dry' area, also turns out to be of importance. In Chapter 2 of this thesis, both departure and the underlying growth processes are treated with the aid of simple models in which the bubble is considered as a segment of a sphere.

Section 2.2 describes the coupled thermal and hydrodynamic processes during growth of a free bubble in a uniformly superheated liquid. Two modes of growth are distinguished, and a general expression for the transition between these two modes is derived.

In Section 2.3, a simple model describing bubble departure under the influence of buoyancy is introduced.

In Section 2.4, the model developed in Section 2.3 is applied to bubbles in a non-homogeneous temperature field. In this way, the empirical relation of Cole and Rohsenow (1969) for the departure radius is explained theoretically.

In Section 2.5, oscillations of spherically symmetric vapour bubbles are considered. It is shown that, at a sufficiently high frequency, the compressibility of the vapour may no longer be neglected.

In Chapter 3, the departure of rotationally symmetric vapour bubbles in water boiling at subatmospheric pressures is investigated theoretically. Departure occurs under the influence of gravity. Deviations from the hemispherical shape are described with the global orthogonal collocation method, and the heat transport process is described with a finite number of terms of the Grünwald series for the Riemann-Liouville operator. In this way, the treatment has been reduced to the numerical solution of a coupled set of non-linear ordinary differential equations.

Experiments have been performed on water boiling at subatmospheric pressures. For a pressure of 10 kPa, the theoretically determined bubble shapes and departure time are compared with experimental data.

Finally, in Chapter 4, the hydrodynamic mechanism of microlayer formation and growth of a dry area under the influence of capillary forces is considered.

The mechanism of microlayer formation is described in Section 4.1. The theoretical results are in good agreement with experimental data of Pike (1977).

In Section 4.2, the growth of a dry area under the influence of surface tension is treated. For vapour bubbles it is shown that the contribution of capillary effects is small with respect to dry area formation by evaporation. For gas bubbles, however, the growth of the bubble foot is determined by capillary effects; this growth process is described in Section 4.3. It is shown experimentally that the well-known equation of Fritz (1935) for the departure radius is not applicable for quasi-statically growing gas bubbles.

## SAMENVATTING

In dit proefschrift wordt het loslaten van een groeiende bel op een horizontale wand theoretisch, alsmede experimenteel onderzocht. Twee soorten bellen kunnen worden onderscheiden:

- 1<sup>e</sup>. *Dampbellen*. Aan een oververhitte wand groeien deze relatief snel als gevolg van verdamping. Tussen bel en wand blijft een dun vloeistoflaagje achter, de zogenaamde microlaag. Verdamping vindt zowel aan het oppervlak van de microlaag plaats als aan de belkap.
- 2<sup>e</sup>. *Gasbellen*. Deze groeien door diffusie van in de vloeistof opgelost gas naar de bel. Hun groei is quasi-stationnair en een microlaag wordt niet gevormd; tussen bel en wand bevindt zich echter een dunne adsorptielaag.

Het loslaten is sterk afhankelijk van de snelheid waarmee de bel groeit. Bij de quasi-stationnaire gasbellen blijkt ook het groeitempo van de adsorptielaag, meestal de "droge" plek genoemd, van belang te zijn.

In hoofdstuk 2 van het proefschrift worden zowel het loslaten, alsmede de daaraan ten grondslag liggende groeiprocessen behandeld m.b.v. eenvoudige modellen, waarin de bel als een bolsegment wordt voorgesteld.

Paragraaf 2.2 beschrijft de samenhang tussen hydrodynamische en thermische effecten tijdens de groei van een vrije bel in een uniform oververhitte vloeistof. Twee groeistadia worden onderscheiden en een algemene uitdrukking die de overgang tussen beide groeistadia beschrijft wordt afgeleid.

In paragraaf 2.3 wordt een eenvoudig model voorgesteld voor het loslaten van dampbellen onder invloed van de zwaartekracht.

In paragraaf 2.4 wordt het in paragraaf 2.3 ontwikkelde model toegepast op bellen in een niet-uniform temperatuurveld. Het aldus verkregen resultaat verklaart goed de empirische formule van Cole en Rohsenow (1969) voor de loslaatstraal.

In paragraaf 2.5 worden oscillaties van bolsymmetrische dampbellen beschouwd. Het blijkt dat bij een voldoende hoge oscillatie-frequentie de compressibiliteit van de damp niet meer verwaarloosd mag worden.

Op grond van de in hoofdstuk 2 verkregen inzichten in het gedrag van de bel en van de mogelijke wiskundige methoden ter beschrijving ervan, wordt in hoofdstuk 3 het loslaten onder invloed van de zwaartekracht van omwentelingssymmetrische dampbellen in water onder subatmosferische drukken theoretisch (numeriek) behandeld.

Afwijkingen van de bolvorm worden beschreven met de globale orthogonale collocatie methode en het warmtetransport wordt beschreven met een eindig aantal termen van Grünwald's reeksontwikkeling voor de Riemann-Liouville operator. Op deze manier is het probleem teruggebracht tot het numeriek oplossen van een gekoppeld stelsel niet-lineaire gewone differentiaal-vergelijkingen.

Er zijn experimenten verricht aan water, kokend onder subatmosferische druk. Bij een druk van 10 kPa worden de theoretisch berekende belvorm en de loslaattijd van een bel vergeleken met experimentele waarden.

In hoofdstuk 4 worden ten slotte het hydrodynamische mechanisme van de vorming van een microlaag en dat van de groei van een droge plek onder invloed van capillaire krachten beschouwd.

Het mechanisme van microlaagvorming wordt beschreven in paragraaf 4.1. De theoretische resultaten zijn in goede overeenstemming met door Pike (1977) gevonden experimentele waarden.

In paragraaf 4.2 wordt de groei van een droge plek onder invloed van de oppervlaktespanning beschreven. Voor dampbellen blijkt dat de bijdrage van capillaire effecten verwaarloosbaar is ten opzichte van droge-plek vorming door verdamping. Bij gasbellen echter wordt de groei van de belvoet bepaald door capillaire effecten; dit groei-proces is beschreven in paragraaf 4.3. Experimenteel wordt aangetoond dat de welbekende formule van Fritz (1935) voor de berekening van de loslaatstraal in het algemeen niet mag worden gebruikt voor quasi-stationnair groeiende gasbellen.

## DANKWOORD

In de eerste plaats dank ik Dr. Sjoerd van Stralen voor de vele enthousiasmerende discussies en de prettige manier van samenwerken. Ook dank ik Dr. David Moalem-Maron van de universiteit van Tel-Aviv voor zijn inspirerende en vriendschappelijke manier van samenwerken. Met name wil ik Jacques Joosten en Frans Ramakers danken voor hun bijdragen aan het onderzoek naar vervormende bellen. In het bijzonder dank ik hiervoor ook Pim Sluijter, die bovendien adviseerde op experimenteel gebied. Voor de experimenten aan de groei van droge plekken ben ik o.m. dank verschuldigd aan Louis Hermans. Het typewerk was in goede handen bij Hermine Weise, Nolly de Leeuw en Els Hermkens; het tekenwerk werd verzorgd door Ruth Gruijters. Correcties in de Engelse tekst werden o.m. aangebracht door Derek Charles van de universiteit van Kingston, Canada. Ik ben dankbaar voor het vertrouwen dat in mij werd gesteld en ik dank alle leden van de vakgroep transportfysica voor de prettige sfeer, die ertoe bijdroeg dat mijn werk in de vakgroep een plezier voor mij was.

## CURRICULUM VITAE

Wouter Zijl werd geboren op 16 augustus 1944 te Amsterdam. In 1962 behaalde hij het MULO-B diploma en in 1966 het diploma HTS-electrotechniek. In 1973 studeerde hij af aan de THE, afdeling der technische natuurkunde, vakgroep transportfysika; het afstudeerwerk was gewijd aan ionisatie-verschijnselen aan de achterwand van een schokbuis. In 1973/74 volgde hij een 'post-graduate' cursus in 'computational fluid dynamics' aan het Von Kármán instituut te Sint-Genesius Rode, België. September 1974 kwam hij in dienst van de THE, waar hij in de vakgroep transportfysica beldynamica en kookverschijnselen bestudeerde, hetgeen leidde tot het schrijven van dit proefschrift.



## STELLINGEN

1. Omdat de zogenaamde "regel der exponenten" al een suggestie voor de oplosmethode inhoudt, verdient de notatie met behulp van fractionele afgeleiden de voorkeur boven de schrijfwijze met integralen.

K.B. Oldham and J. Spanier, *The fractional calculus*, Academic Press, New York (1974).

Dit proefschrift, paragraaf 2.5.

2. Voor het numeriek oplossen van de Navier-Stokes vergelijkingen in een stroming begrensd door een vrij oppervlak, verdient het aanbeveling een zodanige eindige elementenmethode te ontwikkelen dat, door eenvoudige integratie van de impuls-vergelijkingen, een expliciete uitdrukking voor de druk wordt verkregen als functie van de nog te bepalen ontwikkelings-coëfficiënten in de proef-functies.

Dit proefschrift, Appendix C.

3. Scheludko's uitbreiding van de formule van Reynolds voor het dunner worden van een horizontale vloeistoffilm onder invloed van verticale krachten is onjuist.

O. Reynolds, *Phil. Trans. Royal Soc.*, 177, 157 (1886).

A. Scheludko, *Koll. Zeitschr.*, 155, 39 (1957).

4. Bij de groei van een droge plek in een vloeistoffilm op een wand zal een eventuele concentratie-gradient aan het scheidingsvlak tussel vloeistof en gas een verwaarloosbare rol spelen.

5. De correctie van Culick op de formule van Dupré voor de expansiesnelheid van een zwarte plek in een vrij opgespannen zeepvlies is onjuist. De discussie van Frankel en Mysels ter verklaring van de door deze correctie ontstane dissipatie in de energie-balans is daarom evenzeer onjuist.

A. Dupré, *Ann. Chim. Phys.*, 11 (4), 194 (1867).

F.E.C. Culick, *J. Appl. Phys.*, 31, 1128 (1960).

S. Frankel and K. Mysels, *J. Phys. Chem.*, 73, 3028 (1969).

6. Het gebruik van een relatie voor de stroom-spannings karakteristiek bij electrolyse, verkregen naar analogie met een betrekking tussen de warmteflux en het temperatuurverschil bij kokende vloeistoffen, zal niet tot juiste resultaten leiden.
7. Het verschijnsel dat in kokende binaire mengsels de bellen minder snel coalesceren dan in kokende zuivere vloeistoffen, moet worden toegeschreven aan de stabiliserende eigenschappen van de opgeloste stof op de dunne vloeistoflagen tussen bellen. Het Marangoni effect is hierbij slechts van ondergeschikt belang.
8. Het overbekende ervaringsfeit dat water nat is valt niet af te leiden uit de standaard-werken over hydrodynamica.

H. Lamb, *Hydrodynamics*, Cambr. Univ. Press (1974).

L.M. Milne-Thomson, *Theoretical Hydrodynamics*, Macmillan and Co, London (1955).

L.D. Landau and E.M. Lifshitz, *Fluid Mechanics*, Pergamon Press, Oxford (1959).

9. Het verdient aanbeveling om in het Engels één uitdrukking te introduceren voor de Nederlandse taal, ter vervanging van de nu naast elkaar voorkomende uitdrukkingen "Dutch" en "Flemish".

W. ZIJL

19 september 1978